Title
Coastal Septic Systems and Submarine Groundwater Discharge: A Case Study

Author
de Sieyes, Nicholas R.

Publication Date
2011-03-01

Peer reviewed

COASTAL SEPTIC SYSTEMS AND SUBMARINE GROUNDWATER DISCHARGE: A CASE STUDY

A DISSERTATION

SUBMITTED TO THE DEPARTMENT

OF CIVIL AND ENVIRONMENTAL ENGINEERING

AND THE COMMITTEE ON GRADUATE STUDIES

OF STANFORD UNIVERSITY

IN PARTIAL FULFILLMENT OF THE REQUIREMENTS

FOR THE DEGREE OF

DOCTOR OF PHILOSOPHY

Nicholas Reed de Sieyes

March 2011

I certify that I have read this dissertation and that, in my opinion, it is fully adequate in scope and quality as a dissertation for the degree of Doctor of Philosophy.

_____

Alexandria Boehm, Principal Adviser

I certify that I have read this dissertation and that, in my opinion, it is fully adequate in scope and quality as a dissertation for the degree of Doctor of Philosophy.

_____

David Freyberg

I certify that I have read this dissertation and that, in my opinion, it is fully adequate in scope and quality as a dissertation for the degree of Doctor of Philosophy.

_____

Scott Fendorf

Approved for the Stanford University Committee on Graduate Studies

_____

ABSTRACT

The focus of this dissertation is submarine groundwater discharge (SGD), the direct flow of groundwater from the seabed to the sea, and onsite wastewater treatment systems in coastal California. The research focuses primarily on a single coastal community in central California, Stinson Beach, where conventional onsite treatment systems, or septic systems, are used exclusively for wastewater disposal. The overarching goal of the work has been to quantify the magnitude and timing of SGD at the site and to provide insight into how onsite wastewater treatment at Stinson Beach affects local groundwater quality and, via SGD, surface water quality, all with the broader goal of informing and guiding future development along the California coast.

The dissertation includes four research chapters, each focused on one or more important aspects of the issue of SGD and coastal septic systems at Stinson Beach. The first research chapter, *Submarine discharge of nutrient-enriched fresh groundwater at Stinson Beach, California is enhanced during neap tides*, describes a 14-day study investigating the influence of fortnightly spring-neap tidal variability on submarine discharge of fresh and saline groundwaters at the site. Fresh, shallow groundwater at the site was observed to contain high concentrations of nutrients including dissolved inorganic nitrogen, soluble reactive phosphate, and silicate, as well as human fecal bacteria. A groundwater-derived freshening and nutrification of the surf zone was observed at neap tide, and was followed by a 4-day increase in chlorophyll *a* concentrations in the surf zone. Analytical models and a fresh water budget in the surf zone were used to estimate the saline and fresh SGD at both neap and spring tides. Fresh SGD at the site was estimated at between 1.2 and 4.7 L min^{-1} m^{-1} shoreline during neap tides compared to 0.1 and 0.5 L min^{-1} m^{-1} during spring tides. This compares to saline SGD estimates of 15.9 and 22.0 L min^{-1} m^{-1} during neap and spring tides, respectively. Despite the smaller total discharge of groundwater during neap compared to spring tides, the larger fresh discharge component during neap tides raised surf zone silicate, DIN, and SRP by 14%, 35%, and 27%, respectively, relative to spring tides. The observed fortnightly 'pulse' of fresh groundwater-derived nutrients into the surf zone was

consistent with seaward hydraulic gradients across the fresh part of the beach aquifer, which varied due to aquifer overheight, or the mounding of groundwater due to variable infiltration of salt water during tides, adjacent the beach face. Darcy-Dupuit estimates of seaward fresh groundwater flow in this area agreed well with the fresh discharge results of the mass balance.

The second research chapter of the dissertation, entitled *Submarine groundwater discharge to a high-energy surf zone at Stinson Beach, California, estimated using radium isotopes***,** describes and compares results from a pair of two-week long experiments conducted in the dry season (July 2006) and wet season (March 2007) to examine tidal, wave-driven and seasonal variability of SGD at the site using natural radium tracers. Tide stage, tide range, breaker height and season each explained a significant degree of radium variability in the surf zone. A mass balance of excess radium in the surf zone was used to estimate SGD and associated nutrient fluxes during each season, confirming larger discharge rates during the wet season. Our results indicate median groundwater discharge rates of 6 to 8 L min^{-1} m^{-1} in July 2006 and 38 to 43 L min^{-1} m^{-1} in March 2007. SGD from 200 m of Stinson Beach in March 2007 was shown to contribute a flux of phosphate and dissolved inorganic nitrogen approximately equal to that associated with all local creeks and streams within 6 km of the study site at that time.

The third research chapter, *Fresh submarine groundwater discharge from a coastal aquifer forced by the Mediterranean climate of central California*, is a numerical investigation of groundwater flow at the land-sea interface forced by precipitation and evapotranspiration typical of the Mediterranean climate of coastal California. A numerical groundwater model was developed using the variable density groundwater flow code SEAWAT-2000 to examine the influence of seasonally variable recharge conditions typical of coastal California on the magnitude and timing of fresh submarine groundwater discharge from a generic coastal aquifer with a constant head (non-tidal) ocean boundary. Model dimensions and hydrogeologic characteristics were chosen based on a combination of observations from field studies at Stinson Beach, California, and published numerical investigations of coastal groundwater flow. Average monthly recharge was calculated from historical precipitation records and potential evapotranspiration rates calculated from climatological observations made near the field

site. Calculated recharge was approximately sinusoidal across the year, with positive recharge rates dominated by precipitation during the rainy winter and negative recharge rates dominated by evapotranspiration during the hot, precipitation-free summer. Rates of fresh discharge from the model aquifer to the ocean exhibited similar temporal characteristics for two modeled scenarios, a first including a constant head fresh landward boundary condition and a second including a constant flux fresh landward boundary condition. Discharge in both models peaked in January during the period of maximum precipitation and recharge, and declined until reaching a minimum in September, two months after the minimum recharge period in July. Minimum simulated discharge rates for two simulated scenarios were 17% and 18% lower in September than the maximum simulated discharges in winter. Monthly mean discharge from Lagunitas Creek, a creek near Stinson Beach, reached maximum and minimum values in February and September, respectively. The exponential decline in creek discharge was fast compared to the decline in modeled SGD, however, suggesting that fresh SGD and associated nutrient fluxes may play a particularly important role in coastal ecosystems in early summer when surface water discharge has nearly reached a minimum but discharge of substantial quantities of fresh groundwater is still substantial.

The final research chapter, *Nitrogen, fecal indicator bacteria, and coliphage attenuation and flux from a septic leach field to the coastal ocean*, describes a two-year field study to measure the flux and attenuation of nitrogen, fecal indicator bacteria, and bacteriophage in groundwater adjacent to a large coastal septic system in Central California. The study was carried out at Stinson Beach Park, Golden Gate National Recreation Area, sixteen kilometers northwest of the San Francisco Golden Gate Bridge. Long-term measurements of septic effluent quality and volumetric discharge to the leach field, synoptic DC resistivity profiling of the saltwater/freshwater interface, continuous measurements of hydraulic head in the coastal aquifer, and the installation and subsequent monitoring of a dense array of multi-level monitoring wells adjacent to the leach field for chemical and microbiological constituents were carried out. Our results indicate a nitrogen- and inorganic carbon-rich plume of septic effluent flowing from the leach field through the beach to the subterranean estuary, or the mixing zone of fresh and saline groundwaters. Attenuation of *E. coli* and coliphage was complete within the

vadose zone and the first few meters of transport. Enterococci were detected throughout the well network during one sampling event during which no attenuation was observed, and no attenuation of total nitrogen was observed along the flowpath during the experiment. Median estimates of total nitrogen fluxing toward the ocean downgradient from the leach field ranged from 1.6 to 70.6 moles day^{-1}, depending on season and transect location. Except for enterococcus, the behavior of nitrogen and microbial pollutants in the field was consistent with results from laboratory experiments, which demonstrated low denitrification potential in slurry tests, but fast fecal indicator bacteria and virus attenuation rates in saturated column experiments. Comparisons of total nitrogen flux to the subterranean estuary in this study agree well with SGD-associated nutrient flux estimates from prior studies at the site, suggesting that septic systems at the site are a persistent source of nitrogen to the subterranean estuary and may at times also be a source of enterococci. Denitrification potentials measured at the site suggest a possible role for in-situ remediation strategies to optimize nutrient removal in the beach aquifer.

ACKNOWLEDGMENTS

I am most indebted to my principal adviser, Ali Boehm, for her guidance, patience, knowledge, and friendship. I am also grateful to David Freyberg and Scott Fendorf, both of whom provided valuable advice and insight during my doctoral studies. I also extend a warm thanks to Doug Mackay and Art Sylvester, whose kind encouragement was pivotal in my choice to pursue a career in academic research.

This work would not have been possible without the support of the community of Stinson Beach, California. I owe an enormous debt of gratitude to the board of directors and staff of the Stinson Beach County Water District and to the maintenance staff of Stinson Beach Park, specifically Michael Peri and Tima Alexandro, all of whom were enormously helpful in the completion of my field projects. I also thank California Sea Grant and the Environmental Ventures Program of the Woods Institute for the Environment at Stanford University for funding my research.

Warm thanks go to the Boehm Group members of past and present who have contributed to my research in one way or another, including Alyson Santoro, Daniel Keymer, Tim Julian, Blythe Layton, Sarah Walters, and Todd Russell. I also thank the many students who contributed to my work through independent study, including Eric Foote, Elizabeth Joyce, Rachelle Strickfaden, and Cynthia McClain. A very special thanks also goes to fellow Boehm Group member and good friend Kevan Yamahara for his support and friendship through the years.

Lastly, I thank my parents Chuck and Cricket, my brother Evan, Loie, Jamie, and Kim for all their love and encouragement.

TABLE OF CONTENTS

LIST OF TABLES

LIST OF FIGURES

CHAPTER 1: INTRODUCTION

Along coastal margins, an invisible connection exists between groundwater and the ocean. Submarine groundwater discharge (SGD) is any and all fluid flow, regardless of composition or driving force, flowing from the seabed to the sea (Burnett et al. 2006). SGD can contribute nutrients, metals, pollutants, and freshwater to the coastal environment (Johannes 1980, Bone et al. 2007). Driving forces of SGD include meteoric hydraulic head, tide- and wave pumping, seasonal evapotranspiration cycles (Michael et al. 2005), and variations in groundwater density. Additional factors influencing the timing and magnitude of SGD include regional geology, climate, and human activities along the coastline including groundwater pumping and artificial recharge. The importance of combinations of factors controlling SGD vary from site to site, and site-specific studies are often required to fully understand SGD in a given region. These studies are often labor intensive, so relatively few studies have been conducted (Taniguchi et al. 2002). Of these, even fewer have been conducted in California (Oberdorfer et al. 1990; Boehm et al. 2004, Boehm et al. 2006) or other wave-dominated settings. While the existence and variability of SGD along the world's coastlines has been documented researchers are still working to understand the many factors that influence and modulate the timing and magnitude of this important process.

Numerous potential sources of groundwater pollution can contaminate coastal waters via SGD, but few pose as much potential risk to coastal ecosystem and human health as on-site wastewater treatment systems, or septic systems. Septic systems rely on natural attenuative mechanisms to treat wastewater on-site during infiltration. Incomplete treatment in the vadose zone can result in the contamination of surficial aquifers by pathogens, pharmaceuticals, and nutrients (Robertson et al. 1991, Swartz et al. 2006). The usage of on-site wastewater treatment is widespread, with twenty-five percent of the US population serviced by onsite wastewater treatment systems (US Census Bureau 1997) and 1.2 million OWTS in usage in California alone (CWTRC 2003). The Census Bureau estimated that the 24.6 million OWTS in use in the United States in 1990 generated

approximately 5.5 billion gallons of septage annually, making recharge from OWTS the single largest volumetric discharge to groundwater in the United States (Robertson et al. 1991). Given the prevalence of OWTS, septic systems are one of the greatest threats to groundwater quality in the United States (USEPA 2005).

Nowhere is the importance of understanding the environmental effects of on-site wastewater treatment greater than in active regions of groundwater discharge along the coastal margin. In fact, in many coastal communities, septic systems have often been suspected as potential sources of microbial and/or nutrient pollution to the ocean via SGD. The issue has become hotly contested in California communities such as Malibu, Rincon, Bolinas, Los Osos, and Carpinteria, as development pressure increases and communities suffering from water quality problems make the shift from on-site treatment options to centralized wastewater treatment systems. However, in only a few cases have coastal septic systems actually been confirmed as sources of coastal nutrient- and microbial pollution (Ritter 1986; Valiela and Costa 1988; Reay 2004). Additional studies are needed to better understand the ramifications of treating water on-site along coastlines where SGD is occurring, and the research presented in this dissertation has been conducted to fill some off these knowledge gaps.

1.1 CASE STUDY: STINSON BEACH, CALIFORNIA.

My research has had a substantial fieldwork component, the idea being that careful, intensive study at well-characterized field sites can greatly improve our understanding of important physical processes at work elsewhere. My work has focused on the community of Stinson Beach, California (37° 53' 58.387", 122° 38' 45.384"; Fig. 1.1), a small coastal community 30 km north of San Francisco, California uses septic systems exclusively for wastewater disposal. The beach itself is exposed to the open ocean and faces southwest. Tides at the beach are mixed semi-diurnal, and the beach itself is reflective with a spring tide range on the order of 2.5 m, typical breaker heights of 0.5-1.5 m, and a high-energy surf zone. The climate is Mediterranean with 60 to 120 cm of annual average rainfall occurring predominately between October and April (SBCWD 1998). During the dry season, Bolinas Lagoon (37° 54' 24.811" N, 122° 40' 54.732" W), a tidally influenced lagoon, and Webb Creek (37° 53' 7.332" N, 122° 37'

43.392" W), a nearby freshwater stream, are the only potential sources of fresh surface water to the near-shore marine environment within 6 km of town (Fig. 1.1). During the wet season, numerous ephemeral streams in the area discharge the ocean, mostly via Bolinas Lagoon. Water quality advisories are rare at Stinson Beach: in 2006, only 3% of beach water samples were above any California single sample standard (NRDC 2007).

Stinson Beach is home to only 780 permanent residents (US Census Bureau, factfinder.census.gov), although weekend population can swell by an order of magnitude. Summer daytime visitors to Stinson Beach Park can number in the thousands, and summertime water usage in the community increases threefold above wintertime usage due to vacationers and visitors (SBCWD Manager, pers. comm.) Development is generally confined to the lower elevations of the area, and households use on-site septic systems and holding tanks exclusively for wastewater disposal throughout the community. The unconfined aquifer receiving septage at the site is composed primarily of Quaternary alluvium and beach- and dune sands underlain by older greenstones, sandstones, and shales (SBCWD 1996; Blake et al. 2000).

The work at Stinson Beach has focused on two distinct areas: the Calles residential district and Stinson Beach Park, Golden Gate National Recreation Area (GGNRA; Fig. 1.1). The Calles district is a waterfront section of the community that was developed in the 1940's. The area is approximately 750m in the alongshore direction by 250m in the cross-shore direction. Residential lot size in the Calles area are generally small and housing is relatively dense, and the areal density of standard gravity leach fields is approximately one leach field per 650 m2 (SBCWD 1998). The high density of septic systems in this area allows for research is which focused on the cumulative effect of dense septic systems on the quality of groundwater and SGD. Adjacent to the Calles area is Stinson Beach Park, a public park administered by Golden Gate National Recreation Area. In the Park, three large systems are relied upon for on-site sewage treatment for both park staff and the throngs of park visitors. Each system is separated and surrounded by undeveloped park property, providing a unique setting for plume-scale research focused on the flux and attenuation of specific contaminants as septic effluent-impacted groundwater flows through the beach toward the ocean.

1.2 DISSERTATION ORGANIZATION AND MOTIVATING QUESTIONS.

This dissertation contains six chapters: this introduction (Chapter 1), four research chapters (Chapters 2-5) and a final chapter that summarizes and reflects upon my findings in the broader context of SGD, coastal pollution and on-site wastewater treatment at the land-sea interface. Each research chapter is written in the format of a peer-reviewed publication with individual abstracts, introductions, methods, results, and conclusions. Chapters 2 and 3 have been published in Limnology and Oceanography and Estuaries and Coasts, respectively. Chapter 5 is in preparation for another peer-reviewed journal, and includes a Supplemental Information contained in Appendix A of this dissertation.

Each of the four research chapters are focused around a number of key motivating questions pertinent to the issue of SGD and coastal septic systems. Often, these motivating questions are addressed by research described in more than one chapter.

Is SGD occurring at Stinson Beach, and if so, what is the magnitude? What are the important forces driving SGD at the site, and on what timescales do they act?

Resolving the magnitude, driving forces, and timing of SGD at Stinson Beach is fundamental to this dissertation, and work in each of the first three chapters addresses these important issues. In Chapter 2, wave- and tide-driven saline SGD is estimated using analytic models, and fresh SGD is estimated using a salinity mass balance approach in the surf zone. Variation in SGD on the neap-spring tidal timescale is investigated and linked to groundwater fluctuations in the beach aquifer on the same timescale. In Chapter 3, SGD is estimated using a coastal water mass balance of radium isotopes, a well-recognized natural tracer of SGD. Correlations between radium tracer activity and wave height, tide stage, and fortnightly tide range are calculated to elucidate the importance of each of these known forcing mechanisms. Results from experiments conducted during the summer and winter seasons are compared to investigate seasonal variability of total SGD. Lastly, Chapter 4 investigates variability of SGD from a simulated beach aquifer forced by annual precipitation and evapotranspiration conditions typically experienced in the Mediterranean climate of central California.

Is SGD an environmentally relevant source of nutrients or microbiological pollution to the coastal environment?

Estimates of SGD-associated fluxes of nutrients and microbial pollution to the coastal ocean at Stinson Beach, and the environmental importance thereof, are explored in Chapters 2, 3, and 5. In Chapter 2, fresh-, saline-, and total (fresh + saline) groundwater discharge-associated nutrient fluxes are calculated in neap and spring tide and compared. To highlight the importance of site groundwater in the local marine ecosystem, fertilization of the ocean by site groundwater is investigated in the lab using mesocosm phytoplankton growth experiments. Chapter 3 calculates SGD and associated nutrient fluxes during two 14-day studies, and compares SGD-associated nutrient flux with that of surface water discharges in the area. Lastly, Chapter 5 documents research focused on measuring the flux of nitrogen, bacteriophage and fecal indicator bacteria associated with a plume of septic effluent in groundwater emanating from a large septic system and flowing through the beach into the subterranean estuary. Nutrient fluxes associated with the plume are compared to previous estimates of SGD-associated nutrient flux from values reported in Chapter 2.

What role do on-site wastewater treatment systems play in contaminating groundwater at the site? Is attenuation in the saturated zone adequate for in-situ treatment septage-derived contamination before discharge to the ocean?

Having documented high concentrations of nutrients and fecal indicator bacteria in Stinson Beach groundwater in Chapters 2 and 3, Chapter 5 focuses on characterization of a single septic system at the site in order to better understand contaminant fate and transport in the coastal groundwater setting. Specifically, the research described in Chapter 4 tests to what degree the treatment system in question is polluting groundwater with respect to nitrogen, FIB, and virus, and estimates rates of attenuation for each contaminant of concern using a combination of field and laboratory methods.

Figure 1.1. Map of the study area showing the locations of Bolinas Lagoon, Webb Creek, Stinson Beach Park (GGNRA), and the residential Calles district of Stinson Beach, California.

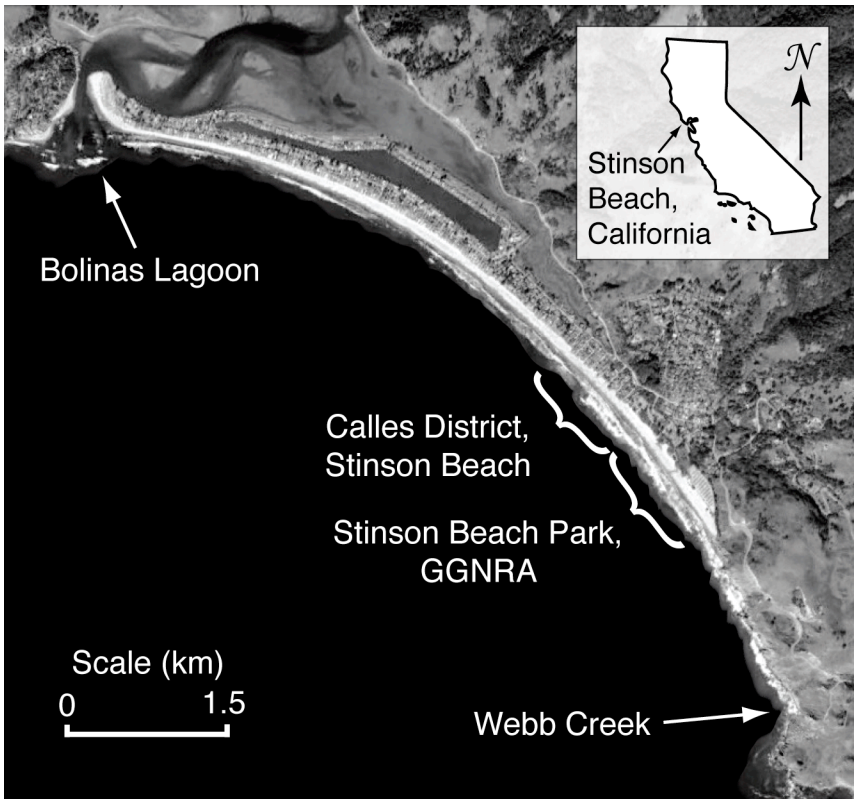

1.3 REFERENCES CITED

Blake, M. C.. Geologic map and map database of parts of Marin, San Francisco, Alameda, Contra Costa, and Sonoma Counties, California. Version 1.0, scale 1:75,000. USGS Miscellaneous field studies no. MF-2337, pub. 2000. OCLC #43723249

Boehm, A. B., G. G. Shellenbarger, and A. Paytan. 2004. Groundwater discharge: Potential association with fecal indicator bacteria in the surf zone. Environ. Sci. Technol. **38**: 3558-3566.

Boehm, A., A. Paytan, G. G. Shellenbarger, and K. A. Davis. 2006. Composition and flux of groundwater from a California beach aquifer: Implications for nutrient supply to the surf zone. Continental Shelf Research **26**: 554-554.

Bone, S. E., M. A. Charette, C. H. Lamborg, and M. E. Gonneea. 2007. Has submarine groundwater discharge been overlooked as a source of mercury to coastal waters? Environ. Sci. Technol. **41**: 3090-3095.

Burnett, W. C., P. K. Aggarwal, A. Aureli, H. Bokuniewicz, J. E. Cable, M. A. Charette, E. Kontar, S. Krupa, K. M. Kulkarni, A. Loveless, W. S. Moore, J. A. Oberdorfer, J. Oliveira, N. Ozyurt, P. Povinec, A. M. G. Privitera, R. Rajar, R. T. Ramessur, J. Scholten, T. Stieglitz, M. Taniguchi, and J. V. Turner. 2006. Quantifying submarine groundwater discharge in the coastal zone via multiple methods. Sci. Total Environ. **367**: 498-543.

California Wastewater Training and Research Center (CWTRC) and U.S. Environmental Protection Agency (EPA), 2003. Status Report: Onsite Wastewater Treatment Systems in California, California State University at Chico.

Census Bureau, United States Department of Commerce. American Housing Survey for the United States - 1995. Issued September 1997.

Johannes, R. E. 1980. Ecological significance of the submarine discharge of groundwater. Mar. Ecol. – Prog. Ser. **3**: 365-373.

Michael, H. A., A. E. Mulligan, and C. F. Harvey. 2005. Seasonal oscillations in water exchange between aquifers and the coastal ocean. Nature. **436**: 1145-1148.

Natural Resources Defense Council (NRDC). 2007. Testing the Waters. NRDC, New York, NY.

Oberdorfer, J. A., M. A. Valentino, and S. V. Smith. 1990. Groundwater contribution to the nutrient budget of Tomales Bay, California. Biodegradation **10**: 199-216.

Reay, W. G. 2004. Septic Tank Impacts on Ground Water Quality and Nearshore Sediment Nutrient Flux. Ground Water **42**: 1079-1089.

Ritter, W.F. 1986. Nutrient budgets for the inland bays. Dover, Delaware: Delaware Department of Natural Resources and Environmental Control Technical Report.

Robertson, W. D., J. A. Cherry, and E. A. Sudicky. 1991. Groundwater contamination from two small septic systems on sand aquifers. Ground Water **29**: 82-92.

Stinson Beach County Water District (SBCWD). 1998. Stinson Beach Hydrologic Survey. www.stinson-beach-cwd.dst.ca.us.

Swartz, C. H., S. Reddy, M. J. Benotti, H. Yin, L. B. Barber, B. J. Brownawell, and R. A. Rudel. 2006. Steroid estrogens, nonylphenol ethoxylate metabolites, and other wastewater contaminants in groundwater affected by a residential septic system on Cape Cod, MA. Environ. Sci. Technol. **40**: 4894-4902.

Taniguchi, M. 2002. Tidal effects on submarine groundwater discharge into the ocean. Geophys. Res. Lett. **29**: 1561.

U.S. Environmental Protection Agency. 2005. Decentralized Wastewater Treatment Systems: A Program Strategy. EPA 832-R-05-002.

Valiela, I., and J. E. Costa. 1988. Eutrophication of Buttermilk Bay, a Cape-Cod Coastal Embayment - Concentrations of Nutrients and Watershed Nutrient Budgets. Environmental Management **12**: 539-553.

CHAPTER 2: SUBMARINE DISCHARGE OF NUTRIENT-ENRICHED FRESH GROUNDWATER AT STINSON BEACH, CALIFORNIA IS ENHANCED DURING NEAP TIDES

The research presented in this chapter was published in 2008 under the above title in the journal *Limnology and Oceanography,* Volume 53, Issue 54, pp. 1434-1445. Coauthors included Kevan Yamahara who contributed enormously in the field, Blythe Layton who conducted the enterococcal surface protein (*esp*) gene analysis, Elizabeth Joyce who assisted with the mesocosm experiments, and Alexandria Boehm. The research was supported by the National Sea Grant College Program of the U.S. Department of Commerce's National Oceanic and Atmospheric Administration under NOAA Grant NA04OAR4170038, Project R/CZ-197, through the California Sea Grant College Program. The views expressed herein do not necessarily reflect the views of California Sea Grant. Eric Foote, Timothy Julian, Daniel Keymer, Holly Michael, Alyson Santoro, Gregory Shellenbarger, Sarah Walters, and Keeney Willis are also acknowledged for assistance in the field and/or suggestions for improving the manuscript. Comments from two anonymous reviewers also improved the manuscript.

2.1 ABSTRACT

The influence of fortnightly spring-neap tidal variability on submarine discharge of fresh and saline groundwater was examined at Stinson Beach, California. Stinson Beach is a residential community that utilizes on-site systems for wastewater disposal. Fresh, shallow groundwater at the site contains high concentrations of nutrients (dissolved inorganic nitrogen (DIN), soluble reactive phosphate (SRP), and silicate), and human fecal bacteria. A groundwater-derived freshening and nutrification of the surf zone during neap tides was observed, followed by a 4-day increase in chlorophyll *a* concentrations. Analytical models and a fresh water budget in the surf zone were used to estimate the saline and fresh discharge of submarine groundwater. We estimate fresh groundwater discharge between 1.2 and 4.7 L min^{-1} m^{-1} shoreline during neap tides compared to 0.1 and 0.5 L min^{-1} m^{-1} during spring tides. This compares to 15.9 and 22.0 L min^{-1} m^{-1} saline groundwater discharge (forced by waves and tides) during neap and spring tides, respectively. Despite the smaller total (fresh + saline) flux of groundwater during neap compared to spring tides, the larger fresh discharge component during neap tides raises surf zone silicate, DIN, and SRP by 14%, 35%, and 27%, respectively, relative to spring tides. This observed fortnightly pulsing of fresh groundwater-derived nutrients was consistent with seaward hydraulic gradients across the fresh part of the beach aquifer, which varied due to aquifer overheight near the beach face. Darcy-Dupuit estimates of seaward fresh groundwater flow in this area agreed well with the fresh discharge results of the mass balance.

2.2 INTRODUCTION

Submarine groundwater discharge (SGD), defined as fresh and saline ground waters discharging along the coastline at the land-sea interface (Burnett et al. 2006), can contribute nutrients, metals, pollutants, and freshwater to the coastal environment (Johannes 1980; Bone et al. 2007). Driving forces of SGD include meteoric hydraulic head, tide- and wave pumping, seasonal evapotranspiration cycles (Michael et al. 2005), and variations in groundwater density. Additional factors influencing the timing and magnitude of SGD include regional geology, climate, and human activities along the coast such as groundwater pumping and artificial recharge. The importance of combinations of factors controlling SGD vary from site to site, and site-specific studies are often required to fully understand SGD in a given region. While a large body of literature has documented the existence and variability of SGD along the world's coastlines (Taniguchi et al. 2002), we are still working to understand the many factors that influence and modulate discharge rates.

Human activities along coasts can influence the quality of SGD (Kroeger et al. 2006). Nutrients emanating from fertilizers applied to residential lawns or agricultural fields may percolate through the vadose zone and increase concentrations in surficial aquifers (Valiela et al. 1992). In some coastal regions, households utilize cesspools or septic systems with leach fields for sewage disposal. These practices can recharge surficial aquifers with freshwater contaminated with pathogens, pharmaceuticals, nitrogen, and phosphorous (Robertson et al. 1991; Scandura and Sobsey 1997; Swartz et al. 2006). A number of studies have investigated SGD in areas where on-site wastewater treatment is prevalent and have shown that SGD can contribute substantial nutrient loads to coastal waters (Giblin and Gaines 1990; Lapointe et al. 1990; Weiskel and Howes 1991). In order to protect human and ecosystem health, it remains important to continually improve our understanding of the magnitude and timing of SGD in areas where septic systems are used for wastewater disposal.

A limited number of studies have documented the importance of spring-neap tides on total SGD (Kim and Hwang 2002; Taniguchi 2002; Boehm et al. 2004) but not on the fresh component of SGD specifically. A single study (Campbell and Bate 1999) has

examined fortnightly variations in fresh SGD. The present study explores the influence of the fortnightly spring-neap tidal cycle on submarine discharge of fresh groundwater from an unconfined, septic effluent-impacted coastal aquifer in Central California. Using a multi-faceted approach that couples analytical models, hydraulic head measurements, and a nearshore freshwater budget, we document a neap tide pulsing of fresh, nutrient-enriched SGD. We link this enhanced neap tide discharge to fortnightly changes in seaward hydraulic gradient across the aquifer induced by aquifer overheight – the buildup or mounding of the water table near the land-sea interface as a result of tidal variation, wave set-up, and wave run-up (Nielsen 1990; Turner et al. 1997; Horn 2002) – near the beach face. Using field data and a controlled mesocosm experiment, we explore the potential role of nutrient-enriched groundwater in causing increases of chlorophyll *a* in the coastal ocean at the site.

2.3 METHODS AND MATERIALS

2.3.1 STUDY SITE.

Field work was conducted from 14 through 28 July 2006 to characterize SGD from the unconfined aquifer over a spring-neap cycle at Stinson Beach, a small residential community 30 km north of San Francisco, California (37° 53' 58.387", 122° 38' 45.384", Fig. 2.1). The beach is an open ocean, southwest facing, reflective beach with mixed semi-diurnal tides, a spring tide range of 2.4 m, typical breaker heights of 0.5-1.5 m, and a high energy surf zone. During the study, neap tide (17 July) preceded the spring tide (24 July).

The climate is Mediterranean with 60 to 120 cm of annual average rainfall occurring predominately between October and April (SBCWD 1998). During the dry season, Bolinas Lagoon (37° 54' 24.811" N, 122° 40' 54.732" W), a tidally influenced lagoon, and Webb Creek (37° 53' 7.332" N, 122° 37' 43.392" W), a nearby freshwater stream, are the only potential sources of fresh surface water to the near-shore marine environment within 7 km of Stinson Beach. There had been no precipitation in the watershed for approximately 2 months at the onset of the study, and no rainfall occurred during the study (data not shown). Easkoot creek, a seasonal groundwater-fed creek, runs

parallel to the shoreline through the field site approximately 200 m from the shoreline (Fig. 2.1). The creek discharges to Bolinas Lagoon and contains very little freshwater during the dry season.

Human development occupies 5% of the 29.3 km^2 Stinson Beach watershed and is primarily contained within 100 m of the coastline (GIS analysis not shown). Households use on-site septic systems and holding tanks exclusively for wastewater disposal. The areal density of standard gravity leach fields in the study area is approximately one leach field per 650 m^2 (SBCWD 1998).

The unconfined aquifer in the experimental area is composed primarily of beach and dune sands (Fig. 2.1, SBCWD 1998). At the beachhead, the sands are underlain by lacustrian clay at a depth of approximately 32 m below mean sea level (Bergquist 1978). The unit overlies the Franciscan Complex, an assemblage of highly fractured sandstone, limestone, and shale (SBCWD 1998).

In systems with a high-energy surf zone, such as Stinson Beach, direct measurement of discharge with seepage meters is not possible (Libelo and MacIntyre 1994; Burnett et al. 2006). Breaking waves dislodge seepage meters and strong currents can induce flow through the seabed when passing over the objects (Huettel et al. 1996). This presents a unique challenge in the measurement of SGD in high-surf areas, and may explain the paucity of studies conducted on high-energy, open ocean coastlines in California and elsewhere. At Stinson Beach, we estimate SGD by combining three indirect methods: measurements of hydraulic head and Darcy-Dupuit calculations, a freshwater budget in the surf zone, and analytical models.

2.3.2 HYDRAULIC HEAD MEASUREMENTS.

Three permanent long-screen monitoring wells (MW06, MW07, and MW09) and two temporary piezometers (MW10 and MW11) were installed into the beach to create a cross-shore array (Fig. 2.1). Well construction details are shown in Table 2.1. Beach topography and well elevations were surveyed relative to mean sea level (MSL). Measurements of hydraulic head were recorded in each well at 1 min intervals using pressure transducers (Solinst, Ontario, Canada). The <1% of head measurements known to be misrepresentative of true aquifer conditions (hydraulic recovery after well

installation and sampling) were removed and estimated by interpolation. All head measurements presented herein are presented as equivalent freshwater head. In the fresh part of the aquifer where hydraulic gradients are shallow (MW06 to MW09), the Dupuit assumptions are made. Namely, we assume that the hydraulic gradient is equal to the slope of the water table, and streamlines are horizontal and equipotential lines are vertical (Fetter 2001). Fortnightly average hydraulic heads at each well were calculated from head measurements collected during the entire experiment. Neap- and spring tide head measurements were calculated by averaging measurements taken during the lunar day following the quarter (17 July) and new (24 July) moons, respectively.

2.3.3 WATER SAMPLING.

At the low-low and high-high tide approximately every other day (n= 42 and 32, respectively), surf zone samples were collected at ankle and waist depths (0.2 and 0.7 m, respectively) along two cross-shore transects extending from the water line out into the surf zone adjacent to the well network (Fig. 2.1). Transects were approximately 100 m apart in the alongshore direction. At low-low tides only, the groundwater immediately adjacent to the water line was characterized by sampling from shallow pits dug into the beach approximately 10 m back from the water line (n=19). In addition, subaerial seepage faces were sampled when they developed at the lowest tides (n=17). Groundwater was sampled from the five wells approximately every seven days ($2 \leq n \leq 5$ for each well). Surface offshore ocean water samples were obtained 180 m, 870 m, and 1615 m from the shore in a cross shore transect from our sampling site on the days of the 3rd-quarter and new moons (n=2 for each offshore location). The ebb flow from Bolinas Lagoon was sampled approximately every four days (n=4). In all cases, clean, triple-rinsed 20 L collapsible low-density polyethylene containers were used for water collection. A total of 100 L for ocean and lagoon samples and 20-80 L for groundwater samples were composited. A 1 L subsample from large volume samples was collected in clean triple-rinsed bottles and used for all chemical and biological analyses.

Tide elevation measurements were obtained from a NOAA tide gage at Point Reyes, approximately 30 km from Stinson Beach (http://tidesandcurrents.noaa.gov,

Station ID 9415020, 37°59'48.12" N, 122°58'30" W). Data were recorded at six-minute intervals. Daily tidal range was calculated from daily maxima and minima.

2.3.4 Sand analysis for hydraulic conductivity (Kh) determination.

A 2 m continuous core was collected near monitoring well MW09, homogenized, and analyzed for grain size distribution using American Society for Testing and Materials (ASTM) standard C136. Hydraulic conductivity (K_h) was estimated from grain size distribution using the method of Hazen (1911).

2.3.5 Salinity, dissolved oxygen, and nutrient analysis.

Salinity and dissolved oxygen were measured in situ using a hand-held probe (Hydrolab, Loveland, CO). Salinity is reported according to the unitless Practical Salinity Scale and is accurate to ±0.01. A 30-mL aliquot of each sample was filtered with 0.45 µm pore size filter and stored at -20°C for nutrient analyses. The concentrations of soluble reactive phosphate (SRP), silicate, nitrate, nitrite, and ammonia were measured by standard methods with a nutrient autoanalyzer (Lachat QuikChem 8000, Loveland, CO). Samples were diluted as necessary to be within the machine's detection limits for each nutrient. Concentrations reported herein reflect both the required sample dilution and the precision of the analytical method. Dissolved inorganic nitrogen (DIN) was determined by adding molar concentrations of nitrogen species. Five percent of nutrient samples were analyzed in duplicate.

2.3.6 Chlorophyll a analysis.

Waist-deep seawater samples were analyzed in duplicate for chlorophyll *a* (Chl *a*) using a modified version of EPA method 445.0 (Arar and Collins 1997). Samples were filtered immediately after collection through Whatman GF/F glass filters and stored at -80°C. Samples were analyzed approximately seven months after collection, longer than the EPA suggested holding time of three weeks. We assume that negative effects related to holding time are distributed equally across all samples, allowing intra-study comparison. During analysis, filters were added to 10 mL 90% acetone in water, shaken vigorously for 60 seconds, and steeped at 4°C for 18 to 24 h. Samples were then centrifuged and the supernatant was analyzed on a fluorometer (Turner Designs,

Sunnyvale, California), acidified, and reanalyzed, as specified in the EPA method. The precision, based on analysis of duplicates, is 5%.

2.3.7 MESOCOSM EXPERIMENTS.

Experiments were conducted to assess whether the addition of fresh groundwater to seawater promoted increases in Chl *a.* Stinson Beach seawater, collected from within the surf zone, was filtered through a 250 μm sieve to remove large zooplankton grazers (Pederson and Borum 1996). Groundwater from MW09 was 0.2 μm filtered to remove particulates. Filtered groundwater was added to sieved seawater to final concentrations (v/v) of 0%, 4%, and 8%. Mesocosms were run in duplicate in 3.5 L clear plastic bottles. Bottles were spaced evenly under constant fluorescent light with illuminance 200 lm m^{-2} and incubated at 15°C for 2 d. Samples were collected and analyzed every 4 to 8 h via EPA Method 445.0 for in vivo fluorescence. A subset of samples were also analyzed for in vitro Chl *a* by the same method. A best-fit curve was used to estimate the concentrations of Chl *a* from in vivo fluorescence for those samples where only fluorescence had been measured. No more than 10% of bottle volumes was removed over the course of the experiment. Data collected on the final day of the experiment were averaged for determining final Chl *a* concentrations.

2.3.8 FECAL INDICATOR BACTERIA ANALYSIS.

Water samples were analyzed for fecal indicator bacteria to determine the degree of contamination by human waste. Fifty mL of each sample were collected in a sterile container, and immediately stored on ice. *Escherichia coli* (EC) and enterococci (ENT) were quantified from 10 mL of water diluted with 90 mL of Butterfield buffer (Weber Scientific, Hamilton, NJ) using Colilert-24 and Enterolert (IDEXX, Westbrook, ME), respectively, within 6 h of collection. Tests were implemented in a 97-well format following manufacturer's direction and allowed for the detection of EC and ENT concentrations between 10 and 24,192 most probable number (MPN) $(100\ mL)^{-1}$. Note that the units MPN $(100\ mL)^{-1}$ are the standard units for reporting indicator bacteria concentrations in water. No duplicate samples were analyzed.

2.3.9 ENTEROCOCCAL SURFACE PROTEIN (ESP) GENE ANALYSIS.

A subset of ENT-positive samples were analyzed for the enterococcal surface protein (*esp*) gene, a putative human-specific marker in ENT (Scott et al. 2005). Media from positive IDEXX wells was removed using a 21 1/2 gauge needle and syringe, and pooled for each sample. One mL of pooled media was enriched in trypic soy broth for 4 to 6 h at 41°C. Deoxyribonucleic acids (DNAs) were extracted from a 1 mL aliquot of enrichment using QIAamp DNA Mini Kit (Qiagen, Valencia, California). Polymerase chain reactions (PCRs) containing 3 µL template were run using the conditions, primers, and buffers described by Scott et al. (2005), except we used Platinum Taq (Invitrogen, Eugene, Oregon). PCR products were run on a 1.5% agarose gel and stained with SYBR Gold (Invitrogen, Eugene, Oregon). Positive and negative PCR and extraction controls were run in conjunction with unknowns.

2.3.10 DATA ANALYSIS.

Pearson correlation coefficients (r_p) between measured parameters were determined using SPSS (Chicago, IL). Groups of data were compared using Student's t-test. Correlations were deemed significant if $p<0.05$.

2.3.11 FLUX CALCULATIONS.

Total SGD (D) can be expressed as $D = D_t + D_w + D_m + D_s + D_d$ (modified from Li et al. 1999) where D_t and D_w represent saline outflow from tidal- and wave-driven circulation of seawater through the beach aquifer, respectively, D_m represents SGD of meteoric and artificially recharged fresh groundwater, D_s represents saline SGD forced by the seasonal recharge-evapotranspiration cycle (Michael et al. 2005), and D_d represents the outflow of density-driven saline waters. We will not consider contributions from D_s or D_d in our estimates for D, and the reasons for and implications of these omissions will be discussed.

The outflow seepage rate driven by wave set up per unit alongshore distance, $D_{w,}$ can be expressed as follows (Longuet-Higgins 1983):

$$D_W = K_h S_W L \tag{2.1}$$

where K_h is hydraulic conductivity of the beach aquifer media, S_w is the slope of the wave setup, and L is the surf zone width defined as the distance between the breaker line and the wave runup line. Expressions for S_w and L can be calculated from the local oceanographic and geologic conditions including breaker height H_b, beach slope S_b, and wave period T_w (Li et al. 1999).

Li et. al. (1999) used Nielsen's solution predicting the height of the water table with time in response to tidal forcing to estimate the tidally driven groundwater outflow seepage rate per alongshore distance (D_t). The resulting discharge rate is tidally averaged, implies quasi-steady-state conditions and should be viewed as a first-order approximation. Following Nielsen (1990, Eq. 31) and Li et. al. (1999),

$$D_t = \frac{n_e A}{\kappa T_t}\exp(-\alpha)\big(\cos(\alpha)-\sin(\alpha)\big) + \frac{\sqrt{2}n_e A^2}{s_b T_t}\exp(-\sqrt{2}\alpha)\cos(\sqrt{2}\alpha) + \frac{n_e A^2}{s_b T_t} \qquad (2.2a)$$

with

$$\kappa = \sqrt{\frac{n_e \omega}{2K_h H}} \qquad (2.2b)$$

and

$$\alpha = \frac{\kappa A}{s_b} \qquad (2.2c)$$

In Equation 2.2a-c, A corresponds to the tidal amplitude, T_t the tidal period, ω the tidal frequency, n_e the effective porosity of the beach sand, and H the aquifer thickness.

Input parameters required for calculating D_w and D_t at our study site are as follows. Beach slope was calculated from surveyed beach topography (s_b=0.0378). Tidal amplitude (A) was set to 0.80 m and 1.12 m for neap and spring tides, respectively. The tidal period (T_t=12.42 h) and frequency (ω=1.41x10^{-4} rad s^{-1}) of the M_2 harmonic were

used. During the study, the period of the dominant swell (T_w) was 9.6 s (http://cdip.ucsd.edu, Station ID 029). Breaking wave heights (H_b) were approximately constant during the study and estimated to be 0.8 m from observations in the field. Porosity was estimated to be 0.4 by displacement of a known volume of sediment in water in a volumetric flask; all porosity was assumed to be effective porosity (n_e). The hydraulic conductivity (K_h) of the sand was measured in the lab with aquifer material and determined to be 3.85 x10^{-4} m s^{-1}, as described earlier. The unconfined aquifer thickness H was estimated to be 34 m from cores collected in the area, with an aquifer base approximately 32 m below sea level (Bergquist 1978; SBCWD 1998).

A mass-balance was applied to the surf zone to calculate D_m at neap and spring tides using salinity as a tracer (Fig. 2.2). The surf zone adjacent to the well network was treated as a triangular prism with alongshore length (L) 300 m (typical distance between rip currents) and a right triangular cross shore section of width 20 m (distance from shoreline to just beyond breakers) and offshore depth $20s_b$ (0.76 m). The salinity in the prism (S_{prism}) was determined for neap and spring tides by averaging all surf zone samples collected during the two lunar days before and after the quarter and new moons, respectively (two transects, both ankle and waist measurements, n=16 and n=32 for neap and spring tide, respectively). Although salinity measurements did not extend past 10 m in the offshore direction, surf zones are typically well-mixed (Inman et al. 1971), so the calculated average salinity applied to the entire 20 m wide prism. Water samples collected at 1615 m offshore on the days of the 3rd-quarter and new moons, which were the most saline and also the furthest from shore, were chosen as the offshore end member salinities ($S_{offshore}$). A salinity of 0 was assigned to the fresh groundwater end member. The following equation was used to estimate D_m per unit length of shoreline:

$$D_m = \frac{(S_{offshore} - S_{prism})V_{prism}}{S_{offshore} L \tau} \tag{2.3}$$

where D_m is meteoric water flux in units of volume per time per unit length of beach, τ is the cross shore residence time of water in the rip cell, L is the length of the shoreline of the prism (a single rip cell), V_{prism} is the volume of the prism, and S_{prism} and $S_{offshore}$ were

defined previously. Following Boehm et al. (2004), we estimate the cross shore residence time of water in a rip cell to be 1 to 4 h. Eq. 3 assumes that D_m is small compared to the input of offshore waters into the surf zone via breaking waves (Fig. 2.2), and thus does not affect the water balance.

Estimation of fresh groundwater discharge across the land/sea interface is complicated by variations in fluid density, the existence of a seepage face, and the effects of tidal pumping. Our monitoring network is not as dense as would be needed for direct, accurate calculation of fresh and saline groundwater flux through the interface using Darcy's Law. However, insight into the rate of fresh groundwater flow toward the land/sea interface, and thus the potential variation in freshwater discharge to the sea between neap- and spring tides, can be provided by calculating groundwater flow through a landward section of unconfined aquifer using Darcy's Law and the Dupuit assumptions (given previously), which are combined in the Dupuit equation (Fetter 2001):

$$Q' = -\frac{1}{2} K_h \left(\frac{h_1^2 - h_2^2}{Y} \right) \tag{2.4}$$

In Eq. 4, Q' is the flow per unit length of shoreline, K_h has been defined previously, and h_1 and h_2 are the saturated thicknesses at a distance Y apart. Flow was calculated between MW07 and MW09, the two furthest inland monitoring wells in the network installed in the unconfined aquifer, which are 178 and 70 m from the mean water line, respectively. The nature of the boundary between the unconfined aquifer and the highly fractured Franciscan Complex basement rock is uncertain, and for the purpose of this estimate we assume that the lacustrian clay at 32 m below MSL extends underneath the unconfined aquifer through this area, and that groundwater is fresh throughout the section. The flow through the landward part of the aquifer may not be exactly equal to D_m. Rather, since short-period (diurnal) tidal effects on head are small at MW07 and MW09 relative to effects of long-period (fortnightly) tides (data not shown), this flow rate can be thought of as the fresh groundwater entering the tidally pumped zone where density effects and

vertical flow become important. It can also be considered a check on the mass balance-based estimates of D_m.

The "potential flux" (F_p) of nutrients to the surf zone via SGD was calculated as follows:

$$F_p = C_{fresh} D_m + C_{sal}(D_t + D_w) \tag{2.5}$$

where C_{fresh} and C_{sal} represent the end member constituent concentrations in fresh and saline groundwaters, respectively. C_{fresh} and C_{sal} were estimated with mixing diagrams of salinity versus nutrient for all groundwater samples (wells, pits, and subaerial seeps, n=55), which were fit with a linear regression. The regression equation was extrapolated to fresh (0) and average offshore marine salinity (32.12) to determine C_{fresh} and $C_{sal,}$, respectively . Multiplying groundwater end-member concentrations by SGD rates, as in Eq. 5, is a common method for estimating nutrient fluxes to the coastal ocean via SGD (Charette et al. 2001; Hwang et al. 2005; Hays and Ullman 2007). However, the method assumes that the nutrient of interest behaves conservatively as it travels through the subsurface from aquifer to sea. In fact, sorption of SRP in groundwater systems is common (Slomp and Van Cappellen 2004) and the potential for nitrification and denitrification in the subterranean estuary has been demonstrated (Santoro et al. 2006; Santoro et al. 2008). Therefore, Eq. 5 should be considered a first-order approximation of the true flux of nutrients.

We used the calculated nutrient discharge values (F_p) to examine if observed changes surf zone nutrient concentrations could be attributable to SGD. The following expression which includes mass fluxes from all SGD components, excluding D_s and D_d, was used to predict the equilibrium concentration of DIN, SRP, and silicate in the surf zone, C_{prism}, under spring and neap tidal conditions:

$$C_{prism} = \left[C_{fresh} D_m + C_{sal}(D_w + D_t) + C_{offshore}\left(V_{prism}/\tau - D_m - D_w - D_t\right)\right](\tau / V_{prism}) \tag{2.6}$$

D_m estimated from the freshwater budget was used. Surf zone residence times (τ) of 1 and 4 h were used. We then determined the predicted percent change of each constituent in

the surf zone during neap relative to spring tides and compared this to the constituent's actual change.

2.4 RESULTS

2.4.1 GROUNDWATER AND COASTAL OCEAN WATER QUALITY.

The fresh groundwater in the unconfined aquifer at Stinson Beach contains high concentrations of fecal indicator bacteria, silicate, DIN, and SRP (Table 2.2). The presence of the *esp* gene in a subset of groundwater samples is consistent with their being impacted by septic discharge (Table 2.2). A nutrient- and fecal indicator bacteria-rich freshwater signature dissipates from inland wells (MW06, MW07, MW09) through the brackish mixing zone (MW10, MW11, pits and subaerial seeps) to the open ocean (surf zone- and offshore samples). Fresh groundwater has, at most, 10, 130, 10, and 2500 times higher silicate, DIN, SRP, and fecal indicator bacteria, respectively compared to surf zone waters.

Tide range was positively correlated to salinity in the surf zone (Fig. 2.3, r_p=0.81, p<0.01) indicating a freshening of the surf zone during the neap tide. Tide range was negatively correlated to silicate, DIN, and SRP in the surf zone (Fig. 2.3, $-0.71 \leq r_p \leq -0.57$, p<0.01, respectively) indicating nutrient enrichment in the surf zone during neap tides. Silicate, nitrate, DIN, and SRP concentrations were significantly negatively correlated to salinity (Fig. 2.3, $-0.73 \leq r_p \leq -0.49$, p<0.01) supporting the idea that the freshening of the surf zone is caused by input of nutrient-enriched fresh waters and not by other large-scale saltwater nutrient sources, such as upwelling, which can act on similar timescales.

The fresh component of discharges from Bolinas Lagoon and Webb Creek had little or no effect on the salinity in the surf zone at the experimental site. The salinity measurements taken during Bolinas Lagoon ebb flow were marine and were not significantly different (p>0.05) than salinities in the surf zone at the study site. An 800 m alongshore transect of ankle-depth surf zone samples extending from the study site toward Webb Creek indicated that salinity was not decreasing with distance toward the creek (data not shown), indicating the creek's freshwater plume does not substantially

influence salinity of the surf zone at our site. Given these observations, we attribute the freshening of the surf zone during neap tides to discharge of fresh groundwater across the land-sea interface, and the corresponding nutrient increase a consequence of discharge of fresh groundwater to the coastal ocean from the surficial aquifer.

Chl *a* concentrations in the surf zone increased substantially following the 3rd-quarter moon. A least-squares regression of all Chl *a* measurements from 17 July (3rd-quarter moon) to 21 July with time (r_p=0.86, p<0.05) indicates an increase of over 1 µg L^{-1} day^{-1}.

Fecal indicator bacteria densities in the surf zone did not correlate significantly to salinity (r_p= 0.16, p=0.17 for EC, and r_p = 0.03, p=0.79 for ENT) or tide range (r_p= 0.17, p=0.13 for EC, and r_p = 0.01, p=0.97 for ENT). Despite the high concentrations of fecal indicator bacteria observed in fresh groundwater, they do not appear to be discharged with the fresh, nutrient-rich groundwater, indicating they may be filtered as groundwater moves through the sand (Hijnen et al. 2005; Bolster et al. 2006).

2.4.2 MESOCOSM EXPERIMENT.

Average Chl *a* with 95% confidence intervals at the start of the experiment (day 0, n=4) and on the final day of the experiment (day 2, n=16) are shown in Fig. 2.4. After incubation for two days, Chl *a* concentrations in bottles containing 4% and 8% groundwater exhibit significant (p<0.001 in each case) increases relative to the seawater control. This experiment illustrates that a dissolved constituent present in the fresh groundwater at Stinson Beach, or a combination thereof, promotes the growth of phytoplankton in seawater when light and temperature are held constant.

2.4.3 HYDRAULIC HEAD MEASUREMENTS.

The head varied over a smaller range at the most inland wells compared to the wells closer to the sea (Table 2.3). The average hydraulic head over the fortnight at the well farthest from the sea, MW06, the only well installed into the bedrock at the landward boundary the surficial beach aquifer, was higher than average heads at other wells installed into the beach aquifer (Table 2.3). This indicates that there was net flow from the bedrock to the surficial aquifer and out toward the sea, assuming a hydraulic connection. At the inland side of the unconfined aquifer, the hydraulic head in wells

MW06 and MW07 was approximately 1 cm above the fortnight average during the neap tide and 4 cm below the fortnight average during the spring tide (Table 2.3). The reduction in head from neap to spring tide at these wells may be attributed to lagged response to low-frequency tidal constituents (Li et al. 2000; Raubenheimer et al. 1999), and/or to the slow seasonal dropping of the water table during the summer months due to discharge and evapotranspiration. Changes to hydraulic head at the seaward side of the aquifer had an opposite and more substantial fortnightly trend. Neap tide average heads at wells MW09, MW10, and MW11 were 5, 19, and 4 cm below the fortnight averages, respectively, while spring tide heads at the same wells were 2, 10, and 6 cm, respectively, above the fortnight averages (Table 2.3). This illustrates an increase in aquifer overheight, or mounding of water at the land-sea interface during spring relative to neap tides.

2.4.4 SGD ESTIMATES.

Based on the freshwater budget in the surf zone, D_m varies from between 1.2 and 4.7 L min^{-1} m^{-1} of shoreline at neap tide to between 0.1 and 0.5 L min^{-1} m^{-1} at spring tide (range reported for 1 and 4 h residence times, Table 2.4). By comparison, estimates of discharge, based on measurements in the fresh part of the aquifer, using the Dupuit equation are 1.2 L min^{-1} m^{-1} (neap tide) and 0.1 L min^{-1} m^{-1} (spring tide). Thus, agreement is excellent between the Dupuit freshwater discharge calculations and the mass balance estimates of D_m calculated with a 4 h residence time.

We calculate that D_w= 7.2 L min^{-1} m^{-1} of shoreline (constant throughout study) and D_t= 8.7 (neap) and 14.8 (spring) L min^{-1} m^{-1} shoreline, respectively (Table 2.4). The sum of these estimates shows that total SGD (D) during spring tides (D_{spring}) is greater than SGD during neap tides (D_{neap}), which is consistent with results from other studies in unconfined aquifers, including those done with seepage meters (Kim and Hwang 2002; Taniguchi 2002; Boehm et al. 2004). Assuming a 1-hour residence time, 2.2% of D_{spring} is fresh groundwater while 22.8% of D_{neap} is fresh groundwater, or 0.5% versus 7.0%, respectively, assuming a 4-hour residence time (Table 2.4).

2.5 DISCUSSION

Fortnightly trends in surf zone nutrients and salinity at Stinson Beach can be linked to changes in the meteoric (fresh) component of total SGD, which in this environment appears to be controlled by tide- and wave-driven aquifer overheight in the unconfined beach aquifer. Increased fresh groundwater discharge at neap tide corresponded with a drop in aquifer overheight at the land-sea boundary and a steepening of the seaward hydraulic gradient in the fresh part of the aquifer. Similarly, increased aquifer overheight near the beach face during spring tide corresponded with a shallowing of the hydraulic gradient in the fresh part of the aquifer, and reduced fresh groundwater discharge to the coastal ocean. Fresh groundwater at the field site is substantially enriched in nutrients, thus the freshening of the surf zone during neap tide is accompanied by nutrification of the surf zone.

The discovery of fecal indicator bacteria and *esp*-positive ENT in monitoring wells at the site suggests that high nutrient concentrations in fresh groundwater are due at least in part to contamination by septic effluent. This is not surprising given the high density of septic systems at the field site. Our field observations indicate that nutrients from fresh groundwater can be transported from the land to the sea through the subsurface, impacting coastal water quality. Interestingly, increased surf zone concentrations of groundwater-derived nutrients were not associated with an increase in fecal indictor bacteria concentrations, although fresh groundwater at the site is enriched with these organisms. This indicates attenuation of bacteria in the unconfined beach aquifer at Stinson Beach is efficient. Future work will concentrate on quantifying attenuation rates of effluent-derived fecal indicator bacteria, pathogens – in particular viruses, and nutrients in individual septage plumes at the site.

During the four days following the nutrient pulse that occurred at neap tide at Stinson Beach, Chl *a* concentrations in the surf zone increased from approximately 2 µg L^{-1} to 6 µg L^{-1}. Numerous studies have implicated SGD in causing algal blooms in the coastal ocean (LaRoche et al. 1997; Hwang et al. 2005*a*; Hwang et al. 2005*b*), with some specifically linking SGD-derived nutrient inputs from septic systems to growth of algae in canals and coastal watersheds (Lapointe et al. 1990; Valiela et al. 1992; Charette et al. 2001). The mesocosm experiments illustrated that the addition of nutrient-rich fresh

groundwater from well MW09 (average nutrient concentrations in Table 2.2) to seawater promoted significant increases in Chl *a* relative to a control with no addition. While we are unable to definitively conclude that nutrification of the coastal ocean by fresh SGD during the neap tide caused the increase in Chl *a* in the coastal ocean soon thereafter, our field observations and mesocosm experimental results are consistent with this linkage. Other possible causes of the increased Chl *a* in the surf zone include changes in resuspension of benthic diatoms (Demers et al. 1987), turbidity (May et al. 2003), water column stability and light penetration (Comeau et al. 1995), and upwelling (Labiosa and Arrigo 2003).

For the purposes of testing whether the observed changes in nutrient concentrations in the surf zone could have been caused by the estimated changes to SGD across the fortnight, theoretical spring- and neap tide nutrient concentrations (C_{prism}) were estimated using the calculated potential nutrient fluxes (Eq. 5). Based on groundwater mixing diagrams of salinity versus nutrient concentration, groundwater end member nutrient concentrations were 422 μmol L^{-1} silicate, 208 μmol L^{-1} DIN, and 13 μmol L^{-1} SRP for fresh groundwater, and 113 μmol L^{-1} silicate, 44 μmol L^{-1} DIN, and 2.5 μmol L^{-1} SRP for saline groundwater (mixing diagrams not shown). Using these end members with the corresponding discharge estimates, the potential flux F_p ranges from 2303 to 3780 μmol min^{-1} m^{-1} silicate, 949 to 1677 μmol min^{-1} m^{-1} DIN, and 55 to 101 μmol min^{-1} m^{-1} SRP, depending on residence time and tidal condition (spring vs. neap) (Table 2.4). Variation in F_p between neap and spring tides is due to the different proportions of D_m and D_t in total SGD (D).

Using F_p, we calculated C_{prism}, the theoretical concentration of nutrients in the surf zone during neap and spring tides. For each nutrient constituent C_{prism} is greater than the actual measured concentration in the surf zone during both tidal conditions (Table 2.4). This is not surprising given that nutrients do not behave conservatively in the subsurface, while our calculation of F_p assumes they do. However, comparisons of the projected change in C_{prism} between spring and neap tides to the actual change in surf zone concentrations agreed reasonably well assuming a 1 h residence time: C_{prism} increases 18% (silicate), 20% (DIN), and 37% (SRP) during neap relative to spring tides, as compared to the measured increases of 14% silicate, 35% DIN, and 27% SRP. Thus, it

appears that if we use the low-end residence time estimate, the fortnightly changes in the flux of fresh and saline groundwater from the beach aquifer to the coastal ocean can account for an increase in surf zone concentrations of nutrients during neap tides. If the residence time is instead 4 h, then our model predicts higher nutrient concentrations during spring compared to neap tides presumably due to increased saline discharge at spring tide. This is counter to our observations, and may indicate that the nutrient flux attributed to the saline groundwater discharge is overestimated by our model.

Neither the seasonal component D_s nor the density-driven component D_d were included in flux calculations. Seepage metering was instrumental in investigating D_s at a low wave-energy field site at Waquoit Bay, Massachusetts (Michael et al. 2005). In systems with a high-energy surf zone such as Stinson Beach, seepage metering is problematic if not impossible (Libelo and MacIntyre 1994; Burnett et al. 2007), and for this reason D_s was not included in our estimate of D. However, since it oscillates on a yearly timescale, we can assume that D_s would have been approximately constant across the 14 d study. We contend that had D_s been included our formulation of D, the percentages fresh SGD of total reported above would be reduced but the relative differences, and our general conclusions, would remain the same. The variability and role of D_d at Stinson Beach is uncertain, but we suggest that because the fresh groundwater at the site is so substantially enriched in nutrients relative to the saltwater end members, the nutrification effects attributed to D_d variability would be small compared to those attributed by the large changes in fresh groundwater flux across the fortnight.

To ground-truth our discharge results, it is useful to compare them with those made in similar environments. At Tomales Bay, a 21 km long embayment along the San Andreas Fault approximately 27 km to the northwest of Stinson Beach, Oberdorfer et al. (1990) estimated D_m using both Darcy's Law and a soil moisture budget approach. Saline discharge was not investigated. D_m estimates for the two methods were 6.6×10^3 m^3 day^{-1} and 25.3×10^3 m^3 day^{-1}, respectively, or 0.12 L min^{-1} m^{-1} and 0.44 L min^{-1} m^{-1} given the approximate length of shoreline along the bay (40 km). During a multi-day experiment, Mulligan and Charette (2006) used Darcy's Law and radon-based methods estimated fresh discharge to Waquoit Bay, Massachusetts, at 2.8 L min^{-1} m^{-1} and 3.9 L min^{-1} m^{-1},

respectively. Kroeger et al. (2007) used Darcy's Law and a water budget to estimate fresh SGD from the Pinellas Peninsula in Tampa Bay, Florida. D_m was estimated at 2.0 L min^{-1} m^{-1} and 0.8 L min^{-1} m^{-1} using the two methods, respectively. Hays and Ullman (2007) dammed subaerial seepage faces which developed during 16 spring tide monitoring events across an 18-month period at Cape Henlopen, Delaware, and measured D_m directly with a weir. They calculated annual average D_m during the study of 0.9 +/- 0.4 L min^{-1} m^{-1}. The range of D_m presented in our study is consistent with the values reported above.

SGD field studies have specifically investigated neap-spring tidal forcing of SGD. Taniguchi (2002) used seepage meters in Osaka Bay, Japan, and found that total SGD increased from neap to spring tide. At a monitoring station in Korea's Yellow Sea, Kim and Hwang (2002) found that groundwater-derived ^{222}Rn and CH_4 concentrations near the sea floor increased sharply from neap to spring tide. Boehm et al. (2004) also found an increase in total SGD between neap and spring tides using radium isotopes as tracers. In all three cases, the results indicate a greater total discharge during spring tide relative to neap tide, and are consistent with the results presented herein. The only study that examined spring-neap variation in fresh SGD specifically, was conducted in South Africa. Campbell and Bate (1999) used a Darcy's Law approach to quantify the flux of fresh groundwater from a South African sand dune complex, and estimated D_m to be 0.11 L min^{-1} m^{-1} during spring tide and 0.23 L min^{-1} m^{-1} during neap tide. The increase in neap tide D_m versus spring tide D_m is also consistent with the results presented here.

The precise physical explanation of the neap tide pulsing phenomenon is unknown, though two numerical experiments have been conducted to examine D_m and D_t at a hypothetical beach under varying tidal amplitude scenarios and no wave action (Ataie-Ashtiani et al. 2001; Robinson et al. 2007), both of which offer some insights.

Ataie-Ashtiani et al. (2001) simulated constant-density steady-state D_m and D_t from a thin isotropic aquifer with a constant-head landward boundary under zero, low-, and high-tidal amplitude scenarios. They showed that increasing tidal range (as would be expected during spring tides) increased both D_t and aquifer overheight at the boundary, and decreased D_m. Despite differences between the simulated and Stinson Beach environments, the results of the simulation are consistent with the results of our study.

Robinson et al. (2007) simulated variable-density steady-state D_m and D_t from a thick isotropic aquifer with a constant-flux fresh landward boundary and multiple tidal ranges. They showed that a saline tidally-driven circulation cell develops approximately between the high and low tide lines. Under certain conditions, a freshwater 'tube' discharges seaward of the tidal circulation cell near the low tide line. As tidal amplitude is increased, the depth and width of the saline circulation cell increase and the freshwater 'tube' is forced to flow deeper in the aquifer and discharge further offshore. It is possible that during our study, fresh groundwater discharged to the surf zone at neap tide but discharged beyond the surf zone at spring tide, thereby producing a freshening of the surf zone at neap tide. While we cannot rule out this possibility, no data collected at the site to date indicate a freshening of nearshore waters beyond the surf zone during spring tides (Table 2.2, additional data not shown).

Given the results described here, we present a qualitative framework for understanding the relationship between tide- and wave-driven overheight and the magnitude and timing of freshwater discharge from unconfined beach aquifers similar to that at our field site (Fig. 2.5). We introduce two variables, H_{fresh} and O_{saline}, where H_{fresh} is the hydraulic head in the fresh portion of the aquifer and O_{saline} is the hydraulic head due to overheight in the saline portion of the aquifer near the beach face. The magnitude of O_{saline} is controlled by a number of factors including wave set-up, wave run-up, tidal height, and meteoric hydraulic pressure. H_{fresh} is measured just beyond the influence of tides and waves and, thus, controlled entirely by meteoric hydraulic head.

In Fig. 2.5, O_{saline} (horizontal axis) is plotted against H_{fresh} (vertical axis). The dashed, horizontal lines represent neap (N) and spring (S) tide conditions at hypothetical beaches where H_{fresh} is relatively constant but O_{saline} varies with tide range, as it does at Stinson Beach. If H_{fresh} is higher than O_{saline} during all tidal conditions, the system is in region I of Fig. 2.5 and shallow fresh groundwater continuously discharges throughout the fortnightly tidal cycle. This may be the case at Waquoit Bay, a site with small tidal range and minimal wave action where researchers have described freshwater discharging to the coastal ocean under a variety of conditions (Michael et al. 2003; Mulligan and Charette 2006). If H_{fresh} is low relative to O_{saline} at both neap and spring tide, then shallow fresh groundwater does not discharge over the fortnightly cycle, and the system

is in region II. This likely was the case in Huntington Beach, CA (Boehm et al. 2006) where very little to no fresh groundwater discharge occurred despite the presence of fresh groundwater just landward of the high tide berm. At Stinson Beach, H_{fresh} is higher than O_{saline} during neap tide but lower during spring tide; thus, the system straddles regions I and II, resulting in a pulsing of fresh groundwater during neap tides with little or no discharge during spring tides.

It is conceivable that at Stinson Beach and elsewhere, aquifers may occupy regions I and/or II during different parts of the year as seasonal waves of meteoric hydraulic pressure force fresh groundwater though the beach and interact with the wave- and tide-driven overheight at the boundary. It is also conceivable that variable wave conditions across neap-spring cycles may interfere constructively or destructively with the neap-spring overheight cycle described herein. For these reasons and numerous others, we expect that not all tide- and wave-driven systems will fit into the above classification scheme. Future work including field experiments and numerical modeling and will explore this concept more fully.

This study illustrates the importance of fortnightly variation in aquifer overheight in tide- and wave-driven systems and presents a qualitative framework for categorizing fresh groundwater discharge from beach aquifer systems similar to Stinson Beach with respect to overheight at the land-sea interface. Understanding the interactions of mechanisms forcing SGD is particularly important in systems similar to Stinson Beach, where fresh submarine groundwater discharge from a polluted unconfined aquifer poses potential risk to nearshore ocean ecosystem health. Further work should be done to examine the importance of neap-spring tides on submarine groundwater discharge in other environments.

2.6 REFERENCES CITED

Arar, E. J, and G. B Collins. 1997. Method 445.0. In vitro determination of chlorophyll-a and pheophytin a in marine and freshwater algae by fluorescence. National Exposure Research Laboratory, Office of Research and Development, U.S. Environmental Protection Agency.

Ataie-Ashtiani, B., R. E. Volker, and D. A. Lockington. 2001. Tidal effects on groundwater dynamics in unconfined aquifers. Hydrol. Process. **15**: 655-669.

Bergquist, J. R. 1978. Depositional history and fault-related studies, Bolinas Lagoon, California. USGS Open-File Report 78-802.

Boehm, A. B., G. G. Shellenbarger, and A. Paytan. 2004. Groundwater discharge: A potential association with fecal indicator bacteria in the surf zone. Environ. Sci. Tech. **38:** 3558-3566.

Boehm, A. B., A. Paytan, G. G. Shellenbarger, and K. A. Davis. 2006. Composition and flux of groundwater from a California beach; Implications for nutrient supply to the surf zone. Cont. Shelf. Res. **26**: 269-282.

Boehm, A. B., G. G. Shellenbarger, and A. Paytan. 2004. Groundwater discharge: Potential association with fecal indicator bacteria in the surf zone. Environ. Sci. Technol. **38**: 3558-3566.

Bolster, C. H., S. L. Walker, and K. L. Cook. 2006. Comparison of *Escherichia coli* and *Campylobacter jejuni* transport in saturated porous media. J. Environ. Qual. **35**: 1018-1025.

Bone, S. E., M. A. Charette, C. H. Lamborg, and M. E. Gonneea. 2007. Has submarine groundwater discharge been overlooked as a source of mercury to coastal waters? Environ. Sci. Technol. **41**: 3090-3095.

Burnett, W. C., P. K. Aggarwal, A. Aureli, H. Bokuniewicz, J. E. Cable, M. A. Charette, E. Kontar, S. Krupa, K. M. Kulkarni, A. Loveless, W. S. Moore, J. A. Oberdorfer,

J. Oliveira, N. Ozyurt, P. Povinec, A. M. G. Privitera, R. Rajar, R. T. Ramessur, J. Scholten, T. Stieglitz, M. Taniguchi, and J. V. Turner. 2006. Quantifying submarine groundwater discharge in the coastal zone via multiple methods. Sci. Total Environ. **367:** 498-543.

Campbell, E. E., and G. C. Bate. 1998. Tide-induced pulsing of nutrient discharge from an unconfined aquifer into an *Anaulus australis*-dominated surf-zone. Water SA. **24:** 365-370.

Charette, M. A., K. O. Buessler, and J. E. Andrews. 2001. Utility of radium isotopes for evaluating the input and transport of groundwater-derived nitrogen to a Cape Cod estuary. Limnol. Oceanogr. **46**: 465-470.

Comeau, L. A., A. F. Vézina, M. Bourgeois, and S. K. Juniper. 1995. Relationship between phytoplankton production and the physical structure of the water column near Cobb Seamount, northeast Pacific. Deep Sea Res. Part I: Oceanogr. Res. Papers. **42**: 993-1005.

Demers, S., J. C. Therriault, E. Bourget, and A. Bah. 1987. Resuspension in the shallow sublittoral zone of a macrotidal estuarine environment: Wind Influence. Limnol. Oceanogr. **32**: 327-339.

Fetter, C.W., 2001. Applied Hydrogeology, 4th Edition. Merrill.

Giblin, A.E., and A.G. Gaines. 1990. Nitrogen inputs to a marine embayment: The importance of groundwater. Biogeochemistry **10**: 309–328.

Hays, R. L., and W. J. Ullman. 2007. Direct determination of total and fresh groundwater discharge and nutrient loads from a sandy beachface at low tide (Cape Henlopen, Delaware). Limnol. Oceanogr. **52**: 240-247.

Hazen, A. 1911. A discussion of "Dams on sand foundations" by A. C. Koenig. T. Am. Civ. Eng. **73**: 199-203.

Hijnen, W. A. M, A. J. Brouwer-Hanzens, K. J. Charles, and G. J. Medema. 2005. Transport of MS2 phage, *Escherichia coli*, *Clostridium perfringens*, *Cryptosporidium parvum*, and *Giardia intestinalis* in a gravel and sandy soil. Environ. Sci. Technol. **39**: 7860–7868.

Horn, D. P. 2006. Measurements and modeling of beach groundwater flow in the swash zone: a review. Cont. Shelf. Res. **26**: 622–652.

Huettel, M., W. Ziebis, and S. Forester. 1996. Flow-induced uptake of particulate matter in permeable sediments. Limnol. Oceanogr. **41**: 309-322.

Hwang, D., G. Kim, Y. Lee, and H. Yang. 2005*a*. Estimating submarine inputs of groundwater and nutrients to a coastal bay using radium isotopes. Mar. Chem. **96**: 61-71.

Hwang, D., Y. Lee, and G. Kim. 2005*b*. Large submarine groundwater discharge and benthic eutrophication in Bangdu Bay on volcanic Jeju Island, Korea. Limnol. Oceanogr. **50**: 1393-1403.

Inman, D. L., R. J. Tait, and C. E. Nordstrom. 1971. Mixing in the surf zone. Geophys. Res. Lett. **76**: 3493-3514.

Johannes, R. E. 1980. Ecological significance of the submarine discharge of groundwater. Mar. Ecol. – Prog. Ser. **3**: 365-373.

Kim, G., and D. Hwang. 2002. Tidal pumping of groundwater into the coastal ocean revealed from submarine ^{222}Rn and CH_4 monitoring. Geophys. Res. Lett**. 29:** 1678, doi.10.1029/2002GL015093.

Kroeger, K. D., M. L. Cole, and I. Valiela. 2006. Groundwater-transported dissolved organic nitrogen exports from coastal watersheds. Limnol. Oceanogr. **51:** 2248-2261.

Kroeger, K. D., P. W. Swarzenski, J. Greenwood, and C. Reich. 2007. Submarine groundwater discharge to Tampa Bay; Nutrient fluxes and biogeochemistry of the coastal aquifer. Mar. Chem. **104:** 85-97.

Labiosa R. G. and K. R. Arrigo. 2003. The interplay between upwelling and deep convective mixing in determining the seasonal phytoplankton dynamics in the Gulf of Aqaba: Evidence from SeaWiFS and MODIS. Limnol. Oceanogr. **48**: 2355-2368.

Lapointe, B. E., J. D. O'Connell, and G. S. Garrett. 1990. Nutrient couplings between on-site sewage disposal systems, groundwaters, and nearshore surface waters of the Florida Keys. Biogeochemistry **10:** 289-307.

LaRoche, J., R. Nuzzi, R. Waters, K. Wyman, P. G. Falkowski, and D. W. R. Wallace. 1997. Brown tide blooms in Long Island's coastal waters linked to interannual variability in groundwater flow. Glob. Change Biol. **3:** 397-410.

Li, L., D. A. Barry, F. Stagnitti, and J.-Y. Parlange. 1999. Submarine groundwater discharge and associated chemical input to a coastal sea. Water Resour. Res. **35:** 3253–3259.

Li, L., D. A. Barry, F. Stagnitti, J. Y. Parlange, and D. S. Jeng. 2000. Beach water table fluctuations due to spring-neap tides: moving boundary effects. Adv. Water Resour. **23**: 817–824.

Libelo, E.L. and W.G. MacIntyre. 1994. Effects of surface-water movement on seepage-meter measurements of flow through the sediment–water interface. Hydrogeol. J. **2:** 49–54.

Longuet-Higgens, M. S. 1983. Wave set-up, percolation and undertow in the surf zone. P. Roy. Soc. Lond. A Mat. **390:** 283–291.

May, C. L., J. R. Koseff, L. V. Lucas, J.E. Cloern, and D. H. Schoellhamer. 2003. Effects of spatial and temporal variability of turbidity on phytoplankton blooms. Mar. Ecol. Prog. Ser. **254**: 111–128.

Michael, H. A., A. E. Mulligan, and C. F. Harvey. 2005. Seasonal oscillations in water exchange between aquifers and the coastal ocean. Nature. **436:** 1145-1148.

Michael, H. A., J. S. Lubetsky, and C. F. Harvey. 2003. Characterizing submarine groundwater discharge: a seepage meter study in Waquoit Bay, Massachusetts. Geophys. Res. Lett. **30**: 1297. doi:10.1029/2002GL016000

Mulligan, A. E., and M. A. Charette. 2006. Intercomparison of submarine groundwater discharge estimates from a sandy unconfined aquifer. J. Hydrol. **327:** 411-425.

Nielsen, P. 1990. Tidal dynamics of the water table in beaches. Water Resour. Res. **26:** 2127–2134.

Oberdorfer, J. A., M. A. Valentino, and S. V. Smith. 1990. Groundwater contribution to the nutrient budget of Tomales Bay, California. Biodegradation **10:** 199-216.

Pederson, M. F., and J. Borum. 1996. Nutrient control of algal growth in estuarine waters. Nutrient limitation and the importance of nitrogen requirements and nitrogen storage among phytoplankton and species of macroalgae. Mar. Ecol. – Prog. Ser. **142**: 261-272.

Raubenheimer, B., and R. T. Guza. 1999. Tidal water table fluctuations in a sandy ocean beach. Water Resour. Res. **35:** 2313–2320.

Robertson, W. D., J. A. Cherry, and E. A. Sudicky. 1991. Groundwater contamination from two small septic systems on sand aquifers. Ground Water **29:** 82-92.

Robinson, C., L. Li, and D. A. Barry. 2007. Effect of tidal forcing on a subterranean estuary. Adv. Water Resour. **30:** 851-865.

Santoro, A. E., A. B. Boehm, and C. A. Francis. 2006. Denitrifier community composition along a nitrate and salinity gradient in a coastal aquifer. Appl. Environ. Microb. **72:** 2102-2109.

Santoro, A.E., C.A. Francis, N.R. de Sieyes, and A.B. Boehm. 2008. Shifts in the relative abundance of ammonia-oxidizing bacteria and archaea in a subterranean estuary. Environ. Microb. **10**: 1068-1079.

Scandura, J. E., and M. D. Sobsey. 1997. Viral and bacterial contamination of groundwater from on-site sewage treatment systems. Water Sci. Technol. **35:** 141-146.

Scott, T. M., T. M. Jenkins, J. Lukasik, and J. B. Rose. 2005. Potential use of a host-associated molecular marker in *Enterococcus faecium* as an index of human fecal pollution. Environ. Sci. Technol. **39:** 283-287.

Slomp, C. P., and P. Van Cappellen. 2004. Nutrient inputs to the coastal ocean through submarine groundwater discharge: controls and potential impact. J. Hydrol. **295:** 64-86.

Stinson Beach County Water District (SBCWD). 1998. *Stinson Beach Hydrologic Survey*. www.stinson-beach-cwd.dst.ca.us.

Swartz, C. H., S. Reddy, M. J. Benotti, H. Yin, L. B. Barber, B. J. Brownawell, and R. A. Rudel. 2006. Steroid estrogens, nonylphenol ethoxylate metabolites, and other wastewater contaminants in groundwater affected by a residential septic system on Cape Cod, MA. Environ. Sci. Technol. **40:** 4894-4902.

Taniguchi, M. 2002. Tidal effects on submarine groundwater discharge into the ocean. Geophys. Res. Lett. **29,** 1561, doi:10.1029/2002GL014987.

Taniguchi, M., W. C. Burnett, J. E. Cable, and J. V. Turner. 2002. Investigation of submarine groundwater discharge. Hydrol. Process. **16:** 2115-2129.

Turner, I. L., B. P. Coates, and R. I. Acworth. 1997. Tides, waves and the super-elevation of groundwater at the coast. J. Coastal Res. **13:** 46-60.

Valiela, I., K. Foreman, M. LaMontagne, D. Hersh, J. Costa, P. Peckol, B. DeMeo-Andreson, C. D'Avanz, M. Babione, C. Sham, J. Brawley, and K. Lajtha. 1992.

Couplings of watersheds and coastal waters: Sources and consequences of nutrient enrichment in Waquoit Bay, Massachusetts. Estuaries **15:** 443-457.

Weiskel, P.K., and B.L. Howes. 1991. Quantifying dissolved nitrogen flux through a coastal watershed. Water Resources Research **27**: 2929–2939.

Table 2.1. Well construction details for the wells used in the study. Elevations are given in meters above mean sea level. Distances are given in meters from the mean water line.

Well ID	Diameter (cm)	Distance from mean water line (m)	Top of casing elevation (m)	Top of screen elevation (m)	Bottom of screen elevation (m)
MW06	10.16	223	1.46	-3.11	-4.63
MW07	10.16	178	1.36	-0.16	-1.69
MW09	10.16	70	3.10	0.05	-3.00
MW10	3.81	48	2.13	-0.92	-1.38
MW11	3.81	36	2.07	-1.13	-1.58

Table 2.2. Arithmetic means for chemical concentrations and log-transformed bacterial concentrations in MPN (100 mL)$^{-1}$ for sample groups. Ninety-five percent confidence intervals are given in parentheses. For bacterial calculations, samples below the detection limit of 10 MPN (100 mL)$^{-1}$ detection limit were substituted with 5 MPN (100 mL)$^{-1}$. The *esp* gene column indicates how many of analyzed samples were positive.

Sample Group	n	Salinity (-)	DO (mg L^{-1})	SRP (µmol L^{-1})	Silicate (µmol L^{-1})	Log EC	Log ENT	*esp* gene
MW06	4	0.22 (0.00)	4.1 (0.6)	0.7 (0.0)	409.03 (31.31)	0.7 (0)	0.7 (0)	-
MW07	4	0.97 (0.30)	1.5 (0.3)	9.2 (4.0)	447.39 (50.17)	4.38 (0)	4.38 (0)	2 of 4
MW09	6	3.44 (3.87)	2.5 (0.9)	18 (3)	435.62 (29.32)	3.48 (0.74)	2.29 (0.91)	-
MW10 & MW11	5	11.86 (5.84)	3.0 (0.2)	16 (17)	229.85 (77.64)	1.45 (0.49)	1.19 (0.69)	-
Pits	19	31.75 (0.24)	3.4 (0.2)	2.8 (0.1)	140.65 (7.84)	0.82 (0.09)	1.14 (0.3)	3 of 3
Seeps	17	30.22 (1.39)	5.8 (0.1)	2.4 (0.2)	102.38 (8.75)	0.79 (0.08)	0.82 (0.14)	-
Surf Zone	84	32.02 (0.05)	6.6 (0.1)	1.7 (0.1)	44.89 (1.16)	1.08 (0.1)	0.96 (0.1)	0 of 2
Offshore	6	32.09 (0.09)	7.0 (0.5)	1.6 (0.2)	40.79 (3.15)	N/A	N/A	-
Bolinas Lagoon	4	32.34 (0.51)	6.0 (0.9)	1.6 (0.1)	45.88 (3.45)	2.32 (0.45)	1.29 (0.88)	1 of 1

Sample Group	n	NO_3^- (µmol L^{-1})	NO_2^- (µmol L^{-1})	NH_4 (µmol L^{-1})	DIN (µmol L^{-1})
MW06	4	76 (2)	0.0 (0.0)	1.1 (0.6)	78 (2)
MW07	4	1.4 (1.6)	1.9 (2.4)	530 (80)	520 (8)
MW09	6	8 (4)	0.3 (0.1)	36 (70)	44 (66)
MW10 & MW11	5	160 (110)	7.6 (6.4)	40 (34)	210 (80)
Pits	19	21 (6)	4.0 (1.0)	2.4 (1.2)	27 (5)
Seeps	17	14 (5)	2.6 (1.0)	5.3 (1.8)	22 (5)
Surf Zone	84	15 (1)	0.4 (0.0)	4.1 (0.4)	19 (1)
Offshore	6	14 (3)	0.3 (0.0)	3.1 (0.6)	18 (3)
Bolinas Lagoon	4	11 (1)	0.3 (0.0)	4.5 (1.7)	16 (2)

Table 2.3. The maximum and minimum equivalent freshwater hydraulic head (m) measured relative to mean sea level is shown for each well. Also shown are average heads during the fortnight, and during neap and spring tides. Sea level maximum, minimum and average values are shown for comparison.

Well ID	Minimum (m)	Maximum (m)	Fortnight average (m)	Neap tide average (m)	Spring tide average (m)
MW06	1.26	1.39	1.32	1.33	1.28
MW07	0.41	0.55	0.48	0.49	0.44
MW09	0.24	0.56	0.42	0.37	0.44
MW10	0.08	1.03	0.45	0.26	0.55
MW11	0.08	1.01	0.43	0.39	0.49
Sea level	-1.28	1.18	0.09	0.11	0.18

Table 2.4. (A) Dupuit equation estimates of seaward groundwater discharge in the fresh part of the unconfined aquifer. (B) Model estimates of D_m, D_t, D_w, D, F_p SiO_4, F_p SRP, and F_p DIN. Estimates vary for 1 and 4 h residence times. (C) Predicted C_{prism} for nutrients predicted using Eq. 6. Actual nutrient concentrations in the surf zone are reported for neap and spring tides for comparison.

(A)	Neap tide	Spring tide
Fresh Discharge (L min^{-1} m^{-1})	1.2	0.1

(B)	Neap tide		Spring tide	
	1 h	4 h	1 h	4 h
D_m (L min^{-1} m^{-1})	4.7	1.2	0.5	0.1
D_w (L min^{-1} m^{-1})	7.2	7.2	7.2	7.2
D_t (L min^{-1} m^{-1})	8.7	8.7	14.8	14.8
D (L min^{-1} m^{-1})	20.6	17.1	22.5	22.1
F_p SiO_4 (µmol min^{-1} m^{-1})	3780	2303	2697	2528
F_p SRP (µmol min^{-1} m^{-1})	101	55	62	56
F_p DIN (µmol min^{-1} m^{-1})	1677	949	1972	989

(C)	Neap tide			Spring tide		
	1 h	4 h	Actual	1 h	4 h	Actual
C_{prism} Silicate (µmol L^{-1})	66	97	49	56	98	43
C_{prism} SRP (µmol L^{-1})	2.6	2.3	1.9	1.9	2.4	1.5
C_{prism} DIN (µmol L^{-1})	30	41	23	25	39	17

Figure 2.1. Map of study area (left) and regional hydrogeology (right). Question marks in right panel indicate that contacts between geologic units in this region are uncertain.

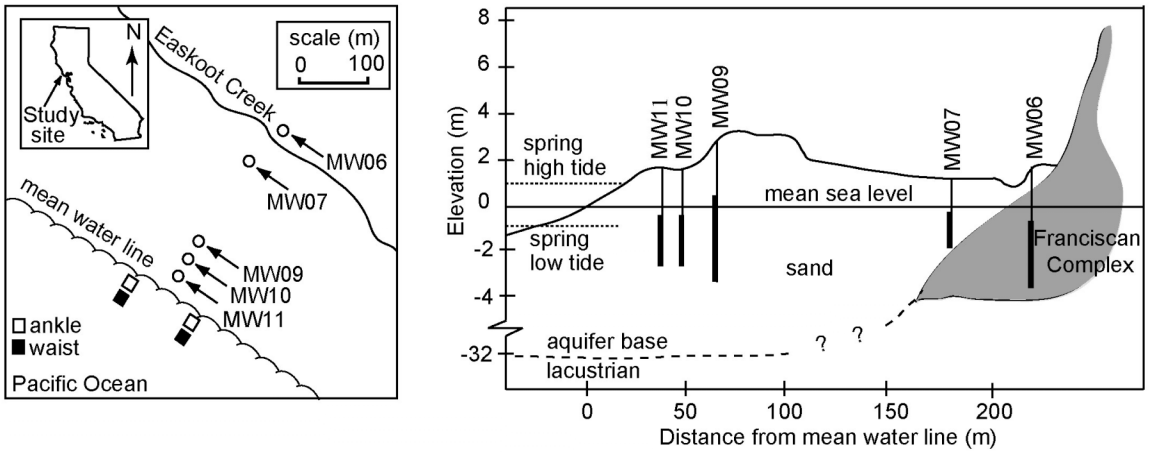

Figure 2.2. Surf zone prism used as a control volume for the freshwater budget. Variables are defined in the text.

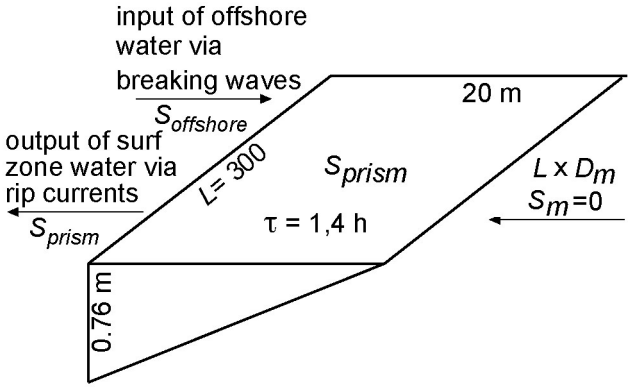

Figure 2.3. Surf zone concentrations of salinity, SRP, DIN, SiO_4, Chl *a* and tidal range plotted versus time during the experiment.

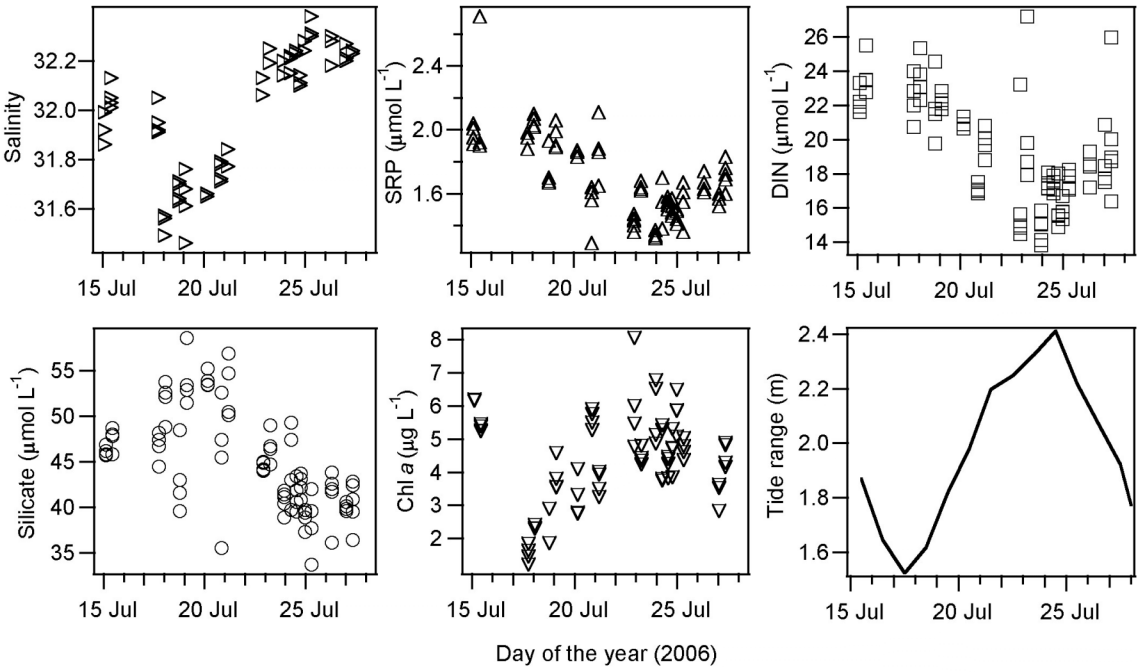

Figure 2.4. Average and 95% confidence intervals of Chl *a* concentrations at time 0 and on day 2 of the mesocosm experiment for treatments (4% and 8% v/v groundwater and seawater) and control (0%). Concentrations in 4% and 8% treatments show significant increases above concentrations at time 0 and above control at day 2, suggesting a dissolved constituent in groundwater is promoting growth of phytoplankton.

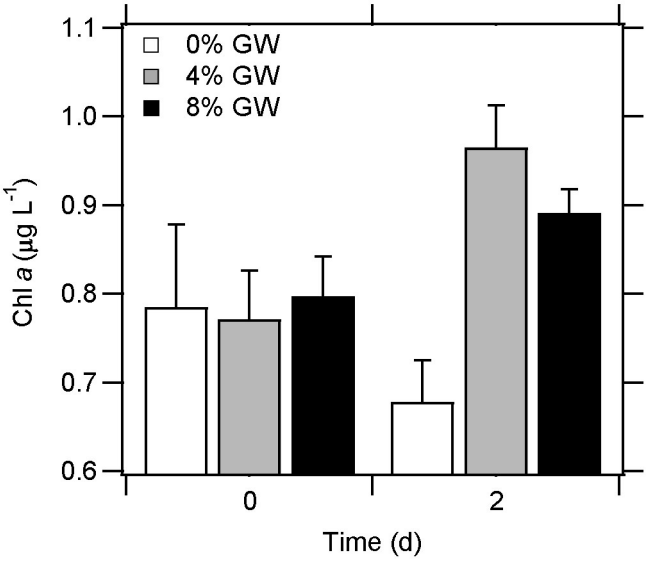

Figure 2.5. A framework for understanding the timing of freshwater discharge at beaches similar to Stinson Beach. The dashed, horizontal lines connect the aquifer overheight (O_{saline}) during neap (N) and spring (S) tides at hypothetical beaches with varying hydraulic heads behind the overheight (H_{fresh}). The solid diagonal line separates region I and II. In region I the aquifer overheight at the beach face is lower than the inland hydraulic head; fresh groundwater discharges to the coastal ocean. In region II, the aquifer overheight is higher than the inland hydraulic head; no freshwater discharge occurs. Fortnightly-pulsed fresh groundwater discharge occurs when a beach straddles region I and II.

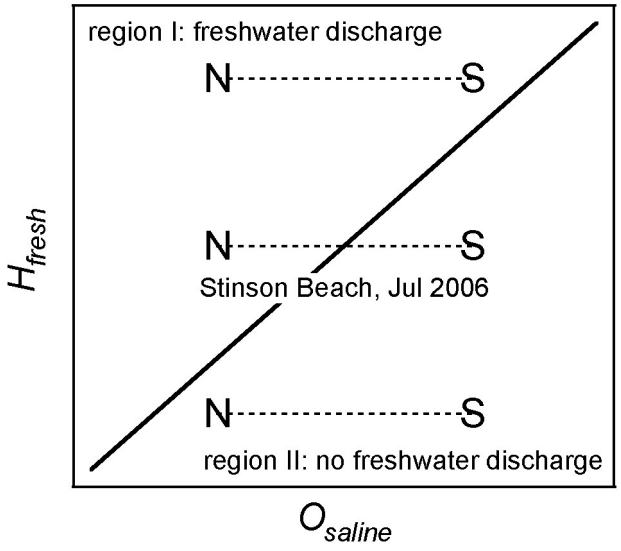

CHAPTER 3: SUBMARINE GROUNDWATER DISCHARGE TO A HIGH-ENERGY SURF ZONE AT STINSON BEACH, CALIFORNIA, ESTIMATED USING RADIUM ISOTOPES

The research presented in this chapter was originally published in 2011 in *Estuaries and Coasts* Vol. 34, pp. 256-268, and is reprinted here with kind permission of Springer Science and Business Media. The research was supported by the National Sea Grant College Program of the U.S. Department of Commerce's National Oceanic and Atmospheric Administration under NOAA Grant NA04OAR4170038, Project R/CZ-197, through the California Sea Grant College Program. The views expressed herein do not necessarily reflect the views of California Sea Grant. Kevan Yamahara contributed greatly to the field experiments and was included as a coauthor along with my adviser Alexandria Boehm. I also acknowledge Karen Knee and Eric Foote for assistance in the field and/or suggestions for improving the manuscript. Comments from the editor and associate editor of *Estuaries and Coasts* and two anonymous reviewers also improved the manuscript.

3.1 ABSTRACT

Two 14-day experiments conducted in the dry summer (July 2006) and wet winter (March 2007) seasons, respectively, examined tidal, wave-driven and seasonal variability of submarine groundwater discharge (SGD) at Stinson Beach, California, using natural radium tracers. Tide stage, tide range, breaker height and season each explained a significant degree of radium variability in the surf zone. A mass balance of excess radium in the surf zone was used to estimate SGD for each season, confirming larger discharge rates during the wet season. Our results indicate median groundwater discharge rates of 6 to 8 L min^{-1} m^{-1} in July 2006 and 38 to 43 L min^{-1} m^{-1} in March 2007. SGD from 200 m of Stinson Beach in March 2007 contributed a flux of phosphate and dissolved inorganic nitrogen approximately equal to that associated with all local creeks and streams within 6 km of the study site at that time.

3.2 INTRODUCTION

Submarine groundwater discharge (SGD) is well documented as an important source of inorganic, organic, and microbial pollutants to the coastal ocean (Boehm et al. 2004; Bone et al. 2007; Santos et al. 2008). Numerous physical forcing mechanisms including meteoric hydraulic head, tide- and wave pumping, seasonal precipitation/evapotranspiration cycles, and variations in groundwater density force the flow of groundwater to the ocean (Burnett et al. 2006). Due to interactions between multiple forcing mechanisms at any given location and time, SGD is temporally- and spatially variable. Site-specific studies are often required to fully understand the timing, magnitude, and importance of SGD in a given region.

Many of the mechanisms that modulate SGD have been investigated numerically and through field studies. Tidal pumping has been explored on both the semidiurnal (Ataie-Ashtiani et al. 1999; Robinson et al. 2007) and fortnightly spring-neap timescales (Boehm et al. 2004; De Sieyes et al. 2008; Kim and Hwang 2002; Santos et al. 2009; Taniguchi 2002). Michael et al. (2005) documented a large, seasonally variable component of SGD controlled by precipitation/evapotranspiration cycles. Wave setup and run-up from breaking waves influence beach water table dynamics and drive SGD at coastal margins (King et al. 2009; Li et al. 2004; Longuet-Higgins 1983). However, breaking waves make direct discharge measurement by seepage meter impossible (Burnett et al. 2006; Huettel et al. 1996; Libelo and McIntyre 1994). This presents a unique challenge in studying SGD along coastlines with high wave energy where wave-driven SGD may be most important. In such environments, it is often necessary to estimate SGD by indirect techniques, such as those based on chemical tracers.

This study explores SGD variability at multiple timescales using naturally occurring radium isotopes as tracers of groundwater discharge. Moore and collaborators pioneered the use of the quartet of naturally occurring radium isotopes, which vary in half-life from 3.7 days to 1600 years, as tracers for ocean mixing and groundwater input to coastal systems (Krest and Harvey 2003; Moore 1997; Moore 2003). The divalent radium cation is bound to soil particles and rocks in fresh water but readily desorbs via

ion exchange in the presence of high ionic strength solutions (Elsinger and Moore 1980). Accordingly, in coastal aquifers where saline groundwater mixes with fresh groundwater, high radium waters result. Open seawater is relatively radium-deplete; therefore, radium activity above that of open seawater suggests a coastal source that in many cases is groundwater. Because radium isotopes behave conservatively in the nearshore after accounting for radioactive decay, the radium quartet is useful for characterizing ocean mixing and rates of submarine groundwater discharge (Charette et al. 2001; Moore 1996; Moore 1999; Moore 2000a; Moore 2000b; Moore 2003).

The present study uses the two short-lived radium isotopes ^{223}Ra ($t_{1/2}$ = 11 d) and ^{224}Ra ($t_{1/2}$ = 3.6 d) and the long-lived isotope ^{226}Ra ($t_{1/2}$ = 1600 y) to investigate how SGD at a wave-dominated California beach is modulated by semidiurnal tides, fortnightly neap-spring tides, swell events, and the seasonal precipitation cycle. The work was conducted at Stinson Beach, a small beach community north of San Francisco, CA, USA. Groundwater at the site is contaminated with nitrogen (nitrate and ammonium, primarily), ortho-phosphate, and human fecal bacteria from septic systems, and previous research at the site has documented nutrification of the nearshore coastal ocean by fresh SGD in the summer (de Sieyes et al. 2008). A previous experiment at this beach during dry summer weather estimated SGD using salinity as a groundwater tracer (de Sieyes et al. 2008). The present study builds on that previous study, but uses an entirely new radium tracer dataset consisting of over 500 measurements to investigate the effects of waves, tides, and season on SGD.

3.3 METHODS AND MATERIALS

3.3.1 STUDY SITE.

Stinson Beach (Fig. 3.1) is an open ocean, southwest facing, reflective beach with mixed semi-diurnal tides, a spring tide range of 2.0 to 2.5 m and a high-energy surf zone. Breakers with heights typically in the range of 0.5 to 2 m result primarily from northwest swells during winter and a combination of northwest and south swells in summer. A short description of local hydrogeology and human development in the area can be found

elsewhere (de Sieyes et al. 2008). Our research site is focused on the beach at the end of Calle de Resaca, a residential street in downtown Stinson Beach (37.899 N, 122.646 W; Fig. 3.1).

The climate at Stinson Beach is Mediterranean with an annual average rainfall of 60 to 120 cm occurring predominately between October and April (Stinson Beach County Water District 1998). During the dry season, Bolinas Lagoon (37.908 N, 122.682 W) and a local coastal hot spring (37.886 N, 122.630 W), are the only other potential sources of radium within 20 km of the study site (Fig. 3.1). Numerous ephemeral creeks deliver fresh water to the coastal ocean during the wet season but generally run dry by late summer (Stinson Beach County Water District 1998). Only Webb Creek (37.885 N, 122.629 W) discharges directly to the nearshore within 7 km of the site; all other creeks discharge to Bolinas Lagoon. (Fig. 3.1)

Radium activities in the surf zone were monitored over semidiurnal and spring-neap tidal cycles during both the dry and rainy seasons. Fourteen-day experiments were conducted from 14 through 28 July 2006 and from 10 through 24 March 2007. During each study, neap tide (17 July 2006 and 11 March 2007, respectively) preceded the spring tide (24 July 2006 and 18 March 2007, respectively).

3.3.2 TIDE, WAVE, AND BEACH CONDITIONS.

Tide elevation measurements were obtained from a NOAA tide gauge at Point Reyes, approximately 30 km from Stinson Beach (http://tidesandcurrents.noaa.gov, Station ID 9415020, 38.00 N, 122.98 W). Tides along this coast are in phase at a spatial scale of 30 km, so this tide gauge gives excellent tide data for Stinson Beach. Data were recorded at six-minute intervals. Daily tidal range was calculated from daily maxima and minima. We define spring- and neap tide as those days during the tidal cycle when tidal range is maximal and minimal, respectively.

Wave measurements were obtained from National Buoy Data Center buoy #46026 at San Francisco (http://www.ndbc.noaa.gov, 37.759 N 122.833 W), the closest directional wave buoy to the site. The buoy is located in 55 m of water 23 km due southwest (offshore) from the site. Spectral wave data were recorded at 1-hour intervals.

A continuous record of surf zone breaker height was estimated from significant wave height and period for the duration of our study using the method of Komar (1998). This calculation assumes that wave energy is conserved from deep water to the surf zone and ignores the effects of refractive focusing, diffraction, bottom friction, currents, and wave-wave interactions. Stinson Beach lies in the wave shadow of nearby Bolinas Point and Duxbury Reef, so a correction factor was necessary to increase the accuracy of the breaker height predictions. Seven synoptic breaker height observations were made in the field using surfers riding breaking waves as benchmarks, a commonly used method for estimating breaker height (Caldwell 2005). These observations were compared to the continuous time series and a correction factor was derived using linear regression. The Komar-estimated significant wave heights were multiplied by the correction factor to obtain a continuous time series of significant breaker heights. These data are used to explore correlative relationships between waves and SGD.

During each study, the surf zone was viewed from a high vantage point above the beach and rip cell spacing was estimated using a geo-referenced map. Beach topography was also surveyed during each study by standard methods using a scope and stick (Fig. 3.2).

3.3.3 WATER SAMPLING.

The tidal regime at Stinson Beach is mixed-semidiurnal. To characterize tidal variation in radium activities, we sampled the surf zone at high-high and low-low tide along two cross-shore transects approximately every other day of each study. The two transects were located 100 m apart in the alongshore direction and extending from the water line out into the surf zone (Fig. 3.1). During both studies, the two sampling transects straddled a rip current, indicating that the two transects sampled distinct rip cells. Local knowledge of the site coupled with aerial observations from a high vantage point during each study confirmed the permanence of the rip cell location. During each sampling at the site, surf zone samples were collected along each transect at 0.2 and 0.7 m water depths referred to as ‘ankle’ and ‘waist depths’, respectively (Fig. 3.2). These depths occurred well within the surf zone. Although a small sand bar was observed during

each experiment, no distinct break was ever noted between an inner and outer surf zone at the site. In order to standardize sample collection depth, 0.2 and 0.7 m heights were noted on the legs of the two individuals who conducted all surf zone sampling. During sample collection, care was taken to collect a mixture of water from the entire water column from surface to sandy bottom. For the surf zone, n_{Jul06}=42 and n_{Mar07}=32.

At low-low tides only, groundwater immediately adjacent to the water line was sampled from shallow pits dug into the beach approximately 10 m back from the water line (n_{Jul06}=18 and n_{Mar07}=14; Fig. 3.2). In addition, subaerial seepage faces were sampled when they developed at the lowest tides (n_{Jul06}=17 and n_{Mar07}=2). On multiple days during each experiment, groundwater was sampled from temporary stainless steel drive-point piezometers installed into the top 2 m of the water table just above the high tide berm (n_{Jul06}=1 and n_{Mar07}=5).

To characterize offshore waters during neap and spring tide, surface offshore ocean water samples were obtained 180 m, 870 m, and 1615 m from the beach along a cross shore transect on the days of the 3rd-quarter and new moons during each experiment (Fig. 3.3).

The ebb flow from Bolinas Lagoon (37.908 N, 122.682 W) was sampled every two to four days during both studies (n_{Jul06}=4 and n_{Mar07}=7). The hot spring (37.886 N, 122.630 W) was sampled on 19 March 2007.

Clean, triple-rinsed 20 L collapsible low-density polyethylene containers were used for water collection. For a given water sample, a total of approximately 100 L was composited. A one liter subsample was collected into a clean triple-rinsed bottle and used for all non-radium chemical analyses. All samples were analyzed for ^{223}Ra and ^{224}Ra. A subset of samples was analyzed for ^{226}Ra including pits, seeps, offshore, Bolinas Lagoon, hot spring and a subset of monitoring wells. In addition, surf zone samples collected at the high- and low tide closest in time to the offshore sampling events during each experiment were analyzed for ^{226}Ra.

3.3.4 CREEK SURVEY.

On 16 and 17 March 2007, creeks flowing within 6 km of the site were surveyed for flow rate and nutrient concentration to provide estimates of creek-associated nutrient

flux to the local coastal ocean. The survey included creeks flowing to Bolinas Lagoon (n=11) as well as those discharging directly to the ocean (n=1). Little to no creek discharge occurs during late summer at the site, precluding a similar survey during July 2006. First-order estimates of flow rate in each creek were measured via the float method (Weight and Sonderegger 2001) whereby velocity is measured by timing the travel of a float down a straight reach of a creek. Measurements were made following USGS guidelines as outlined in Rantz et al. (1982). Surface velocities were converted to a depth-averaged velocity using a correction factor of 0.85 and multiplied by cross-sectional area to calculate flow rate. Reflecting the order-of-magnitude nature of our measurements, we conservatively assume 25% standard deviation associated with these flow rate measurements (Rantz 1982). Estimates of creek-associated nutrient flux were calculated by multiplying nutrient concentration by flow rate. Standard deviations of nutrient flux are calculated by propagating standard deviations of nutrient concentration and flow rates.

3.3.5 Nutrient analysis.

The concentrations of orthophosphate, silicate, dissolved inorganic nitrogen were previously reported for all July 2006 water samples in de Sieyes et al. (2008). During the March experiment, a 30 mL aliquot of water was 0.2 μm PES filtered (Millipore, Billerica, MA) and stored at -20°C for nutrient analyses. The concentrations of orthophosphate, silicate, nitrate, nitrite, and ammonium were measured by standard methods with a nutrient autoanalyzer (Lachat QuikChem 8000, Loveland, CO). Detection limits are 0.2 μM nitrate, 0.1 μM nitrite, 0.1 μM phosphate, 1.0 μM silicate, and 0.1 μM ammonium. Dissolved inorganic nitrogen is reported as the sum of nitrate, nitrite, and ammonium. Five percent of nutrient samples were analyzed in duplicate, and standard deviation was <5% for each analyte.

3.3.6 Radium analysis.

Dissolved radium was extracted from ~100 L water samples in the field by filtering through columns of MnO_2-impregnated acrylic fiber at a flow rate not exceeding 1 L min^{-1} (Moore and Arnold 1996; Rama et al. 1987). Untreated acrylic fiber plugs were used to prevent the contamination of the MnO_2 fiber by particulates. The fibers were

removed from the columns and stored in plastic bags until processing, at which time they were rinsed with de-ionized water and hand-squeezed to remove excess water. Activities of the short-lived isotopes ^{223}Ra and ^{224}Ra were measured within three days of collection using a delayed coincidence counter (Moore 2003; Moore and Arnold 1996). Errors associated with radium analysis via this method are 10% (Moore 2003). Samples were not re-analyzed after collection to quantify ^{228}Th-supported ^{224}Ra activity. However, samples collected during subsequent experiments at the Stinson Beach site showed that ^{228}Th-supported ^{224}Ra activity accounts for approximately 3% or less of the original ^{224}Ra activity (Black et al. 2009; Rama et al. 1987). Because ^{228}Th-supported ^{224}Ra activity at the site is small compared to the error associated with the ^{224}Ra method, we assume for the purposes of this paper that all ^{224}Ra in samples is excess ^{224}Ra, i.e. ^{224}Ra unsupported by ^{228}Th decay in the sample.

^{226}Ra activity was measured via its ^{218}Po daughter following Kim et al. (2001). Mn-impregnated fibers were aged for at least six months to allow for decay of the short-lived isotopes. Fibers were then moistened with de-ionized water to obtain constant recoil efficiency, sealed in an air-tight helium-flushed glass tube, and incubated for at least three weeks to allow in-growth of ^{222}Rn daughter product to reach activities within 0.1% of secular equilibrium. Standard error calculated from duplicate (n=34), triplicate (n=3) and quadruplicate (n=6) analysis of individual fibers was 13%.

3.3.7 Data analysis.

Statistical analysis was performed using Matlab (Natick, Massachusetts). Parametric statistical methods were chosen because groups of data in general were normally distributed based on the Lilliefors test of normality. Correlation coefficients between measured continuous parameters were determined using Pearson's product-moment correlations, and sample groups were compared using Student's t-test. Statistical results were deemed significant if $p<0.05$. Unless otherwise noted, summarized data reported in the text are average ± standard deviation.

3.4 RESULTS

3.4.1 ENVIRONMENTAL CONDITIONS.

Tide stage, daily calculated tide ranges, observed breaker heights, as well as times of surf zone and offshore sampling events are shown for both experiments in Figure 3.3. Tidal range during July 2006 was approximately sinusoidal with a fortnightly period, with highest tidal range occurring around the day of the new moon. In March 2007, one or more long-period tidal oscillations slightly reduced the tide range during the new moon.

Breaker heights calculated from buoy data following Komar (1998) were compared with observations made in the surf zone, as described in the methods. A correction factor of 0.36 was used based on linear regression of observed and predicted breaker heights. This correction factor was applied to the entire predicted breaker dataset. Corrected predictions of breaker height are plotted with observed breaker heights in Figure 3.3. Root mean square error between observed and predicted breaker heights was 19%.

Breaker heights in the surf zone during the July 2006 experiment were smaller and more stable (71 ± 12 cm) compared to the March 2007 experiment when breakers were significantly larger and more variable (104 ± 23 cm; t=-4.8, $p<0.05$; Fig. 3.3). Field observations confirmed the arrival of multiple large swell events at the beach during the March 2007 experiment.

According to Stinson Beach County Water District records, 2.1 cm and 24.7 cm of rainfall had fallen in the three months prior to the July 2006 and March 2007 studies, highlighting the Mediterranean climate at the site. Rainfall during the actual experiments themselves was slight, with only 0.05 and 0.3 cm falling during the July 2006 and March 2007 studies, respectively.

3.4.2 NUTRIENTS.

Nutrient concentrations for all sample groups are reported in Table 3.1. Nutrient measurements from July reported by de Sieyes et al. (2008) are included for comparison.

Pit and seep samples were significantly enriched in phosphate, silicate, and dissolved inorganic nitrogen above both surf zone and offshore samples ($p<0.05$ for both July 2006 (de Sieyes et al. 2008) and March 2007).

3.4.3 ^{223}Ra and ^{224}Ra.

All samples were analyzed for the two short-lived radium isotopes ^{223}Ra and ^{224}Ra (Table 3.1). As with nutrient concentrations, activities of ^{223}Ra and ^{224}Ra activities were enriched in pit and seep samples compared to surf zone and offshore samples, suggesting groundwater-associated discharge of radium to the nearshore. In March 2007, a single sample collected from Webb Creek, the only major creek in the area discharging directly to the ocean, contained ^{223}Ra and ^{224}Ra activities of 0.5 dpm $(100L)^{-1}$ 4.3 dpm $(100L)^{-1}$.

When activities of ^{223}Ra are plotted as a function of ^{224}Ra for all samples, data generally fall along a line with a slope of 19, suggesting a common source for both isotopes (Fig. 3.4). A single sample from a hot spring with a ^{224}Ra/^{223}Ra isotopic ratio of approximately 56 deviates substantially from this common mixing line, suggesting it represents a distinct end member. However, none of the other samples fall along a mixing line between seawater and the hot spring end member, indicating that the hot spring has little or no influence on ^{223}Ra and ^{224}Ra activities in surface water and groundwater at our site.

To investigate homogeneity of Ra activities in the alongshore direction during each experiment, we tested whether ^{223}Ra and ^{224}Ra activities measured at the two cross-shore transects (Fig. 3.1) were significantly different using Student's t-test (t-statistics not shown). For both the July 2006 and March 2007 studies, ^{223}Ra and ^{224}Ra activities collected from pits along the two transects were not significantly different ($0.34\leq p\leq 0.90$) suggesting groundwater activities are relatively homogeneous at this spatial scale. No significant differences were found between the samples collected at ankle depth along the two transects ($0.55<p<0.69$) or at waist depth along the two transects ($0.36<p<0.99$). The lack of significant differences between surf zone activities along the two transects indicates that radium activities are relatively homogeneous in the surf zone in the alongshore direction on the hundred-meter scale.

We tested whether the surf zone was well mixed in the cross shore direction with respect to ^{223}Ra and ^{224}Ra by comparing activities of ankle and waist depth samples for each experiment. In July 2007, ^{223}Ra samples collected at ankle- and waist depth were not significantly different ($t_{223,Jul06} = 1.28$, $p = 0.20$). In all other comparisons, activities at ankle depth were significantly higher than at waist depth ($t_{223,Mar07} = 2.57$, $p = 0.01$; $t_{224,Jul06} = 2.24$, $p = 0.028$; $t_{224,Mar07} = 3.59$, $p < 10^{-3}$). The cross shore variation within the surf zone was on the order of 10-25% of the mean radium activity at ankle depth. This variability is small compared to the differences between the surf zone and other major sample groups including Bolinas Lagoon, offshore waters, pits, and seeps. For the purposes of further analysis, we group ankle- and waist-deep surf zone samples for each isotope, referring to them collectively as the surf zone sample group.

If groundwater discharge at the shoreline is the major source of radium to the nearshore, then it follows that tracer activities should show a decreasing trend from groundwater to nearshore to offshore waters. Statistical testing was conducted to confirm this relationship; t- and p-values for the following tests are reported in Table 3.2. Pit samples were significantly enriched above seep samples during the July 2006 experiment (Fig. 3.5) but not during the March 2007 experiment when only two seepage face samples were collected. For both isotopes during both experiments, surf zone activities were significantly lower than both pit samples and seepage face samples. Similarly, the surf zone was significantly enriched in both radium isotopes compared to offshore waters during both experiments.

Ebb flow from Bolinas Lagoon was enriched in ^{223}Ra and ^{224}Ra relative to offshore waters during both experiments (Table 3.2; Fig. 3.5), suggesting submarine groundwater discharge to the lagoon throughout the year. During the March 2007 experiment, the lagoon was also enriched in both isotopes relative to surf zone waters whereas during the July 2006 experiment, the lagoon was significantly enriched over surf zone activities in ^{224}Ra but differences in ^{223}Ra activities were not significant. Mean ^{223}Ra and ^{224}Ra activities in Bolinas Lagoon were higher than mean surf zone activities by 170% and 190% in March 2007 and by 40% and 50% in July 2006. In comparison, Bolinas Lagoon waters contained significantly less of each isotope than groundwater

samples from pits during the July 2006 experiment. The same relationship was true for ^{224}Ra in March 2007 but differences in ^{223}Ra were not statistically significant.

Radium activities in sample groups were compared between the two experiments to test for seasonal differences. ^{223}Ra and ^{224}Ra activities in pit and seep samples were not different between summer and winter, indicating a seasonally stable groundwater end member with respect to ^{223}Ra and ^{224}Ra activities (Table 3.2; Fig. 3.5). Activities of the longer-lived isotope ^{223}Ra in the surf zone were not significantly different between the two experiments but ^{224}Ra activities in the surf zone were significantly lower during the March 2007 experiment relative to July 2006 by 22%. Differences between offshore ^{223}Ra and ^{224}Ra activities during the two studies were insignificant. Bolinas Lagoon was significantly enriched in ^{223}Ra and ^{224}Ra by 86% and 49%, respectively, during the March 2007 experiment compared to the July 2006 experiment.

To test the role of tide level in explaining radium variability in the surf zone, the four samples collected in the surf zone during each low tide sampling event were grouped and compared by paired t-test to the corresponding four samples collected during the previous high tide. In July 2006, ^{223}Ra and ^{224}Ra activities in the surf zone were significantly higher at low tides than at preceding high tides ($t_{223,Jul06}$ = -4.89, $p<10^{-4}$; $t_{224,Jul06}$ = -6.65, $p<10^{-6}$), with mean ^{223}Ra and ^{224}Ra activities at low tides 87% and 95% higher than at preceding high tides, respectively. In March 2007, mean ^{223}Ra and ^{224}Ra activities were 80% and 60% higher at low tides than at preceding high tides, respectively, but the difference was only statistically significant for ^{223}Ra ($t_{223,Mar07}$ = -3.36, p=0.0024; $t_{224,Mar07}$ = -2.00, p= 0.055).

Radium activity in the surf zone was compared to daily tidal range in order to examine the role of fortnightly neap-spring tidal variability on surf zone radium activity. Neither ^{223}Ra nor ^{224}Ra activity in the surf zone was significantly correlated to tidal range when grouped by experiment ($r_{223,Jul06} = 0.22$, $p = 0.055$; $r_{223,Mar07} = 0.12$, $p = 0.37$; $r_{224,Jul06} = 0.16$, $p = 0.18$; $r_{224,Mar07} = 0.24$, p=0.070). When samples from both experiments were grouped together, a significant, positive correlation emerged between tidal range and both ^{223}Ra and ^{224}Ra ($r_{223} = 0.20$, p=0.019; $r_{224} = 0.26$, p=0.0022).

A similar comparison was made for each experiment to investigate the correlation between average daily breaker height on surf zone radium activity. During the July 2006 experiment, ^{223}Ra and ^{224}Ra activities in the surf zone were significantly negatively correlated with breaker height (r_{223} = -0.44, p=0.0001; r_{224} = -0.43, p=0.0001). Interestingly, during the March 2007 experiment when breaking waves in the surf zone were noticeably larger, the short-lived isotope ^{224}Ra in the surf zone was significantly positively correlated with breaker height (r_{224} = 0.38, p=0.0043). No significant relationship existed between daily mean breaker height and ^{223}Ra in the surf zone during the March 2007 experiment (r_{223} = 0.19, p=0.14).

3.4.4 ^{226}RA.

^{226}Ra activities for sample groups are compared in Figure 3.6. During the July 2006 experiment, pit samples were significantly enriched in ^{226}Ra above surf zone activities, consistent with a groundwater ^{226}Ra source (t=3.47; p=0.0014). However, offshore samples were also significantly enriched in ^{226}Ra above surf zone activities (t_{Jul06}= -3.97; $p<10^{-3}$), inconsistent with a coastal groundwater source (Fig. 3.6). By comparison, during the March 2007 experiment, ^{226}Ra activities in pit and surf zone samples were not significantly different (t=-0.85; p=0.40) but the surf zone was enriched relative to offshore waters (t_{Mar07}=2.68; p=0.012). ^{226}Ra activities in Bolinas Lagoon were not significantly different than those in the surf zone during either experiment (t_{Jul06} = -1.76, p=0.095; t_{Mar07} = -0.47, p=0.64). The lagoon was enriched in ^{226}Ra relative to offshore waters in March 2007 (t = -3.23; p=0.0042) but not in July 2006 (t_{Mar07} = 1.19, p=0.24). A March 2007 water sample from the hot spring located on the shoreline approximately 1.8 km from the research site contained very high ^{226}Ra activities of 148 dpm $(100L)^{-1}$, approximately an order of magnitude above that of beach groundwater.

3.4.5 CREEK SURVEY.

A survey of local creeks was conducted during the March 2007 experiment in order to provide an estimate of total creek-associated nutrient flux during the wet season for comparison with SGD-associated nutrient flux estimates (Table 3.3). Total flux from all creeks discharging to Bolinas Lagoon and directly to the ocean near Stinson Beach at

the time of the March experiment was estimated at 10 ± 1 mmol min^{-1} phosphate, 3 ± 1 mol min^{-1} silicate, and 200 ± 50 mmol min^{-1} dissolved inorganic nitrogen.

3.5 DISCUSSION

3.5.1 TIDE LEVEL.

During both the summer and winter studies, ^{223}Ra activities in the surf zone were significantly higher at low tides than at preceding high tides. For ^{224}Ra, the same trend was observed although results were statistically significant only for the July 2006 experiment. The increased ^{223}Ra and ^{224}Ra activities observed during low tides suggest discharge of tidally pumped, radium-enriched groundwater out of the beach aquifer during ebb tides. This interpretation is consistent with results from other studies documenting tidal pumping (Boehm et al. 2004). An alternative explanation for the increased radium activity between low and high tide is that the surf zone becomes enriched in radium at low tide by the outflow of Bolinas Lagoon. However, it should be noted that sediment transport studies suggest that ebb outflow from Bolinas Lagoon typically flows towards the northwest, away from our sampling sites (Philip Williams & Associates 2005). This suggests that Bolinas ebb flow is not directed to the south, towards our study site.

3.5.2 FORTNIGHTLY TIDES.

The magnitude of SGD forced by tidal pumping is directly affected by the magnitude of tidal range, or the difference in elevation between high and low tide (Ataie-Ashtiani et al. 2001). Assuming constant rates of cross-shore mixing, one might expected that SGD-associated radium would increase in the surf zone during periods of highest tidal range. Indeed, tidal range during our studies did explain 4% and 7% of the variation in ^{223}Ra and ^{224}Ra in the surf zone, respectively. This significant positive correlation is consistent with previous studies concluding that tidal range does influence the magnitude of tidal pumping of groundwater from the beach aquifer, with greatest discharge occurring at or around spring tide (Li et al. 1999; Rapaglia 2005; de Sieyes et al. 2008).

An alternative interpretation of the radium enrichment of the surf zone at spring tide is that Bolinas Lagoon is disproportionately enriching the surf zone with radium at that point in the fortnightly tidal cycle. While increases in tidally pumped groundwater during periods of increased tidal range are consistent with the numerical simulations of others (Ataie-Ashtiani et al. 2001), we cannot discount this possibility. However, as mentioned before, the limited available data on ebb flow from the lagoon mouth is not consistent with this interpretation (Philip Williams & Associates 2005). More specific work following radium activity in the ebb plumes from the lagoon is needed to quantitatively evaluate the contribution of this source.

3.5.3 WAVES.

The role of wave setup and wave run-up in driving SGD has been explored by other researchers numerically and using field measurements. Increases in breaker height have been shown to increase wave pumping of SGD (Longuet-Higgins 1983) but also increase cross-shore mixing in the nearshore (Pearson et al. 2002). Significant negative correlations were observed between breaker height and activities of ^{223}Ra or ^{224}Ra in the surf zone during the July 2006 experiment, with breaker height explaining 44% and 43% of activity for the two isotopes, respectively. The negative correlations in the summer experiment suggest either reduced discharge during periods of higher breaking waves, increased cross-shore mixing with radium-poor offshore waters, or both. Given the expected role of waves in driving groundwater flow (larger waves, larger set up and thus larger wave pumped SGD), our results suggest that during summer, when breaker height is comparatively small, the net effect of increased breaker height is increased mixing with radium-poor offshore waters rather than decreased discharge. During the March 2007 experiment when breaker height was larger and more variable compared to the summer, surf zone activities of the short-lived isotope ^{224}Ra were significantly positively correlated with breaker height. In March, variations in breaker height explained 38% of the radium variability. This relationship is consistent with increased wave-driven SGD during large winter swell events. To the best of our knowledge, no other studies have observed a significant relationship between breaker height and groundwater tracer concentrations in open waters receiving SGD.

3.5.4 SGD ESTIMATES AND SEASONAL COMPARISON.

Numerous lines of evidence support the use of the two short-lived radium isotopes ^{223}Ra and ^{224}Ra as tracers of beach groundwater flow to the ocean. The decrease in activity from groundwater to surf zone and Bolinas Lagoon waters to offshore waters is consistent with the conceptual model of a groundwater tracer source discharging in this setting. Conversely, no consistent, statistically significant patterns emerged that suggested beach groundwater as the primary source of the long-lived isotope ^{226}Ra to the nearshore. This lack of a clear pattern may be a combination of the multiple sources of the long-lived isotope ^{226}Ra in this environment, including beach groundwater, ^{226}Ra from hot springs, the outflow of Bolinas Lagoon, and possibly the outflow of San Francisco Bay, which was not investigated in this study. Point Reyes is a major upwelling center, and upwelled waters may also be another important source of ^{226}Ra to the coastal ocean in this area. ^{226}Ra activities monitored during the experiment were inconsistent with the assumptions required of methods using the offshore decay of groundwater-derived ^{226}Ra to calculate groundwater discharge (Moore 2000b; Moore 2003). For this reason, we chose to estimate SGD using a mass balance of short-lived radium isotopes in the surf zone (Boehm et al. 2004; Paytan et al. 2006).

To estimate total groundwater discharge using the short-lived isotopes, we rely upon a surf zone 'box' model which treats a single surf zone rip cell as a prism-shaped continuous flow reactor with constant volume and residence time (Fig. 3.2). This box model approach was previously utilized at Stinson Beach to estimate fresh groundwater discharge using salinity as a conservative tracer (de Sieyes et al. 2008) as well as at other locations (Shellenbarger et al. 2006). Observations of rip cell characteristics were logged and beach topography surveyed during each experiment (Fig. 3.2), and prism cell volume V_{prism} was calculated from these characteristics. The average estimated surf zone width w, the distance from shoreline to just beyond breakers, was estimated at 20 m in July 2006 and 50 m in March 2007, and the breaker depth was calculated as the product of surf zone width w and beach slope s_b. The following equation was then used to estimate total groundwater discharge volume per unit length of shoreline D using a Monte Carlo approach:

$$D = \left(\frac{A_{prism} - A_{offshore}}{A_{groundwater}} \right) \frac{V_{prism}}{L\tau} \quad (3.1)$$

where τ is the cross shore residence time of water in the rip cell. During each of 100,000 iterations, the model calculated D from random, normally-distributed radium activities for the surf zone prism A_{prism}, groundwater end member $A_{groundwater}$, and offshore end member $A_{offshore}$, based on mean and standard deviations measured for each group (Table 3.1). Each iteration incorporates random, evenly-distributed values of surf zone residence time between 1 and 4 h, the range of surf zone residence times used previously for estimating SGD at this site (de Sieyes et al. 2008). Uncertainties on V_{prism} were not considered because they were not quantified as part of this study. It should be noted that Eq. 1 assumes that D is small compared to the input of offshore waters into the surf zone via breaking waves and thus does not affect the water balance.

Given that the ^{223}Ra and ^{224}Ra activities were lower in Webb Creek than in offshore waters, they very likely do not contribute significant short-lived radium isotopes to the nearshore. For this reason, inputs from the creek are ignored in the mass balance. The mass balance assumes that all radium in the surf zone is derived from beach groundwater and not from other sources including Bolinas Lagoon, upwelled seawater, or San Francisco Bay.

Results of the surf zone mass balance are reported in Figure 3.7. Shown are 1st, 2nd, and 3rd quartile estimates of SGD. Median (2nd quartile) estimates of D based on ^{223}Ra and ^{224}Ra activities were 6 and 8 L min^{-1} m^{-1} in July 2006 and 38 and 43 L min^{-1} m^{-1} in March 2007, respectively.

SGD estimates were previously reported for this site using salinity as a tracer and models of saline groundwater discharge and found to be between 17 and 23 L min^{-1} m^{-1} during the dry season (de Sieyes et al. 2008). Those estimates are a factor of two to three higher than the median radium-based discharge rates reported here for the dry season. Disecrepancies in SGD estimates obtained by independent methods is not unusual (Burnett et al. 2006).

A comparison of our radium-derived SGD estimates with those from locations with similar climates (Southern California and Israel) indicates our estimates are within

the range of those previous reported. Boehm et al. (2006) estimated dry season discharge rates between 4.2 and 8.9 L min^{-1} m^{-1} at Huntington Beach, California, using a radium-based eddy diffusivity approach. Shellenbarger et al. (2006) reported annual average discharge rates of 1.0 to 4.5 L min^{-1} m^{-1} in the Gulf of Aqaba, Israel, based on a coastal box model approach using radium as a groundwater tracer. These ranges match well with the median discharge estimates of 6 and 8 L min^{-1} m^{-1} we report for Stinson Beach for dry weather.

SGD estimates were significantly greater in March 2007 than in July 2006 based on both ^{223}Ra (t=-40.5, $p<10^{-10}$) and ^{224}Ra (t=-38.7, $p<10^{-10}$). This difference is driven mathematically by seasonal differences in radium activities and surf zone volume (V_{prism}), as V_{prism} is larger in winter than in summer due to larger waves breaking farther offshore in winter months. The large degree to which our median SGD estimates vary from summer and winter may result from the strongly seasonal precipitation-evapotranspiration cycle experienced in the Mediterranean climate of coastal Central California.

Using Monte Carlo simulations allowed us to incorporate quantifiable uncertainties of input terms into our SGD estimates. Specifically, the radium activities incorporated in each model run were chosen based on standard deviations about mean radium activities for each sample group. The model also used a wide range of surf zone residence times, 1 to 4 hours, reflecting the uncertainty of that model input for the surf zone at the field site. Uncertainty was not quantifiable for the rip cell volume term (V_{prism}), which was assumed constant in all simulations for a given experiment. Future work should examine uncertainty in this parameter.

Bolinas Lagoon was significantly enriched in both ^{223}Ra and ^{224}Ra during the March 2007 experiment compared to the July 2006. Because flow in this lagoon is dominated by tidal exchange (Philip Williams & Associates 2005; Ritter 1973), we can assume that residence time therein likely remains approximately stable on the seasonal timescale. It follows that higher ^{223}Ra and ^{224}Ra activities in the lagoon in March are evidence of increased groundwater flux during the winter experiment, consistent with the seasonal variation in SGD reported above for the Stinson Beach shoreline. An estimate of either residence time or tidal exchange ratio could be used in conjunction with the

radium activities presented here to estimate SGD to Bolinas Lagoon. Unfortunately, to the best of our knowledge, no published values exist for these parameters, and such a calculation is not possible at this time. The role played by SGD in the Bolinas Lagoon ecosystem, which has itself been recognized as an internationally significant ecological resource, should be a focus of future research.

Our previous work at the site has shown that groundwater at Stinson Beach is a major source of nutrients to the coastal ocean, with nutrient pollution in fresh groundwater due at least in part to the high density of septic systems in the community. A comparison between groundwater-associated nutrient flux and that from creeks discharging locally during the March 2007 experiment further supports this conclusion. Total creek-associated nutrient flux (± standard deviation) in March 2007 was estimated at 10 ± 3 mmol min^{-1} phosphate, 4 ± 1 mol min^{-1} silicate, and 200 ± 50 mmol min^{-1} dissolved inorganic nitrogen. Assuming SGD-associated flux in March 2007 is the product of the median ^{223}Ra-based SGD estimate, 38 L min^{-1} m^{-1}, and mean pit nutrient concentrations of 2.6, 130, and 30.4 μM phosphate, silicate, and DIN, respectively, total SGD-associated flux at the study site in March 2007 was 99 μmol phosphate min^{-1} m^{-1}, 4940 μmol silicate min^{-1} m^{-1}, and 1160 μmol DIN min^{-1} m^{-1}. In other words, SGD from the short 200 m stretch of Stinson Beach where our experiments were conducted was responsible for a nutrient flux approximately equal to the total creek-associated flux of phosphate and dissolved inorganic nitrogen discharged within 6 km of the study site in March 2007. Surface water runoff in late summer along this area of coast was negligible, so a similar calculation for the July 2006 experiment was not made, but we can conclude that discharge of nutrient-enriched groundwater discharge at Stinson Beach likely plays a particularly significant role in the local marine nutrient budget during the summer months. This highlights the importance of groundwater protection at Stinson Beach and similar coastal settings where discharge of groundwater to the coastal ocean occurs.

3.6 CONCLUSIONS

Submarine groundwater discharge was documented at Stinson Beach during two experiments. With the exception of ^{224}Ra during the March 2007 experiment, short-lived

radium isotope activities in the surf zone were significantly higher at low tide relative to high tide, indicating the importance of tidal pumping along this coastline. Tidal range correlated significantly with ^{223}Ra and ^{224}Ra activity in the surf zone suggesting that the magnitude of discharge is controlled to some degree by the tidal range, with maximal discharge occurring during spring tide. Increases in wave action at the beach had a significant but opposite effect on radium activities in the surf zone during the summer and winter studies, highlighting the roles of waves in driving both SGD and cross-shore mixing. The arrival of large swell events at the beach in winter appeared to increase radium-enriched SGD to the surf zone.

This study did not investigate the potential effects of large-scale changes in flow and mixing from tides, wind, waves, upwelling and other physical processes which may be influencing radium activities in the nearshore. Future studies investigating these processes would be useful in fully understanding the sources, fate, and transport of radium in coastal waters.

^{226}Ra was enriched in offshore waters relative to surf zone waters at the site, indicating shoreline groundwater discharge was not the sole source of ^{226}Ra to the nearshore. Bolinas Lagoon, San Francisco Bay, upwelling, and hydrothermal springs may all be substantial sources of ^{226}Ra to the coastal ocean. ^{226}Ra was not useful as a tracer for calculating SGD at this site.

SGD at Stinson Beach is seasonally variable, with increased discharge occurring in the winter. Nutrient fluxes associated with SGD during winter months were large, even compared to nutrient loading associated with surface runoff in the area. The high degree of nutrient loading is consistent with previous studies at the site, which attribute the high concentrations of nitrogen and phosphate to the high density of septic systems used for wastewater treatment in the community. This study highlights the importance of groundwater quality protection in areas such as Stinson Beach and nearby Bolinas Lagoon, where SGD-associated nutrient flux can be a major component of the local marine biogeochemical budget.

3.7 REFERENCES CITED

Ataie-Ashtiani, B., R. E. Volker, and D. A. Lockington. 1999. Numerical and experimental study of seepage in unconfined aquifers with a periodic boundary condition. Journal of Hydrology **222:** 165-184.

Ataie-Ashtiani, B., 2001. Tidal effects on groundwater dynamics in unconfined aquifers. Hydrological Processes **15:** 655-669.

Black, F. J. and others. 2009. Submarine Groundwater Discharge of Total Mercury and Monomethylmercury to Central California Coastal Waters. Environmental Science & Technology **43:** 5652-5659.

Boehm, A. B., G. G. Shellenbarger, and A. Paytan. 2004. Groundwater discharge: Potential association with fecal indicator bacteria in the surf zone. Environmental Science & Technology **38:** 3558-3566.

Boehm, A. B., A. Paytan, G. G. Shellenbarger, K. A. Davis. 2006. Composition and flux of groundwater from a California beach aquifer: Implications for nutrient supply to the surf zone. Continental Shelf Research **26**: 269-282.

Bone, S. E., M. A. Charette, C. H. Lamborg, and M. E. Gonneea. 2007. Has submarine groundwater discharge been overlooked as a source of mercury to coastal waters? Environmental Science & Technology **41:** 3090-3095.

Burnett, W. C. and others 2006. Quantifying submarine groundwater discharge in the coastal zone via multiple methods. Science of the Total Environment **367:** 498-543.

Caldwell, P. C. 2005. Validity of North Shore, Oahu, Hawaiian Islands Surf Observations. Journal of Coastal Research. 21(6):1127-1138.

Charette, M. A., K. O. Buesseler, and J. E. Andrews. 2001. Utility of radium isotopes for evaluating the input and transport of groundwater-derived nitrogen to a Cape Cod estuary. Limnology and Oceanography **46:** 465-470.

de Sieyes, N. R., K. M. Yamahara, B. A. Layton, E. H. Joyce, and A. B. Boehm. 2008. Submarine discharge of nutrient-enriched fresh groundwater at Stinson Beach, California is enhanced during neap tides. Limnology and Oceanography **53:** 1434-1445.

Elsinger, R. J., and W. S. Moore. 1980. 226Ra behavior in the Pee Dee River-Winyah Bay estuary. Earth and Planetary Science Letters **48:** 239-249.

Huettel, M., W. Ziebis, and S. Forster. 1996. Flow-induced uptake of particulate matter in permeable sediments. Limnology and Oceanography **41:** 309-322.

Kim, G., W. C. Burnett, H. Dulaiova, P. W. Swarzenski, and W. S. Moore. 2001. Measurement of Ra-224 and Ra-226 activities in natural waters using a radon-in-air monitor. Environmental Science & Technology **35:** 4680-4683.

Kim, G., and D. W. Hwang. 2002. Tidal pumping of groundwater into the coastal ocean revealed from submarine Rn-222 and CH4 monitoring. Geophysical Research Letters **29**.

King, J. N., A. J. Mehta, and R. G. Dean. 2009. Generalized analytical model for benthic water flux forced by surface gravity waves. Journal of Geophysical Research-Oceans **114**.

Komar, P. D. Beach Processes and Sedimentation. Prentice Hall. Upper Saddle River, N.J. 1998. 543 pp.

Krest, J. M., and J. W. Harvey. 2003. Using natural distributions of short-lived radium isotopes to quantify groundwater discharge and recharge. Limnology and Oceanography **48:** 290-298.

Li, L., D. A. Barry, F. Stagnitti, and J. Y. Parlange. 1999. Submarine groundwater discharge and associated chemical input to a coastal sea. Water Resources Research **35:** 3253-3259.

Li, L., N. Cartwright, P. Nielsen, and D. Lockington. 2004. Response of coastal groundwater table to offshore storms. China Ocean Engineering **18:** 423-431.

Libelo, E. L., W. G. McIntyre. 1994. Effects of surface-water movement on seepage-meter measurements of flow through the sediment–water interface. Hydrogeology Journal**:** 49-54.

Longuet-Higgins, M. S. 1983. Wave Set-Up, Percolation and Undertow in the Surf Zone. Proceedings of the Royal Society of London A **390:** 283-291.

Michael, H. A., A. E. Mulligan, and C. F. Harvey. 2005. Seasonal oscillations in water exchange between aquifers and the coastal ocean. Nature **436:** 1145-1148.

Moore, W. S. 1996. Large groundwater inputs to coastal waters revealed by Ra-226 enrichments. Nature **380:** 612-614.

Moore, W. S. 1997. High fluxes of radium and barium from the mouth of the Ganges-Brahmaputra river during low river discharge suggest a large groundwater source. Earth and Planetary Science Letters **150:** 141-150.

Moore, W. S. 1999. The subterranean estuary: a reaction zone of ground water and sea water. Marine Chemistry **65:** 111-125.

Moore, W. S. 2000a. Ages of continental shelf waters determined from Ra-223 and Ra-224. Journal of Geophysical Research-Oceans **105:** 22117-22122.

Moore, W. S. 2000b. Determining coastal mixing rates using radium isotopes. Continental Shelf Research **20:** 1993-2007.

Moore, W. S. 2003. Sources and fluxes of submarine groundwater discharge delineated by radium isotopes. Biogeochemistry **66:** 75-93.

Moore, W. S., and R. Arnold. 1996. Measurement of ^{223}Ra and ^{224}Ra in coastal waters using a delayed coincidence counter. J. Geophys. Res. **101:** 1321–1329.

Paytan, A. and others 2006. Submarine groundwater discharge: An important source of new inorganic nitrogen to coral reef ecosystems. Limnology and Oceanography **51:** 343-348.

Pearson J. M., I. Guymer, J. R. West and L. E. Coates. 2002. Effect of Wave Height on Cross-Shore Solute Mixing. Journal of Waterway, Port, Coastal and Ocean Engineering. **128**: 1-11.

Philip Williams & Associates. 2005. Bolinas Lagoon Ecosystem Restoration Feasibility Project.

Rama, J. F. Todd, J. L. Butts, and W. S. Moore. 1987. A new method for the rapid measurement of ^{224}Ra in natural waters. Mar. Chem. **22:** 43–54.

Rantz, S.E. 1982. Measurement and computation of streamflow: U.S. Geological Survey Water-Supply Paper 2175. 2 v., 631 p.

Rapaglia, J. 2005. Submarine groundwater discharge into Venice Lagoon, Italy. Estuaries **28:** 705-713.

Ritter, J. R. 1973. Bolinas Lagoon, Marin County, California, Summary of Sedimentation and Hydrology, 1967-69. p. 80.

Robinson, C., L. Li, and D. A. Barry. 2007. Effect of tidal forcing on a subterranean estuary. Advances in Water Resources **30:** 851-865.

Santos, I. R., W. C. Burnett, J. Chanton, N. Dimova, and R. N. Peterson. 2009. Land or ocean?: Assessing the driving forces of submarine groundwater discharge at a coastal site in the Gulf of Mexico. Journal of Geophysical Research-Oceans **114**.

Santos, I. R., W. C. Burnett, J. Chanton, B. Mwashote, I. Suryaputra, and T. Dittmar. 2008. Nutrient biogeochemistry in a Gulf of Mexico subterranean estuary and

groundwater-derived fluxes to the coastal ocean. Limnology and Oceanography **53:** 705-718.

Shellenbarger, G. G., S. G. Monismith, A. Genin, and A. Paytan. 2006. The importance of submarine groundwater discharge to the nearshore nutrient supply in the Gulf of Aqaba (Israel). Limnology and Oceanography **51:** 1876-1886.

Stinson Beach County Water District. 1998. Stinson Beach Hydrologic Survey.

Taniguchi, M. 2002. Tidal effects on submarine groundwater discharge into the ocean. Geophysical Research Letters **29**.

Weight, W. D., and J. L. Sonderegger. 2001. Manual of Applied Field Hydrogeology. McGraw Hill Publishing Company.

Figure 3.1. Sampling locations at Stinson Beach. Panel A shows location of Stinson Beach within California. Panel B shows the location of the Calle de Resaca field site with respect to Bolinas Lagoon (BL), Webb Creek (WC), and the hot spring (HS). In the main figure, the locations of ankle, waist, and pit samples, as are the monitoring wells and location of the rip current flowing between the two surf zone transects. Offshore sampling locations are not shown but are given within the text. See houses for approximate scale. Aerial photograph copyright © 2002-2009 Kenneth & Gabrielle Adelman, California Coastal Records Project, http://www.californiacoastline.org.

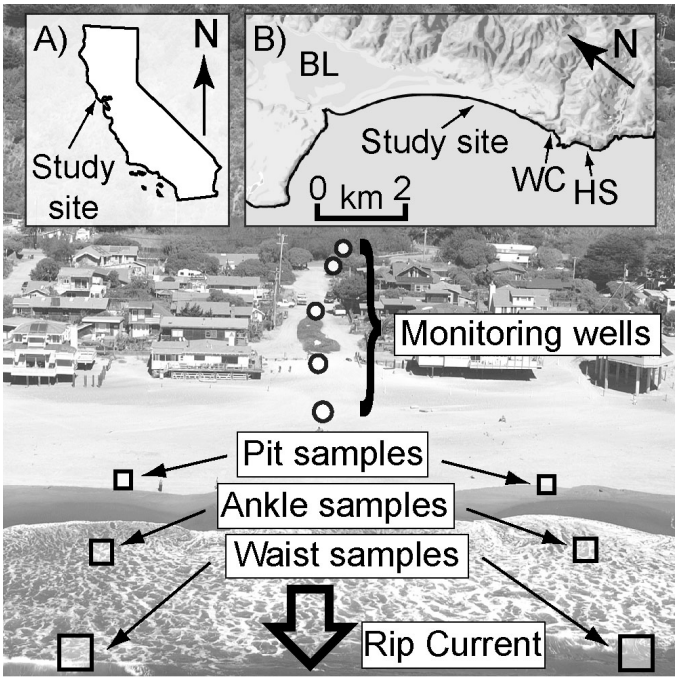

Figure 3.2. Diagram showing beach topography and the geometry of the surf zone box with sampling locations for July 2006 at high tide (Panel A), March 2007 at high tide (Panel B), July 2006 at low tide (Panel C), and March 2007 at low tide (Panel D). In each panel, the ocean is shown on the right side and the beach on the left side. Beach topography from surveys made with scope and stick is shown in meters relative to mean sea level on the y-axis and in meters relative to a known permanent datum on the x-axis. The geometry of the surf zone box is shown as a gray prism. Breaking wave symbols delineate the outer limits of the surf zone box, and the surf zone width in meters is shown for each experiment. The approximate locations of the ankle and waist depths are shown as asterisks, and the approximate locations of pit samples collected at low tides are shown with the letter 'p'.

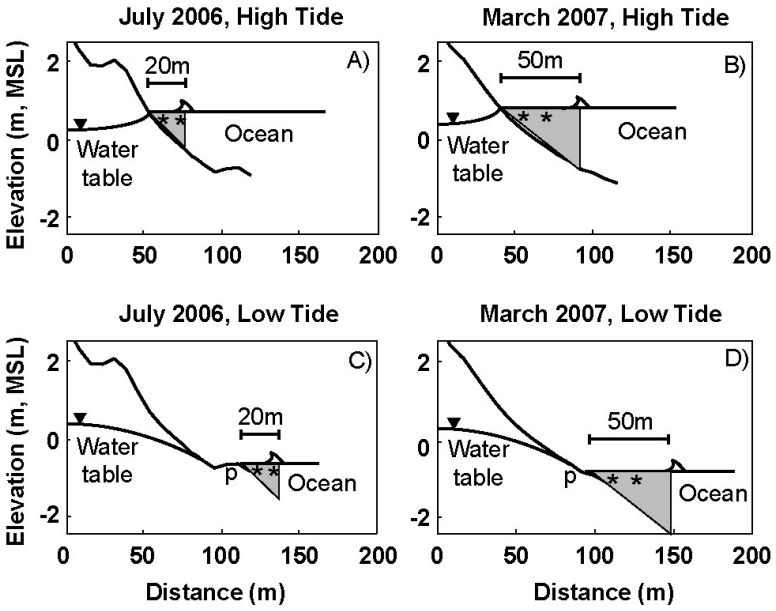

Figure 3.3. Tidal stage (m) relative to mean sea level, daily tidal range (m), and corrected breaker heights for both the July 2006 and March 2007 studies. In the tidal record insets (top), the timing and tide stage during surf zone sampling events are shown as filled triangles and the timing of offshore sampling events on the days of the 3rd-quarter and new moons are shown as asterisks. In the breaker height insets, breaker observations from the field are shown as filled circles, and the corrected, continuous record calculated using San Francisco buoy data is shown as a black line.

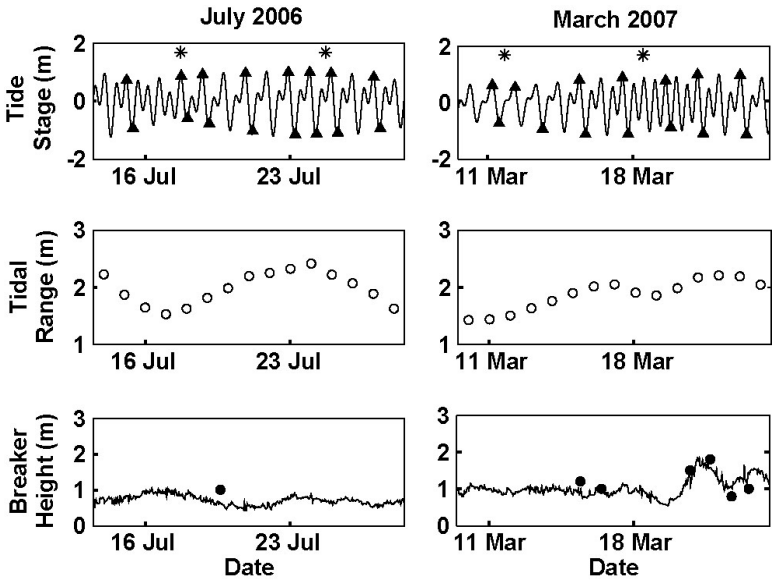

Figure 3.4. ^{224}Ra activity as a function of ^{223}Ra activity for all samples collected as part of this study. Offshore and surf zone samples are open circles, groundwater samples including pits, seeps, and monitoring wells are filled circles, Bolinas Lagoon samples are open boxes and the hot spring is a filled box.

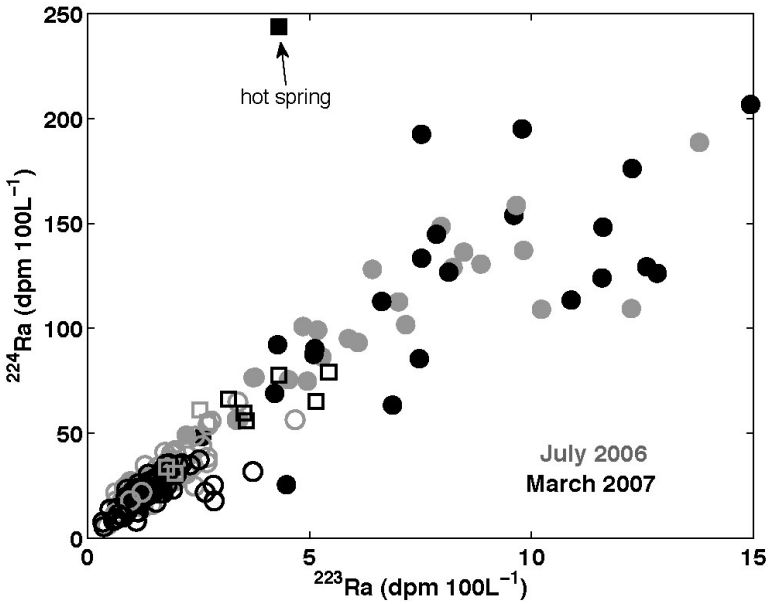

Figure 3.5. ^{223}Ra (A) and ^{224}Ra (B) activities by sample group during the July 2006 and March 2007 experiments.

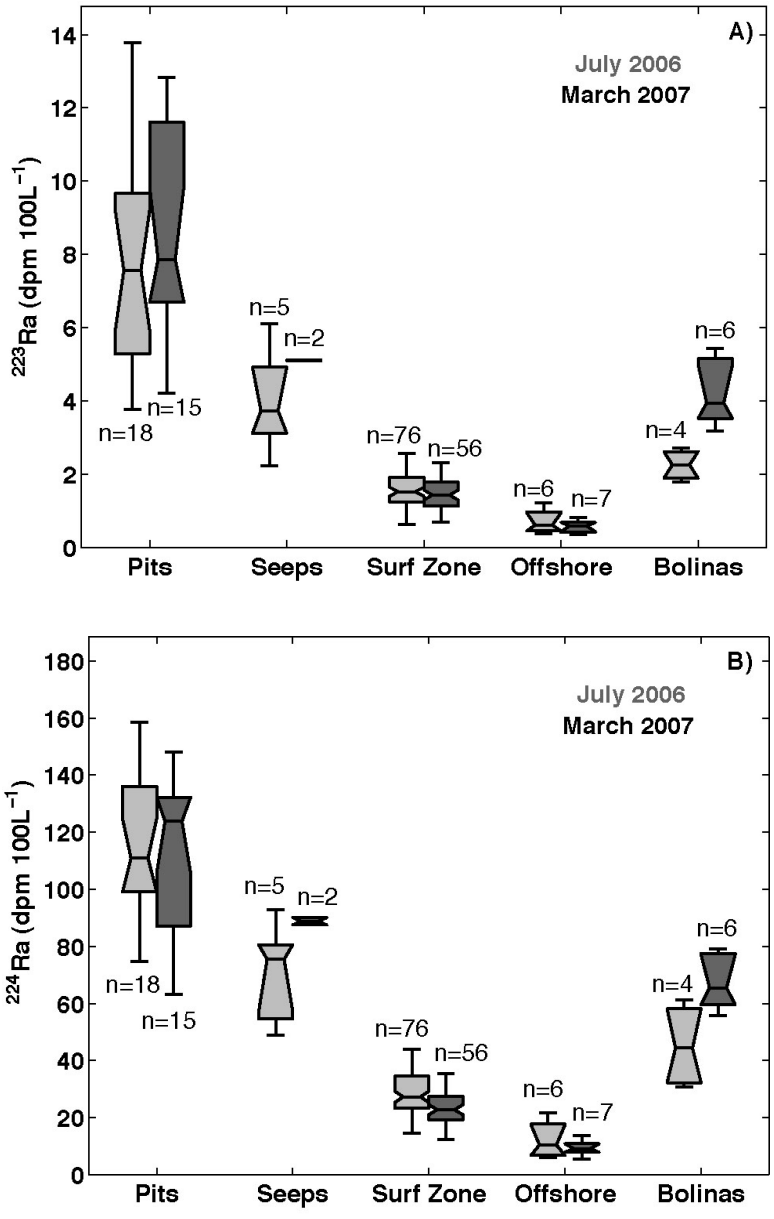

Figure 3.6. ^{226}Ra activities by sample group during the July 2006 and March 2007 experiments. Included in *n* are duplicate and triplicate analyses for individual samples. The hot spring sample collected in March 2007 (148 dpm $(100L)^{-1}$) is not shown.

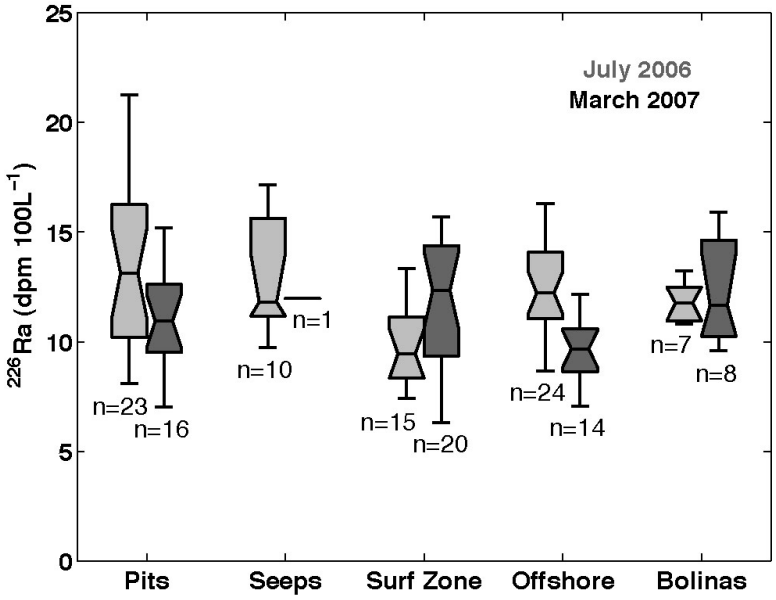

Figure 3.7. Discharge estimates as calculated by Equation 1 using a Monte Carlo approach. Q1, Q2, and Q3 are the 1st, 2nd, and 3rd quartiles of discharge estimates, respectively.

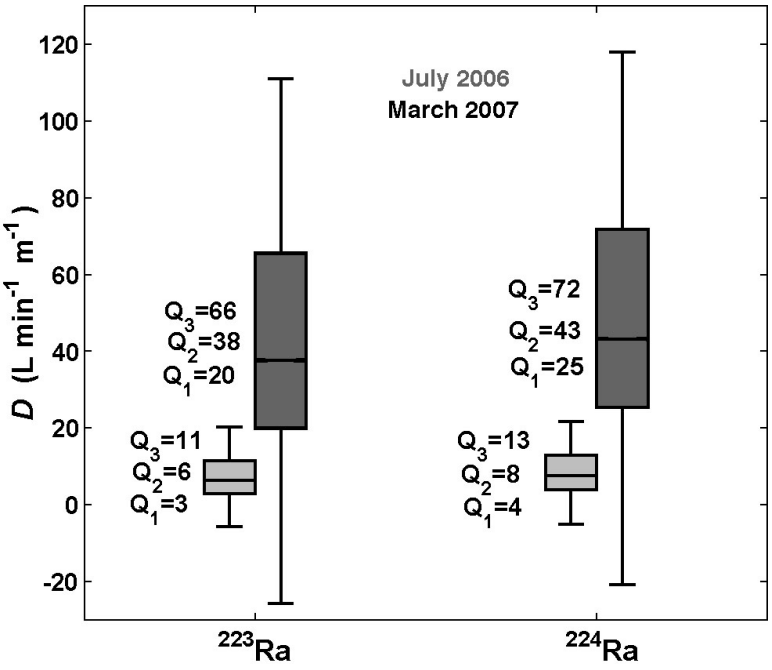

Table 3.1. Average concentrations ± standard deviation of phosphate, silicate, dissolved inorganic nitrogen (DIN), ^{223}Ra and ^{224}Ra as a function of sample type for both experiments. Phosphate, silicate, and DIN for July 2006 are reported in de Sieyes et al. (2008).

Experiment	Group	Phosphate (μM)	Silicate (μM)	DIN (μM)	^{223}Ra (dpm 100L^{-1})	^{224}Ra (dpm 100L^{-1})
July 2006	Pits	2.7 ± 0.2	140.6 ± 17.8	27.0 ± 12.3	7.8 ± 2.7	117.9 ± 29.6
	Seeps	2.4 ± 0.3	102.4 ± 18.4	22.3 ± 9.4	4.0 ± 1.4	70.1 ± 17.5
	Surf Zone	1.7 ± 0.2	44.9 ± 5.4	19.3 ± 3.2	1.7 ± 0.7	30.0 ± 10.3
	Offshore	1.6 ± 0.3	40.8 ± 3.9	17.9 ± 3.5	0.7 ± 0.3	12.2 ± 6.3
	Bolinas	1.6 ± 0.1	45.9 ± 3.5	16.1 ± 1.9	2.2 ± 0.4	45.2 ± 15.2
March 2007	Pits	2.6 ± 0.3	130.1 ±15.4	30.4 ± 6.5	8.4 ± 3.0	106.7 ± 35.2
	Seeps	2.1 ± 0.1	105.9 ± 15.7	29.7 ± 4.4	5.1 ± 0.0	88.8 ± 1.8
	Surf Zone	1.2 ± 0.3	26.0 ± 5.5	15.4 ± 3.5	1.5 ± 0.6	23.5 ± 6.7
	Offshore	1.1 ± 0.1	28.8 ± 9.6	15.6 ± 2.1	0.6 ± 0.2	9.3 ± 2.7
	Bolinas	1.4 ± 0.1	40.6 ± 8.9	9.3 ± 2.4	4.2 ± 0.9	67.2 ± 9.4

Table 3.2. t- and p-values for ^{223}Ra (upper right half) and ^{224}Ra (lower left half) comparisons across groups and experiments.

		July 2006					March 2007				
		Pits	Seeps	Surf Zone	Offshore	Bolinas	Pits	Seeps	Surf Zone	Offshore	Bolinas
July 2006	Pits		t=2.97 p=0.007	t=-17.7 $p<10^{-30}$	n/a	t=-4.0 $p<10^{-3}$	t=-1.23 p=0.22	n/a	n/a	n/a	n/a
	Seeps	t=3.42 p=0.003		t=-6.8 $p<10^{-8}$	n/a	n/a	n/a	n/a	n/a	n/a	n/a
	Surf Zone	t=-21.3 $p<10^{-36}$	t=-8.1 $p<10^{-11}$		t=3.38 p=0.011	t=1.71 p=0.092	n/a	n/a	t=1.13 p=0.26	n/a	n/a
	Offshore	n/a	n/a	t=4.16 $p<10^{-4}$		t=6.47 $p<10^{-3}$	n/a	n/a	n/a	t=0.99 p=0.34	n/a
	Bolinas	t=-2.5 $p<10^{-3}$	n/a	t=2.82 p=0.006	t=4.83 p=0.0013		n/a	n/a	n/a	n/a	t=-3.85 p=0.0049
March 2007	Pits	t= 0.27 p=0.78	n/a	n/a	n/a	n/a		t=0.71 p=0.49	t=-6.1 $p<10^{-7}$	n/a	t=-1.4 p=0.17
	Seeps	n/a	n/a	n/a	n/a	n/a	t=0.78 p=0.45		t=-22.2 p=0.029	n/a	n/a
	Surf Zone	n/a	n/a	t=1.13 p=0.26	n/a	n/a	t=-14.8 $p<10^{-22}$	t=-19.5 p=0.033		t=4.41 $p<10^{-4}$	t=10.13 $p<10^{-13}$
	Offshore	n/a	n/a	n/a	t=1.09 p=0.30	n/a	n/a	n/a	t=5.50 $p<10^{-6}$		t=10.19 $p<10^{-8}$
	Bolinas	n/a	n/a	n/a	n/a	t=-2.85 p=0.021	t=-4.0 p=0.021	n/a	t=14.61 $p<10^{-20}$	t=15.7 $p<10^{-8}$	

Table 3.3. Results of the creek survey. Concentrations are reported in units of micromoles per liter (μM), flow rates are in liters per minute (L min^{-1}), and calculated nutrient fluxes have units of millimoles per minute (mmol min^{-1}). Standard deviations of nutrient fluxes are 25%, the result of propagated standard deviations of nutrient concentration (5%) and flow rate (25%). Culvert #1 is an unnamed storm drain and Stinson Gulch #1, #2, and #3 are the three branches draining Stinson Gulch.

Watershed	Latitude	Longitude	Phosphate (μM)	Silicate (μM)	DIN (μM)	Flow Rate (L min^{-1})	$F_{phosphate}$ (mmol min^{-1})	$F_{silicate}$ (mmol min^{-1})	F_{DIN} (mmol min^{-1})
Audobon Creek	37.930	-122.681	1.8	290	4.9	900	2	300	4
Black Rock Creek	37.898	-122.635	0.9	330	26.8	300	0.3	100	8
Bolinas Creek	37.920	-122.693	1.7	376	22.0	4000	7	2000	100
Culvert #1	37.932	-122.698	0.7	365	16.9	70	0.1	30	1
Fitzhenry Creek	37.900	-122.637	0.9	338	34.7	700	0.7	200	30
McKinnan Gulch	37.913	-122.660	1.1	264	14.9	2000	2	500	30
Pike County Gulch	37.932	-122.688	0.3	262	2.2	100	0.1	40	0.3
Stinson Gulch #1	37.907	-122.651	0.8	207	8.2	400	0.3	90	4
Stinson Gulch #2	37.907	-122.651	0.7	265	6.6	300	0.2	80	2
Stinson Gulch #3	37.907	-122.651	0.4	291	3.2	900	0.3	300	3
Volunteer Canyon	37.925	-122.675	0.6	284	1.1	100	0.1	40	0.2
Webb Creek	37.887	-122.626	0.5	299	20.9	700	0.3	200	10

CHAPTER 4: FRESH SUBMARINE GROUNDWATER DISCHARGE FROM A COASTAL AQUIFER FORCED BY THE MEDITERRANEAN CLIMATE OF CENTRAL CALIFORNIA

The research presented in this chapter was supported by the National Sea Grant College Program of the U.S. Department of Commerce's National Oceanic and Atmospheric Administration under NOAA Grant NA04OAR4170038, Project R/CZ-197, through the California Sea Grant College Program. The views expressed herein do not necessarily reflect the views of California Sea Grant. Doug Rumbaugh, Christian Langevin, Alyssa Dausman, and David Freyberg provided guidance during the development of the model.

4.1 ABSTRACT

A numerical groundwater model was developed using the variable density groundwater flow code SEAWAT-2000 to examine the influence of seasonally variable recharge conditions typical of coastal California on the magnitude and timing of fresh submarine groundwater discharge from a generic coastal aquifer with a constant head (non-tidal) ocean boundary. Model dimensions and hydrogeologic characteristics were chosen based on a combination of observations from field studies at Stinson Beach, California, and published numerical investigations of coastal groundwater flow. Average monthly recharge was calculated from historical precipitation records. Monthly evapotranspiration rates were assumed equal to the potential evapotranspiration rates calculated using climatological observations from the field site. Calculated recharge was approximately sinusoidal in nature, with positive recharge rates dominated by precipitation during the rainy winter season and negative recharge rates dominated by evapotranspiration during the hot, precipitation-free summer season. Temporal trends in fresh discharge from the model aquifer to the ocean were similar for two modeled scenarios, a first including a constant head fresh landward boundary condition and a second including a constant flux fresh landward boundary condition. Specifically, discharge in both models peaked in January during the period of maximum precipitation and recharge, and declined until reaching a minimum in September, two months after the minimum recharge period in July. Minimum discharge rates for two model scenarios were 17% and 18% lower in September than the maximum discharges in winter, respectively. Monthly mean discharge from Lagunitas Creek, a creek near Stinson Beach, reached maximum and minimum values in February and September, respectively. However, the exponential decline in modeled SGD was slower than that of creek discharge, suggesting that SGD and the nutrient fluxes associated with it may play a particularly important role in coastal ecosystems in early summer when surface water discharge has nearly reached a minimum but discharge of substantial quantities of fresh groundwater is still occurring.

4.2 INTRODUCTION

Submarine groundwater discharge (SGD), fluid flow from the seabed to the sea regardless of driving force or composition, has been shown to be a globally important contributor of nutrients, pollutants and freshwater to the coastal zone (Burnett et al. 2006). Confirmed driving forces of SGD include meteoric hydraulic head, tide- and wave pumping (Longuet-Higgins 1983; Li et al. 1999), and variations in groundwater density, and a great deal of research is being conducted to understand the combinations of factors that modulate rates of SGD at sites around the world.

Recently, seasonal cycles of precipitation and evapotranspiration have been shown to greatly influence the magnitude and timing of both saline and fresh groundwaters. Michael et al. (2005) recognized that wave- and tide-driven SGD could not account for the large seasonal differences observed in the activity of radium, a natural tracer of submarine groundwater, in Waquoit Bay, Massachusetts. A numerical model was developed to investigate the role of precipitation and potential evapotranspiration (PET) in forcing discharge of radium-rich SGD at the Waquoit Bay site. The model was recharged based on monthly mean precipitation and PET rates calculated using Thornthwaite (1957). Although monthly precipitation at Waquoit Bay showed no clear seasonal trend, the seasonal variability of PET was strong enough to force a substantial seasonal shift in the location of the fresh/saline interface in the groundwater model. The seaward movement of the fresh/saline interface following the winter season forced the discharge of a substantial flux of saline groundwater to surface waters, thereby explaining a great deal of the observed radium variability in the bay.

The Mediterranean climate of coastal California is characterized by hot, dry summers and cool, wet winters. In such a climate, precipitation and PET peak during opposite times of the year, causing alternating periods of highly positive and negative recharge during the winter and summer, respectively. These alternating periods of positive and negative recharge suggest a similar but perhaps stronger seasonal component of SGD than was documented previously for Waquoit Bay, Massachusetts. A numerical model was developed using SEAWAT-2000 (Langevin et al. 2003), a variable density groundwater flow code, to investigate the issue of seasonally variable SGD from a coastal

unconfined aquifer forced by a Mediterranean climate. The study focuses specifically on understanding the timing and relative magnitude of fresh SGD at sites similar to Stinson Beach, California, a coastal community northwest of San Francisco where substantial SGD-derived nutrient fluxes have been documented due to nutrient-enrichment of fresh groundwater by on-site wastewater treatment systems (de Sieyes et al. 2008, 2010).

4.3 METHODS

A numerical model was developed using SEAWAT-2000 (Langevin et al. 2003), a variable density groundwater code based on the popular groundwater flow code MODFLOW-2000 (Harbaugh et al. 2000) and the multi-species solute transport code MT3DMS (Zheng and Wang 1999). For SEAWAT-2000, Guo and Langevin (2002) derived the governing equation for variable-density groundwater flow in three dimensions as a function of equivalent freshwater head:

$$\frac{\partial}{\partial\alpha}\left[\rho K_{f\alpha}\left(\frac{\partial h_f}{\partial\alpha}+\frac{\rho-\rho_f}{\rho_f}\frac{\partial Z}{\partial\alpha}\right)\right]+\frac{\partial}{\partial\alpha}\left[\rho K_{f\beta}\left(\frac{\partial h_f}{\partial\beta}+\frac{\rho-\rho_f}{\rho_f}\frac{\partial Z}{\partial\beta}\right)\right]$$
$$+\frac{\partial}{\partial\alpha}\left[\rho K_{f\gamma}\left(\frac{\partial h_f}{\partial\gamma}+\frac{\rho-\rho_f}{\rho_f}\frac{\partial Z}{\partial\gamma}\right)\right]=\rho S_f\frac{\partial h_f}{\partial t}+\theta\frac{\partial\rho}{\rho C}\frac{\partial C}{\partial t}-\rho_s q_s \tag{4.1}$$

where α, β, and γ are orthogonal coordinate axes aligned with the principal directions of permeability, K_f (LT^{-1}) is freshwater hydraulic conductivity, S_f (L^{-1}) is the freshwater storage coefficient, t (T) is time, θ is the effective porosity (-), ρ (ML^{-3}) is fluid density, ρ_f (ML^{-3}) is freshwater density, and ρ_s and q_s are the density and flow rate per unit volume of aquifer of the source or sink (T^{-1}). Equivalent freshwater head h_f (L) is calculated as a function of head h (L) in native groundwater using the following equation:

$$h_f=\frac{\rho}{\rho_f}h+\frac{\rho-\rho_f}{\rho_f}Z \tag{4.2}$$

where Z (L) is elevation at the measurement point. SEAWAT-2000 uses a linear equation of state to express fluid density as a function of salt concentration (C):

$$\rho = \rho_f + \frac{\partial \rho}{\partial C} C \tag{4.3}$$

where $\frac{\partial \rho}{\partial C} = 0.7143$ ($M_{fluid}\ M_{salt}^{-1}$).

The governing equation for conservative transport of dissolved species in the model is (Zheng and Wang 1999):

$$\frac{\partial (\theta C_k)}{\partial t} = \frac{\partial}{\partial x_i}\left(\theta D_{ij} \frac{\partial C_k}{\partial x_j}\right) - \frac{\partial}{\partial x}\left(\theta v_i C_k\right) + q_s C_k^s \tag{4.4}$$

where C_k (ML^{-3}) is the concentration of dissolved species k, D_{ij} (L^2T^{-1}) is the hydrodynamic dispersion tensor, v_i (LT^{-1}) is the linear porewater velocity, and C_k^s is the concentration of species k from the source or sink.

Groundwater flow (Eq. 1) and salt transport (Eq. 2) are mutually-dependent, coupled processes that are solved simultaneously by the program using a cell-centered finite-difference approximation. In each cell, Equations 1 and 2 are explicitly coupled to calculate fluid density using concentrations from the previous time step.

A model was developed to represent a cross-shore section of an idealized coastal aquifer with a fresh landward boundary and a saline, constant head seaward boundary (Fig. 4.1). Model aquifer characteristics were chosen not to mimic Stinson Beach conditions specifically, but do in a few cases closely match observations of key aquifer characteristics from the field, specifically aquifer thickness (b = 32 m; SBCWD 1998), hydraulic conductivity (K = 6 m day^{-1}; Chapter 5 from this dissertation), precipitation and evapotranspiration rates calculated from actual data collected near the site, and fresh groundwater flow entering the beach from the inland boundary of the model (see Chapter 5 from this dissertation). For this reason, we consider this model a hybrid whose results

can be compared with those from other similar numerical groundwater simulations (Michael et al. 2005), but which may also have direct implications for the Stinson Beach site specifically.

The domain is 350 m long by 35 m tall and includes two distinct zones, an aquifer zone (A) and an ocean zone (B), all underlain by a no-flow boundary representing an impermeable aquifer base (Fig. 4.1). The ocean zone is characterized by high hydraulic conductivity (10^6 m day^{-1}), 100% effective porosity, and constant salt concentrations of 35 ppt. Representing open water as highly conductive porous media has been used in a number of recent SGD studies (Mao et al. 2006; Robinson et al. 2007) but has limitations. Specifically, the application of Darcy's Law may not be theoretically valid in high hydraulic conductivity cells due to large local flow rates. However, the effects of this limitation on our model results are expected to be relatively small, since only the mass balance of water and salt in the aquifer zone is reported. The aquifer zone is homogeneous and anisotropic, and has hydraulic characteristics typical of a beach sand aquifer, including hydraulic conductivity typical for clean, consolidated beach sands (K_x=6 m day^{-1}; K_z=3 m day^{-1}), 35% porosity, and 25% effective porosity (Fetter 2001). Longitudinal dispersivity (α_L=0.5 m) and transverse dispersivity (α_T=0.05 m) were chosen to minimize unrealistic backward dispersion of salt into the fresh portion of the aquifer, following Robinson et al. (2007). These values are at the lower end of typical values (Gelhar et al. 1992) and are thus expected to provide conservative estimates of mixing (Robinson et al. 2007). At the seaward edge of the domain, bordering both the open water zone and the undersea aquifer zone beneath it, is a constant-head, constant concentration ocean boundary of marine salinity (h=0 m; C=35 ppt). Two landward boundary conditions were simulated in two model runs, Model 1 and Model 2. Model 1 included a constant head (h=2 m) constant concentration (C = 0 ppt) boundary condition. For comparison, Model 2 included a constant concentration (C = 0 ppt) constant flux (q_{cell}=6.86 x 10^{-2} m) landward boundary condition where q_{cell}, the darcy flux of water into the domain from each cell, equals the product of hydraulic gradient i (0.014, or 2 m head drop per 175 m distance) and hydraulic conductivity K_x (6 m day^{-1}). The beach face between the open water and aquifer is characterized by a 10% grade and a 5 m depth at the seaward break in slope. This slope is steeper than Stinson Beach (0.037; de Sieyes et

al. 2008) and was chosen as a compromise between accurate representation of Stinson Beach site characteristics and the development of a seepage face, a feature of shallow sloping beaches which can not be modeled accurately using SEAWAT-2000 (Robinson et al. 2007; see description of drying/rewetting function below). The intersection of mean sea level and the beach face occurs 175 m from both the seaward and landward edges of the domain.

SEAWAT-2000 uses a drying/rewetting function to simulate dewatering of cells at the phreatic surface. When the calculated head in a cell drops below the elevation of the bottom of the cell, the cell is made inactive. In the case of a rising water table, cells are re-wetted once the water level in adjacent cells rises above a threshold value. Discharge only occurs between active cells in the aquifer and ocean zones; the model does not allow for the development of a seepage face, although subaerial seepage has been shown to be an important route for groundwater discharging to the ocean (Urish and McKenna 2004). The inability to properly model a seepage face is a major limitation of the present model.

Recharge to the model was applied to the phreatic surface in the highest active (non-dry) cells. Average monthly recharge was calculated as the sum of average monthly precipitation (positive) and average monthly evapotranspiration (ET; negative). Average monthly precipitation was calculated from a 79-year dataset recorded at Kentfield, California, 8.5 km from Stinson Beach (ncdc.noaa.gov, Station #044500; 37°57'N/122°33'W). For the purposes of our modeling exercise, ET was assumed equal to PET, which itself was calculated following Thornthwaite (1957) using monthly mean temperatures from 70 years of data measured at Muir Woods, California, 6.8 km from the site (ncdc.noaa.gov, Station #046027; 37°54'N/122°34'W). The Thornthwaite method was previously used by Michael et al. (2005) to estimate PET at the Waquoit Bay site, and we chose it over other widely accepted methods for calculating PET primarily for the purposes of direct comparison. The use of PET as ET assumes complete ground coverage and shading by a short green crop of uniform height, and adequate water for evapotranspiration. These assumptions are valid for the Stinson Beach field site in winter, when grassy ground cover is nearly complete and the water table is very shallow, but may

fail in summer when the water table recedes. For this reason, the assumption that PET equals ET may overestimate ET at the Stinson Beach site during summer.

Numerical simulations included a single steady-state stress period followed by a series of transient stress periods. Initial conditions included a salt distribution roughly characteristic of a diagonal saltwater wedge extending inland with depth, as predicted by the Ghyben-Hertzberg relationship (Fetter 2001), and initial heads set to the top elevation of each cell in the domain. The initial stress period included zero recharge and was run to steady state. Following the initial steady-state stress period, the top active cells in the aquifer zone landward of the mean water line are recharged as outlined above during month-long stress periods, each repeating annually over an 3-year period. Model simulations were ceased when pseudo steady state was reached such that discharge from the aquifer zone for all months in the annual cycle agreed to within 0.1% with the results from the same month a year prior.

The predicted hydrograph of simulated discharge per month is compared with monthly mean discharge data from a 25-year stream gauge record for Lagunitas Creek, a local creek 24 km north-northwest of Stinson Beach which drains a 212 km^2 area of similar geology and is gauged at Point Reyes Station, California (waterdata.usgs.gov; ID# 11460600; 38°05'N/122°47'W).

To compare the timing of the decline in discharge for Models 1 and 2 and Lagunitas Creek, each monthly discharge was normalized to the maximum and minimum discharge values in each series using the equation:

$$Q_{t,norm} = 1 - \frac{(Q_{\max} - Q_t)}{(Q_{\max} - Q_{\min})} \qquad (4.5)$$

where Q_{max} and Q_{min} are the maximum and minimum monthly discharge in the series, and Q_t and $Q_{t,norm}$ are the discharge and normalized discharge for each month t. The rate of decay of $Q_{t,norm}$ from Q_{max} to Q_{min} was then quantified for each time series using least squares regression.

4.4 RESULTS

Mean monthly precipitation rates from the 79-year Kentfield record are reported in Figure 4.2. Precipitation is approximately sinusoidal on the annual timescale, peaking at 18.2 cm $month^{-1}$ in January and reaching a minimum of 0.3 cm $month^{-1}$ in July. Also shown in Figure 4.2 are monthly average PET rates predicted by Thornthwaite (1957) using temperature data from the Muir Woods site. By convention, PET is shown as a negative rate, representing a loss term. PET follows a pattern similar to that of precipitation, reaching a minimum of -2.1 cm $month^{-1}$ in December and January and a maximum of -11.2 cm $month^{-1}$ in July. Lastly, Figure 4.2 shows recharge to the model aquifer per month, calculated as the sum of precipitation and PET. As with precipitation and PET, recharge is approximately sinusoidal on the annual timescale, reaching a minimum of -10.9 cm $month^{-1}$ (extraction) in July and a maximum of 16.5 cm $month^{-1}$ (infiltration) in January.

The steady state salt distribution achieved in the model domain prior to applying recharge in transient stress periods is shown in Figure 4.3. The distribution is typical of simulated coastal aquifer systems in which SGD is occurring. Specifically, fresh groundwater flows seaward from the landward boundary, meeting dense saline groundwater beneath the beach face. The dense saltwater displaces freshwater at depth, recreating the classic Ghyben-Hertzberg relationship for coastal groundwaters whereby a freshwater lens thinning towards the beach face overlies a saltwater wedge extending inland at depth.

Pseudo-steady state discharge results for Models 1 and 2 are presented for each month in Figure 4.4. Also shown for comparison are monthly mean discharges for Lagunitas Creek as calculated from the 25-year record measured at the Point Reyes Station gauge. In Models 1 and 2, peak discharge Q_{max} occurred in January at 4.4 and 3.1 $m^3\ day^{-1}\ m^{-1}$, respectively, coincident with the period of highest recharge (Fig. 4.2). By comparison, Lagunitas Creek Q_{max} occurred in February at a rate of $1.0 \times 10^6\ m^3\ day^{-1}$. Discharge in each time series decayed approximately exponentially to a minimum (Q_{min}) in September. Simulated discharge in Models 1 and 2 at that time was 3.7 and 2.6 $m^3\ day^{-1}\ m^{-1}$, respectively. Q_{min} for Lagunitas Creek occurred in September at $1.8 \times 10^4\ m^3\ day^{-1}$. These minimum discharges lag the period of minimum recharge (July) by two months.

For Models 1 and 2, the Q_{min} values predicted for September represent declines of 17% and 18% from the Q_{max} values predicted for January. By comparison, the decline in Lagunitas Creek discharge between Q_{max} in February and Q_{min} in September is 98%.

Monthly values of $Q_{t,norm}$ calculated using Eq. 4 and plotted in Figure 4.5. In each time series, $Q_{t,norm}$ appeared to decay approximately exponentially from the maximum to minimum values, so an exponential function was fit to each dataset. The exponential decay in $Q_{t,norm}$ was faster for Lagunitas Creek (k = -1.15; R^2 = 0.96) than for Model 1 (k = -0.953; R^2 = 0.95) or Model 2 (k = -0.896; R^2 = 0.90).

4.5 DISCUSSION

Precipitation and potential evapotranspiration was approximately sinusoidal on the annual timescale, creating a sinusoidal annual recharge curve with highest infiltration rates in winter and highest evapotranspiration rates in summer. These results highlight the highly seasonally variable recharge characteristics typical of the Mediterranean climate of coastal California.

Discharge of both modeled groundwater and Lagunitas Creek peaked in January and February, respectively, approximately coincident with the period of highest precipitation. The lack of a substantial lag time between peak recharge and peak groundwater discharge was surprising, considering the results of a similar published study by Michael et al. (2005), who modeled discharge from a coastal aquifer in Waquoit Bay, Massachusetts, with forcing only by annual recharge cycles typical for the northeastern United States. In their study, differences between the minimum and maximum simulated SGD values were on the order of 20%, similar to the values reported herein, but peak simulated SGD lagged peak recharge by two- to three months. By comparison, our simulations shows peak SGD occurring coincident with peak recharge. Differences in boundary conditions and model design may explain the difference in predictions. Specifically, Michael et al. (2005) simulated recharge to an aquifer extending 500 m inland of the ocean boundary, 325 m longer than the model aquifer described herein. In their model, the inland edge of the aquifer was bounded by a no-flow boundary, and all fresh water in the model came only from recharge to the phreatic surface. By comparison, our shorter simulated aquifer is recharged at the phreatic surface

and also at the inland boundary, with between 0% and 20% of the fresh discharge coming from recharge and the rest coming from the inland constant-head boundary. For this reason, we do not consider the magnitude of the sustained annual discharge, which varied substantially between Models 1 and 2, to be particularly instructive or predictive of real world conditions. Rather, we focus our attention on the seasonal variation in discharge, which agreed well between the two models despite their different boundary conditions.

Specifically, if we assume that the simulated monthly SGD values presented here accurately reflect the general seasonal trends, if not the precise magnitude of actual SGD from some coastal California aquifers, the subtle differences between the normalized records of simulated SGD and creek discharge may be environmentally important. As per the exponential curve fits of $Q_{t,norm}$, modeled SGD declined slower from winter to fall than did Lagunitas Creek discharge, which declined relatively quickly. For example, by June, $Q_{t,norm}$ for Lagunitas Creek was at 6%, while $Q_{t,norm}$ for Models 1 and 2 were at 16% and 39%, respectively. The difference was more stark in July, when Lagunitas Creek $Q_{t,norm}$ had dropped to just 1% but $Q_{t,norm}$ for Models 1 and 2 remained comparatively high at 9% and 27%, respectively. Because nutrient concentrations in fresh coastal groundwaters are often much higher than in surface waters (Slomp and Van Cappellen 2004), sometimes by orders of magnitude (de Sieyes et al. 2008, 2010), the sustained discharge of fresh SGD through summer may represent an important nutrient source for mid-summer phytoplankton blooms in California. This idea was recently proposed by Santoro et al. (2010), who observed a significant positive linear correlation between mean summer chlorophyll a concentrations in the Southern California Bight and total rainfall the prior winter, and theorized that nutrient inputs from either runoff or SGD might be sustaining nearshore phytoplankton growth through the summer months. Our results are consistent with the theory that substantial SGD-associated nutrient flux might be occurring in mid-summer, and additional research should be conducted to further investigate this potentially important process.

To increase confidence in the temporal trends in simulated discharge observed in this study, additional simulations should be conducted and should include a variety of realistic aquifer geometries, aquifer properties, and boundary conditions. Additionally, our assumption that ET equals PET likely overestimates ET in the mid- to late summer

when water table drops below the root zone and grasses die off, thereby reducing transpiration. More robust estimations of ET should be incorporated into future simulations.

Figure 4.1. Model layout showing model dimensions, zones, and boundary conditions. Distance and elevation are shown on the x- and y-axis, respectively. The aquifer zone (Zone A) is shaded gray and the open water zone (Zone B) is white. Also shown are the constant-head, constant-concentration condition at the landward boundary (h = 2 m; C = 0 ppt; left side) used in Model 1, and the seaward boundary (h = 0 m; C = 35 ppt) used in both Model 1 and Model 2. The beach slope is θ where tan(θ)=0.1.

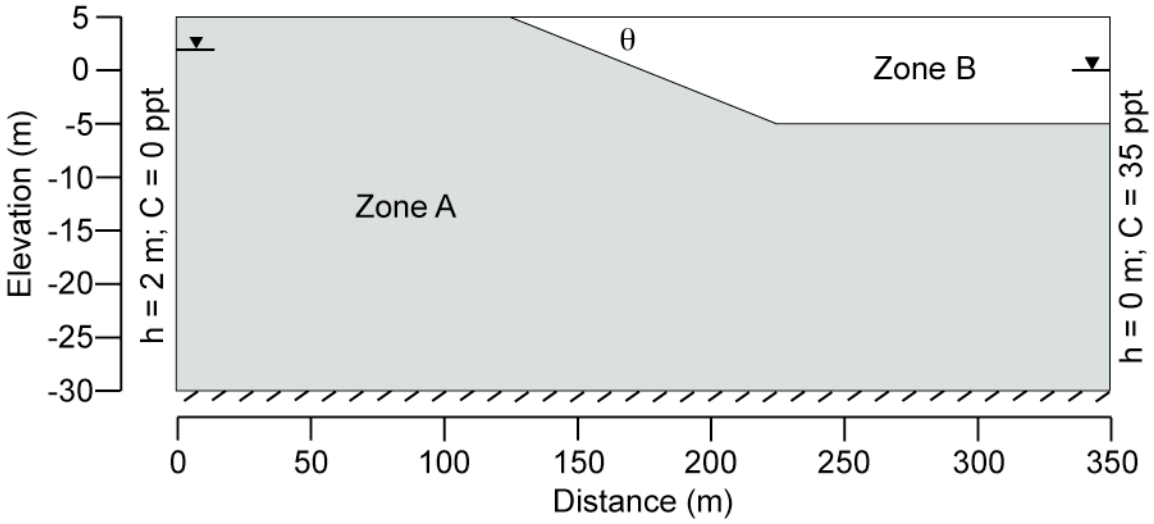

Figure 4.2. Monthly time series of mean precipitation measured at Muir Woods, California, mean potential evapotranspiration (PET) calculated using Thornthwaite (1957) from temperature data recorded at Kentfield, California, and mean recharge calculate as the difference between precipitation and PET. The model assumes that potential and actual evapotranspiration are equal.

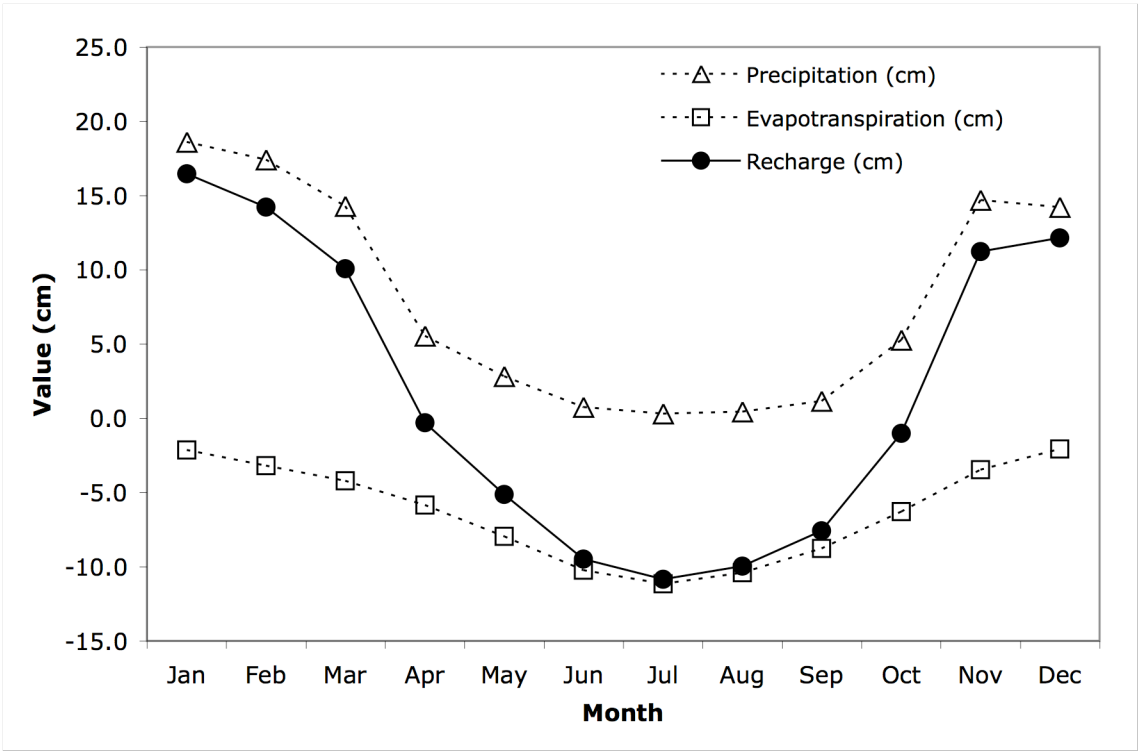

Figure 4.3. Distribution of salt and equivalent freshwater head in the domain of Model 1 under steady-state conditions with no recharge and a constant head boundary condition at the inland (left) edge. A similar steady state distribution of head and salt was observed for Model 2. Heads are contoured with an interval of 0.2 m.

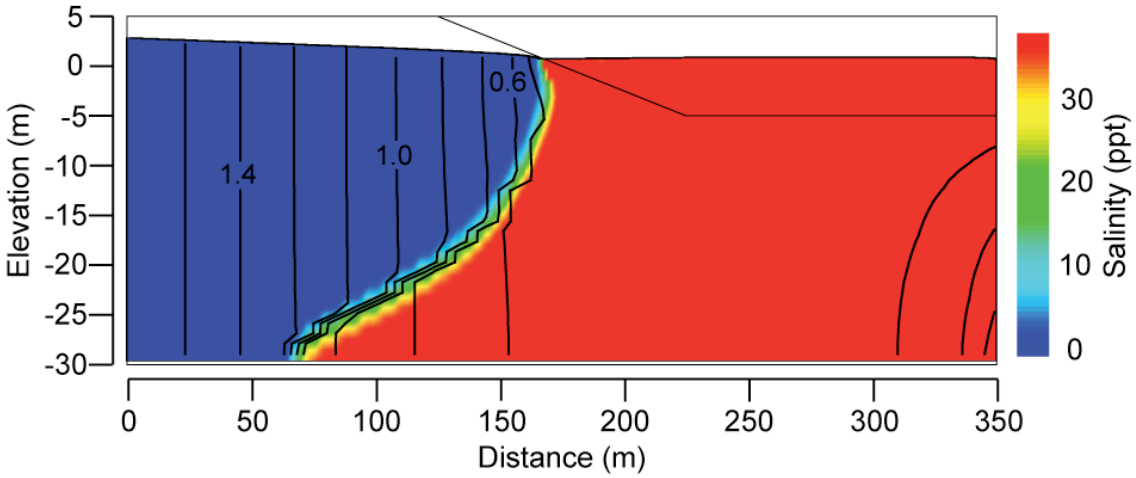

Figure 4.4. Hydrograph of pseudo steady state simulated fresh discharge from the model aquifer zone to the ocean zone by month. Also shown for comparison are monthly mean discharges for Lagunitas Creek, as measured at the Point Reyes Station gauge.

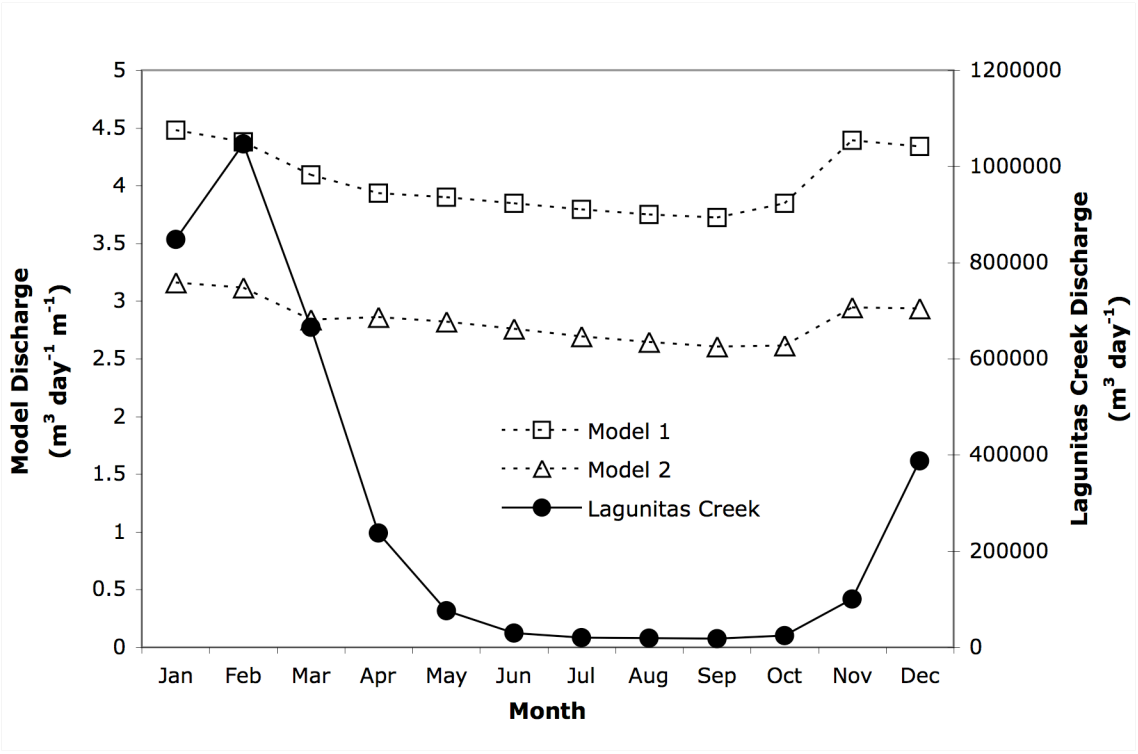

Figure 4.5. Hydrograph of normalized discharge from Models 1 and 2 and Lagunitas Creek. For each data series, $Q_{t,norm}$ each month is normalized to the maximum and minimum discharge values in the series using Eq. 5, and only data for the period of maximum to minimum discharge is shown.

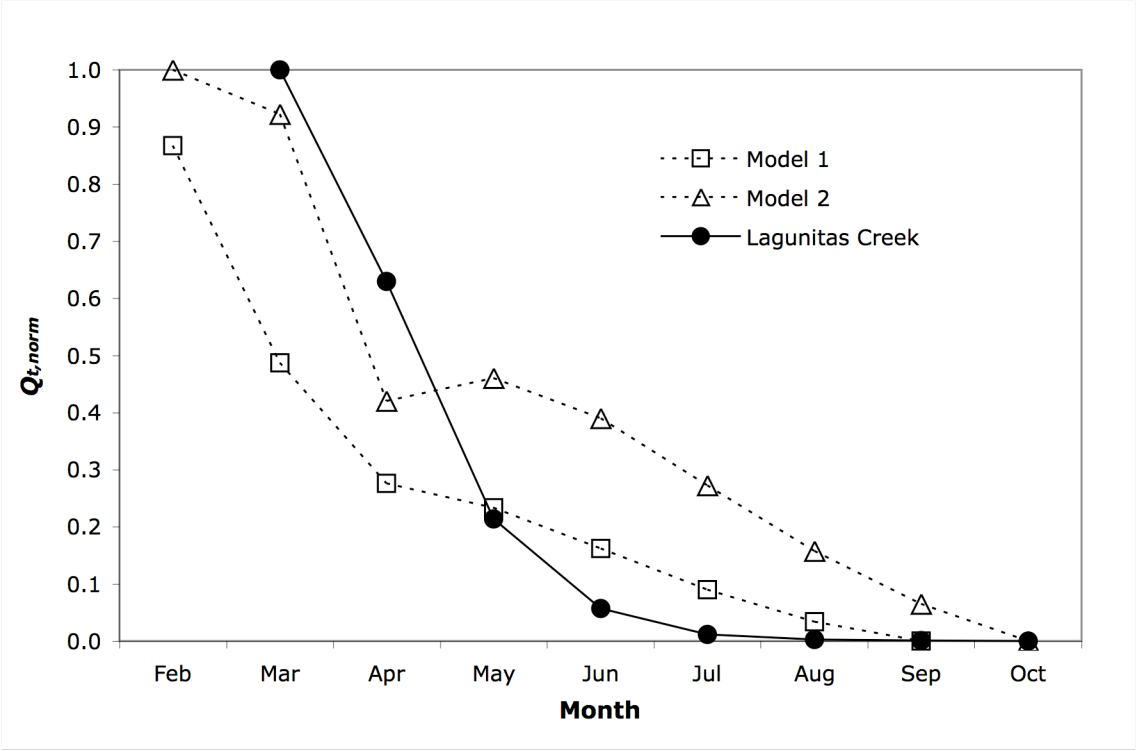

4.6 REFERENCES CITED

de Sieyes, N. R., K. M. Yamahara, B. A. Layton, E. H. Joyce, and A. B. Boehm. 2008. Submarine discharge of nutrient enriched fresh groundwater at Stinson Beach, California is enhanced during neap tides. Limnology and Oceanography **53**: 1434-1445.

de Sieyes, N. R., K. M. Yamahara, A. Paytan, and A. B. Boehm. 2011. Submarine groundwater discharge to a high-energy surf zone at Stinson Beach, California, estimated using radium isotopes. Estuaries and Coasts **34**: 256-266.

Gelhar, L.W., C. Welty, and K.R. Rehfeldt. 1992. A critical review of data on field-scale dispersion in aquifers. Water Resources Research. **28**: 1955–74.

Guo, W., and C. D. Langevin. 2002, User's guide to SEAWAT: A computer program for simulation of three-dimensional variable-density ground-water flow: U.S. Geological Survey Techniques of Water- Resources Investigations, book 6, chap. A7, 77 p.

Harbaugh, A.W., E.R. Banta, M.C. Hill, and M.G. McDonald. 2000. MODFLOW-2000, The US Geological Survey modular ground-water model – user guide to modularization concepts and the ground-water flow process, US Geological Survey Open File Report 00-92; 2000

Langevin, C., W. B. Shoemaker, and W. Guo. 2003. Modflow-2000, The US Geological Survey modular ground-water model – documentation of the Seawat-2000 version with the variable density flow process (VDF) and the integrated MT3DMS transport process (IMT). US Geological Survey Open-File Report 03-426.

Li, L., D. A. Barry, F. Stagnitti, and J.-Y. Parlange. 1999. Submarine groundwater discharge and associated chemical input to a coastal sea. Water Resour. Res. **35**: 3253–3259.

Longuet-Higgens, M. S. 1983. Wave set-up, percolation and undertow in the surf zone. P. Roy. Soc. Lond. A Mat. 390: 283–291.

Mao, X., P. Enot, D.A. Barry, L. Li, A. Binley, and D-S. Jeng. 2006. Tidal influence on behaviour of a coastal aquifer adjacent to a low-relief estuary. Journal of Hydrology **327**:110–127.

Michael, H. A., A. E. Mulligan, and C. F. Harvey. 2005. Seasonal oscillations in water exchange between aquifers and the coastal ocean. Nature. **436**: 1145-1148.

Santoro, A.E., N.J. Nidzieko, G.L. van Dijken, K.R. Arrigo, and A.B. Boehm. 2010. Contrasting spring and summer phytoplankton dynamics in the nearshore Southern California Bight. *Limnology and Oceanography*. **55**: 264-278.

Slomp, C. P., and P. Van Cappellen. 2004. Nutrient inputs to the coastal ocean through submarine groundwater discharge: controls and potential impact. J. Hydrol. **295**: 64-86.

Thornthwaite, C. W. 1957. Instructions and tables for computing potential evapotranspiration and the water balance. Publications in Climatology X, 185-243.

Urish, D.W., and T.E. McKenna. 2004. Tidal Effects on Ground Water Discharge Through a Sandy Marine Beach. Ground Water. **42**: 971–982.

Zheng, C., and M.C. Wang. 1999. MT3DMS - A modular three-dimensional multispecies transport model for simulation of advection, dispersion and chemical reactions of contaminant in ground-water systems; documentation and user's guide. US Army Corps of Engineers Contract Report SERDP-99-1.

CHAPTER 5: NITROGEN, FECAL INDICATOR BACTERIA, AND COLIPHAGE ATTENUATION AND FLUX FROM A SEPTIC LEACH FIELD TO THE COASTAL OCEAN

This chapter benefited greatly from the assistance of Todd Russell, who conducted the denitrification potential slurry assays and saturated column experiments, Nigel Crook, who assisted with the collection of resistivity data in the field, and Cynthia McClain, who assisted with the estimation of hydraulic conductivity using the tidal efficiency method. Tim Julian and Kevan Yamahara are acknowledged for assistance in the field and laboratory. The research was supported by a grant from the Environmental Ventures Program of the Woods Institute for the Environment at Stanford University and by the National Sea Grant College Program of the U.S. Department of Commerce's National Oceanic and Atmospheric Administration under NOAA Grant NA04OAR4170038, Project R/CZ-197, through the California Sea Grant College Program. The views expressed herein do not necessarily reflect the views of either California Sea Grant or the Woods Institute for the Environment.

5.1 ABSTRACT

A two-year field study was conducted to measure attenuation and flux of nitrogen, fecal indicator bacteria, and bacteriophage in groundwater adjacent to a coastal septic system in Central California. The study was carried out at Stinson Beach Park, an open ocean marine beach located northwest of the San Francisco. Septic effluent quality and volumetric discharge to the leach field, synoptic DC resistivity profiling of the saltwater/freshwater interface, continuous hydraulic head in the coastal aquifer, and chemical and microbiological concentrations within dense array of multi-level monitoring wells adjacent to the leach field were measured. A nitrogen- and inorganic carbon-rich plume of septic effluent flowed from the leach field through the beach to the subterranean estuary, or the mixing zone of fresh and saline groundwaters. Attenuation of E. coli and coliphage was complete within the vadose zone. Enterococci were detected in the well network during two of three sampling events. Median estimates of total nitrogen flux toward the ocean downgradient from the leach field ranged from 1.6 to 70.6 moles day-1, depending on season and transect location. Consistently increasing fluxes of nitrate and decreasing fluxes of ammonium with distance from the leach field suggest nitrification as groundwater flows toward the tidal boundary. Laboratory experiments demonstrated fast fecal indicator bacteria and virus attenuation rates in saturated column experiments. However, one field sampling event demonstrated increasing enterococci fluxes with distance from the leach field, suggestive of growth or exogenous inputs along the flowpath. The septic system currently appears to be an occasional soure of enterococci and a persistent source of nitrogen to the subterranean estuary. However, laboratory measurements of aquifer denitrification potential suggest a possible role for advanced in-situ remediation of nitrogen under optimized field conditions.

5.2 INTRODUCTION

In the United States, nearly 25% of the population uses on site treatment systems, or septic systems, for wastewater disposal (US Census Bureau 1997). Incomplete treatment of septage as it infiltrates through the vadose zone from a leach field can result in contamination of surficial aquifers by pathogens, fecal bacteria, and nutrients (Robertson et al. 1991, Swartz et al. 2006). Thus, septic systems are considered one of the greatest threats to groundwater quality in the United States (US EPA 2005). Of particular concern is the potential for groundwater polluted by septic systems to enter surface water systems, thereby threatening the health of aquatic ecosystems and recreational users.

The present study investigates the degree to which a coastal septic system pollutes groundwater, and the potential for that septage-contaminated coastal groundwater to adversely impact coastal water quality via submarine groundwater discharge (SGD). SGD is the direct flow of groundwater to the ocean, regardless of composition or driving force (Burnett et al. 2006). It is a globally important process and a documented source of ecologically important elements, nutrients, and contaminants to the coastal ocean (de Sieyes et al. 2008, Bone et al. 2007, Kroeger et al. 2007).

This study focuses on fate and transport of three key septage-borne groundwater contaminants - nitrogen, fecal indicator bacteria, and coliphage – and chemical markers typical of septic effluent-impacted groundwater at a single coastal septic system adjacent to the subterranean estuary, the mixing zone of fresh and saline groundwaters at the land/sea interface. Specifically, the study quantifies the system's direct impacts on groundwater quality with respect to each contaminant, attenuation along the flowpath downgradient from the leach field, and total contaminant flux to the subterranean estuary. Field work is complemented with several lab experiments to quantify contaminant removal potential. A dense well network including three multilevel well transects was installed, allowing for the calculation of seaward contaminant flux using the Theissen polygon transect method (Einarson & Mackay, 2001; Borden et al. 1997). The work was conducted at Stinson Beach, a central California residential beach community sixteen kilometers north of San Francisco.

There is a well-established conceptual model of the fate of septage constituents (Wilhelm et al. 1994). Specifically, low-Eh septage rich in ammonium and organic nitrogen, carbon, fecal indicator bacteria and virus (FIBV) is pumped to a leach field, dispersed into the unsaturated zone, and travels vertically through the vadose zone to the saturated zone. In the vadose zone, DO is readily available and NH_4^+ is nitrified to NO_3^-, DON and DOC are oxidized aerobically, releasing NO_3^-, DIC and acid. FIBV are removed by mechanical filtration, adsorption, and die-off. In the saturated zone downstream from the leach field, DO is consumed during further oxidation of DOC, increasing DIC and decreasing pH. Additional removal of FIBV occurs if treatment in the vadose zone is incomplete. Stratification of DIN in saturated groundwater may occur due to redox-dependant nitrogen cycling influenced by the availability of labile organic carbon and dissolved oxygen (DO). While this conceptual model has been confirmed at inland locations (Wilhelm et al. 1996), it has not been tested in a coastal setting. Our experiment design allows the investigation of the conceptual model described above by testing the significance of relationships between key products, reactants, and porewater characteristics above, including DIC, DOC, DIN, DON, pH and Eh.

5.3 METHODS AND MATERIALS

5.3.1 STUDY SITE.

The Stinson Beach (37.899 N, 122.646 W; Fig. 5.1) climate is Mediterranean with annual precipitation of 60 to 120 cm occurring between October and April (SBCWD 1998). The beach aquifer is composed of seasonally deposited fine-grained, well-sorted beach sands (de Sieyes et al. 2008) and alluvium underlain by lacustrian clays. The entire unit is underlain by the Franciscan Complex (SBCWD 1998). The town and adjacent Stinson Beach Park use on site conventional septic systems for wastewater treatment exclusively. Our research focuses on contaminant flux and attenuation adjacent to one large septic system at Stinson Beach Park. In this system, effluent is piped from five septic tanks servicing various Park buildings into a large central 18.9 m^3 wet well for temporary storage before being pumped to a 200 m^2 leach field near the beach (Fig. 5.1). Float-triggered pumps deliver 3.8 m^3 pulses of septage to the leach field; the timing of

each pumping event is logged. Additional information about site hydrogeology and septic system characteristics can be found in the SI.

5.3.2 Well installation.

Seventeen 2" PVC water table wells and an array of 116 nested ¼" LDPE and ¾" PVC samplers were installed. The 2" wells were installed within 200 m of the leach field to monitor hydraulic head and background groundwater quality. The nested samplers each consisted of three ¼" LDPE tube samplers with 1.5 m screens nested around a central ¾" PVC sampler with a 1.5 m screen, all staggered vertically for depth-descrete sampling. Three transects of samplers, Transects A, B, and C (Fig. 5.1), were installed approximately orthogonal to groundwater flow 5, 10, and 15 m downgradient from the leach field. A detailed description of well construction and installation at the site is included in the SI.

5.3.3 Head measurements.

From May 2008 to January 2010, manual synoptic head measurements were collected approximately quarterly in the 2" wells using a standard water level indicator (Slope Indicator, Mukilteo, WA). During the same period, continuous head measurements were collected using an array of continuous datalogging pressure transducers (Solinst, Georgetown, Ontario, Canada) installed in a subset of the 2" well array. Monthly head data were binned for each well, and linear regression was used to create a time series of monthly hydraulic gradients +/- standard deviation across the site for each month (see SI for additional details).

5.3.4 Electrical resistivity profiling.

Synoptic DC electrical resistivity transect (ERT) profiling was conducted on 22-23 November 2008 and again on 4-5 April 2009 to characterize and monitor changes to aquifer electrical resistivity (σ) over tidal- and seasonal timescales. Porewater conductivity primarily controls subsurface resistivity in coastal hydrogeologic environments, and we assume that substantial variation in σ at depth is due to variation in porewater salinity (Stieglitz 2005). ERT surveys were conducted at low-low, high-high, high-low, and low-high tide along 40 m cross-shore lines extending from the leach field

to the water line (Fig. 5.1) using a 48-electrode Syscal R1+ system in a Wenner configuration. Total reciprocal error was <10% for each survey. In order to improve data quality, measurements with reciprocal errors >5% (~20% of measurements) were omitted. Each σ model was interpreted using a quadrangular finite element-based forward solution with 'Occam's' style inversion (Constable et al. 1987).

5.3.5 HYDRAULIC CONDUCTIVITY ANALYSIS AND RESIDENCE TIME ESTIMATION.

Eleven estimates of hydraulic conductivity (K) were produced using the tidal efficiency method (Ferris 1951). This method enables measurement of aquifer characteristics based on the propagation of tides through the aquifer, and improves upon slug testing and bench-top methods because it incorporates spatial variability (Millham and Howes, 1995). The SI provides details of the method.

An estimate of residence time τ (days) for water within the well network was made using a formulation of Darcy's Law:

$$\tau = \frac{Ln_e}{Ki} \tag{5.2}$$

where L is length (m), n_e is effective porosity (-), K is hydraulic conductivity (m day^{-1}), and i is hydraulic gradient (-).

5.3.6 WATER SAMPLING.

Sampling of the wet well was conducted approximately every two months between June 2008 and August 2009. Sampling of the entire monitoring network was conducted in three site-wide day-long "snapshot" sampling events on 22 November 2008, 5 April 2009, and 9 August 2009. During each snapshot event, samples were collected from the wet well, all clustered multi-level samplers in the well network, and all 2" monitoring wells upgradient from the leach field. Prior to sampling a well, three well volumes were purged using a dedicated LDPE sample tube. Samples were then collected for chemical and microbiological analysis using dedicated 10% HCl acid-washed all-plastic syringes. Care was taken to sample slowly to avoid bubbling and cross-contamination from vertical flow in nested wells. Measurements of pH were made in the

field using an electrode (Thermo Scietific, Beverly, MA). Whenever samples were collected from the wet well or along the centerline of the plume in the well network (wells A05, B05.5, and C06, Fig. 5.1), measurements of temperature, electrical conductivity, dissolved oxygen, pH, and oxidation-reduction potential were made using a peristaltic pump, a flow-through cell and sonde (Hydrolab, Loveland, CO).

5.3.7 CHEMICAL AND MICROBIOLOGICAL ANALYSIS.

60 mL of water was 0.2 μm PES filtered (Millipore, Billerica, MA) and stored in 10% HCl acid-washed high-density polyethylene bottles at -20°C for nutrient analyses including nitrate, nitrite, ammonium, total nitrogen (TN), dissolved inorganic nitrogen (DIN), dissolved organic nitrogen (DON). Details and detection limits for the standard analytical methods used are in the SI.

Twenty-two mL of water were 0.2 μm PES filtered and stored without headspace in 10% HCl acid-washed amber glass vials at 4°C for dissolved carbon analyses including total dissolved carbon (TC), dissolved inorganic carbon (DIC), and dissolved organic carbon (DOC). Analytical methods and detection limits are in the SI.

Unfiltered samples were collected for analysis of two fecal indicator bacteria (FIB), *E. coli* and enterococci using EPA methods 1603 and 1600, respectively (USEPA 2000a, 2000b; see SI for details). The upper and lower detection limits for each method are 1000 and 2 colony forming units (cfu) $(100\ mL)^{-1}$, respectively. Unfiltered samples were also collected for two viral indicators of fecal pollution in groundwater, male specific (F+) and somatic coliphage, which were analyzed by the single agar layer method following EPA method 1602 (USEPA 2001), within 24 h of collection. The lower and upper detection limits of detection for this method were 2.5 and 250 plaque forming units (pfu) $(100\ mL)^{-1}$.

Contaminant flux calculations. Nutrient and microbiological fluxes associated with septage pumped to the leach field were calculated based on mean and standard deviation values of septage discharge rate and contaminant concentrations in the wet well. Fluxes associated with groundwater flowing through multi-level monitoring well transects downstream from the septic leach field were made using the Theissen polygon transect method (Borden et al. 1997) with a Monte Carlo approach. The Theissen

polygon method enables the estimation of total contaminant flux through a flow-orthogonal control plane as a sum of the fluxes through the component sections making up that control plane. Contaminant flux in each component sections can be calculated as the product of the concentration *C* flowing through the component section, the section area *A,* and a Darcy velocity *K*i*, where *K* is hydraulic conductivity and *i* is hydraulic gradient orthogonal to the section. The method assumes that well transects bisect the entire plume such all plume mass flows through each transect. Further details about the Theissen polygon transect method can be found in the SI. A Monte Carlo model was developed to calculate contaminant flux through each transect in each of 10,000 iterations for each of three monitoring snapshots. For each iteration, random normally-distrubuted values of *i* and log(*K*) were chosen based on all *K* estimates and monthly binned *i* values for the month of the snapshot in question. Each iteration also incorporated direct surveyed measurements of *A* and field measurements of *C* collected during the snapshot. For the purposes of flux calculations, concentrations below the detection limit were assigned a value of zero. Net transformation rates for chemical and microbial constituents were quantified using a linear-least squares approach (Borden et al. 1997). The main assumptions in this approach are that the system is in steady state with respect to constituent input, microbial and physcio-chemical removal mechanisms, and advection-dispersion within the aquifer, and that the monitoring network captures the entire plume emanating from a source of constant, steady input. These assumptions are revisited in the discussion of the results.

5.3.8 FIB V ATTENUATION COLUMN EXPERIMENTS.

Removal rates for enterococci, and somatic and F+ coliphage were quantified in laboratory column experiments for comparison with field data. Aquifer and groundwater samples were collected adjacent to the leach field and the high tide berm to quantify representative attenuation rates in fresh and saline saturated sediments, respectively (Fig. S1, further collection methodologies are in the SI). Specimens were transported to the lab on ice and stored at 15°C until use (within 1 d). Column experiments were conducted at 15°C, a few degrees cooler than the ambient groundwater temperature in the beach (Table S4).

Sterile 22-cm long, 2.5-cm diameter glass columns were wet-packed with homogenized sediment following Jin et al. (1997) and flushed with 4 pore volumes of unammended groundwater. The influent was then switched to a solution containing 90% groundwater, 10% screened raw sewage from the Palo Alto Water Quality Control Plant, and sodium bromide tracer. Darcy flow velocities of approximately 70 cm/day were maintained to match velocities expected in the field. Column effluent was sampled every 20 minutes for 18 hours. Bromide was measured in effluent fractions using a probe (Thermo Scietific, Beverly, MA). Enterococci and coliphage were enumerated using EPA methods 1600 and 1602, respectively. To calculate first-order removal rates, the advection-dispersion equation was fit to the tracer breakthrough curve to calculate velocity and dispersion coefficient using the CXTFIT2 package of the UC Riverside & US Salinity Laboratories code STANMOD V2.2. These coefficients were then used to calculate first order removal rates from FIB and bacteriophage data (van Genuchten and Alves, 1982). Additional details are in the SI.

5.3.9 Denitrification potential assays.

Samples collected upgradient (DNP1, Fig. S1) and downgradient (DNP2-7) of the leach field were assayed for denitrification potential using the acetylene block slurry method (Tiedje 1982). The downgradient samples were collected by augering to the water table along the approximate centerline of the plume. A sonde and flow-through cell was used to record water quality parameters in each bore, as previously described (Table S5). A eighth sample (DNP8) was collected 50 m alongshore to the northwest of the leach field. Details of sample collection and methodology can be found in the SI. Sand from DNP2 was autoclaved for 60 min at 121°C and run as a negative control. The quantification limit of the method was 5.9×10^{-3} nmol N hr^{-1} g^{-1}.

5.3.10 Data analysis.

Unless stated otherwise, concentrations presented are mean +/- standard deviation. Percentages of total carbon, total nitrogen, and dissolved inorganic nitrogen are calculated directly from raw data. For all other statistical testing and summarization, microbial and nutrient concentrations were $\log_{10}$ transformed, and summaries of those data are presented as mean +/- standard deviation of log-transformed data. For the

purposes of statistical testing using log-transformed data, nutrient values below method detection limits (BDL) were replaced with the value of the detection limit. For the purposes of flux calculations, zeros were substituted for BDL values. Statistical analyses were performed using Matlab (Natick, MA). Data comparisons between groups were made using Student's *t* test. Correlation coefficients were determined by calculating Pearson's product-moment correlation coefficients. Statistical results were deemed significant if $p<0.05$.

5.4 RESULTS

5.4.1 HEAD MEASUREMENTS AND HYDRAULIC GRADIENTS.

A region of persistent high hydraulic head was observed in the northern corner of the field site closest to the Easkoot Creek drainage (Fig. 5.1). Flow lines perpendicular to equipotential lines swept south and southeast down the length of the parking lot, eventually curving southwest toward the beach face tidal boundary. Maximum winter hydraulic heads across the site were approximately 0.9 m higher than minimum summer heads. The primary impact of the seasonal head change was a steepening of seaward hydraulic gradient across the site from a minimum value of 0.028 in September 2008 to a maximum of 0.039 in March 2009 (Fig. S2).

5.4.2 RESISTIVITY PROFILES.

Similar subsurface features were observed during all tidal conditions investigated and configurations (Figs. 5.2 and S3). In each profile, a highly conductive region extended 30 m from the seaward boundary to the high tide berm and progressed inland at depth (Fig. 5.2); σ in this region ranges between 0.5 and 3.5 Wm. A low conductivity region was observed in the area of the well network and extended out over the conductive region, shallowing toward the beach face. In this region, σ ranged from 3.5 to 295 Wm.

5.4.3 HYDRAULIC CONDUCTIVITY AND RESIDENCE TIME.

The geometric mean conductivity estimate obtained using the tidal efficiency method was 5 m day^{-1} (Table S2). This value is lower than a previous hydraulic

conductivity measurement made for beach sands at the site (33 m day^{-1}; de Sieyes et al. 2008) but is reasonable considering the hydrogeologic setting as described in the SI.

Considering a plume centerline *L* of 15 m between the leach field and Transect C, mean annual *i* of 0.031, mean *K* of 5 m day^{-1}, and n_e estimated at 0.25 for clean beach sands (Fetter 2001), mean annual groundwater velocity is 0.625 m day^{-1} and residence time in the network is approximately 24 days.

5.4.4 Septic effluent characteristics.

Generally, septage was low in dissolved oxygen (DO) (< 1 mg L^{-1}), neutral in pH (7.1), fresh in salinity (0.3), and had a mean temperature of 19.5°C and Eh of +300 mV, based on 14 measurements over 17 months (Table 5.1). Log-mean total carbon (TC) in septage was 0.79 +/- 0.06 log(μM) and ranged from 0.69 to 0.95 log(μM) (n=22 including replicates). Log-mean dissolved inorganic carbon (DIC) in the same samples was 0.68 +/- 0.04 log(μM) and ranged from 0.62 to 0.77 log(μM). On average, 19% of TC in a given septage sample was dissolved organic carbon (DOC). The log-mean of total nitrogen (TN) was -0.03 +/- 0.32 log(μM) and ranged from -0.46 to 0.46 log(μM) (n=27 including replicates). Dissolved organic nitrogen (DON) ranged from 0 to 50% of TN; for the average septage sample, 91% and 9% of total nitrogen was in the inorganic and organic forms, respectively, and over 99.5% of dissolved inorganic nitrogen (DIN) was ammonium. Log-mean *E. coli* (n=25) and enterococci (n=18) concentrations in septage were 4.3 +/- 0.7 log(CFU (100 mL)$^{-1}$) and 3.6 +/- 0.6 log(CFU (100 mL)$^{-1}$), respectively. Log-mean F+ coliphage (n=12) and somatic coliphage (n=8) concentrations were 1.5 +/- 0.2 log(PFU (100 mL)$^{-1}$) and 1.8 +/- 0.5 log(PFU (100 mL)$^{-1}$), respectively.

5.4.5 Monitoring network data.

Temperature, salinity, DO, pH, and Eh along the approximate centerline of the plume during each snapshot were measured (Table 5.2). Groundwater temperatures were between 16 and 20°C, and exhibited seasonal trends. Salinity along the centerline ranged from 0.4 to 0.6 and did not change significantly between snapshots. Mean DO was in the range of 0.3 to 0.8 mg/L and was significantly lower in August 2009 (0.32 mg L^{-1}) than either April 2008 (0.72 mg L^{-1}; p=0.038) or November 2008 (0.64 mg L^{-1}; p=0.005). Eh

ranged from +300 to +420 mV, and was significantly higher in November 2008 (+414 mV) than in April 2009 (+303 mV; p=0.036). Across the site, pH measurements from the initial snapshot in November 2008 were thrown out due to a faulty probe; mean pH measurements during the sunsequent snapshots were 6.4 +/- 0.2 and ranged from 6.36 to 7.16.

In general, samples collected from transects downstream of the leach field were high in both nitrogen and carbon species, typical of a septic effluent plume (Wilhelm et al. 1998). An example of the cross-sectional chemical data collected during the experiments is shown in Figure 5.3, a contour plot of TC, DIC, DOC, nitrate, ammonium, and TN concentrations at Transect B in November 2008. Contour plots of the nitrogen and carbon species at other transects during other snapshots exhibited similar patterns (Figs. S4-S12.)

TC in the monitoring network ranged from 3.34 to 4.11 log(μM) and had a log-mean of 3.85 +/- 0.15 log(μM). DIC ranged from 3.21 to 4.00 log(μM) with a log-mean of 3.74 +/- 0.16 log(μM) and was highly, positively correlated to TC (r=0.80, $p<10^{-5}$), with DIC often making up the bulk of TC. DOC was also significantly correlated to TC (r=0.25, p=1.2x10^{-4}), had a log-mean of 2.54 +/- 1.08 log(μM) and ranged from BDL to 4.05 log(μM). Upgradient samples (n=11) were not significantly different from downgradient samples (n=253) for TC (p=0.14), DIC (p=0.21), or DOC (p=0.48), likely due to high background concentrations of dissolved carbon in site groundwater.

Log-mean TN concentrations in the multi-level network downgradient from the leach field were 2.57 +/- 0.47 log(μM) and ranged from BDL to 3.79 log(μM). Spatially, samples collected downgradient from the leach field had significantly higher TN concentrations than samples from wells upgradient from the leach field ($n_{upgradient}$=10; $n_{downgradient}$=253; $p<10^{-6}$). Log-mean DIN concentrations in the downgradient network were 2.54 +/- 0.46 log(μM) and ranged from BDL to 3.77 log(μM). DON generally made up a smaller component of the TN than DIN, with log-,mean DON concentrations of 0.78 +/- 0.90 ranging from BDL to 3.10 log(μM); over 60% of samples contained DON concentrations below the detection limit. Log-mean ammonium concentrations were 2.14 +/- 0.73 log(μM) and ranged from BDL to 3.11 log(μM). By comparison, log-mean nitrate concentrations were 0.75 +/- 1.25 log(μM), ranging from BDL to 3.76 log(μM).

TN concentrations in the network were higher in August 2009 than in either November 2008 ($p<10^{-5}$) or April 2009 (p=0.015). Generally, samples contained either nitrate or ammonium but rarely both. Sample elevation was significantly positively correlated with nitrate (r=0.38, $p<10^{-5}$) and negatively correlated with ammonium (r=-0.47, $p<10^{-5}$). DIC was positively correlated with ammonium (r=0.42, $p<10^{-5}$) and negatively correlated to nitrate (r=-0.23, p=0.0004). Additionally, nitrate was positively correlated to DON (r=0.52, $p<10^{-5}$).

Sonde measurements along the plume centerline during each snapshot allowed for the evaluation of relationships between products of likely chemical transformations occurring in the plume. Specifically, elevation was positively correlated to Eh (r=0.59, p=0.002) and negatively correlated to DIC (r=-0.43, p=0.025). Eh was positively correlated to nitrate (r=0.63, p=0.0004) and negatively correlated to both ammonium (r=-0.50, p=0.009) and DIC (r=-0.46, p=0.016). DO was positively correlated with TOC (r=0.46, p=0.015).

During each snapshot, all samples from Transect A (Fig. 5.1), the closest transect to the leach field, were analyzed for F+ and somatic coliphage while all samples from the sampler network were analyzed for enterococci and *E. coli*. In November 2008, Transect A samples were negative for coliphage, and neither enterococci nor *E. coli* were detected in the well network except in the two multilevel samplers upgradient from the leach field, UG1 and UG2 (Fig. 5.1). Here maximum enterococci and *E. coli* concentrations were 28 and 6 cfu (100 mL)$^{-1}$, respectively. During the April 2009 snapshot, samples from Transect A were negative for somatic coliphage; F+ coliphage data were discarded due to a faulty negative control. Two samples from Transect A contained 4 cfu (100 mL)$^{-1}$ enterococci, and no *E. coli* was detected in the network. In August 2009, all Transect A samples were negative for somatic and F+ coliphage. All samples from the sampler network were negative for *E. coli*, but 15 of 87 samples were positive for enterococci with concentrations ranging from 2 to 74 cfu (100 mL)$^{-1}$. Enterococci was detected in each transect, and the geometric mean of positive samples was 8 cfu (100 mL)$^{-1}$. No fecal indicator bacteria or coliphage were detected in the 2” wells upgradient from the leach field during this snap shot.

5.4.6 CONTAMINANT FLUX ESTIMATES.

Septage discharge rates to the leach field were 4.9 x 10^3 +/- 1.9 x 10^3 L day^{-1}. Considering the septage water quality, fluxes to the leach field during the experiment were 6.7 +/- 4.7 moles day^{-1} TN, 6.2 +/- 0.3 log pfu day^{-1} F+ coliphage, 6.4 +/- 0.5 log pfu day^{-1} somatic coliphage, 9.0 +/- 0.7 log cfu day^{-1} *E. coli*, and 8.3 +/- 0.6 log cfu day^{-1} enterococci.

Nitrate, nitrite, ammonium, DIN, DON, TN, and enterococci fluxes to the leach field are compared with fluxes at the three downstream multi-level well transects during each snapshot in Figure 5.4. Fluxes of F+ coliphage, somatic coliphage and *E. coli* were not calculated because they were not detected in the sampler network downgradient from the leach field. Monthly transect TN fluxes ranged from 1.6 to 70.6 moles day^{-1}. On average, DIN and nitrate fluxes at each transect accounted for 86% and 40% of TN flux at a given transect. Maximum fluxes of TN, DIN, and nitrate each occurred in August 2009, when concentrations of each analyte were highest in the network.

In Table 5.3, rates of production and loss with distance downgradient are presented with 95% confidence intervals. Fluxes of nitrate and nitrite consistently increased significantly with distance downgradient during each snapshot. For nitrate, rates of increasing flux with distance ranged from 0.15 moles d^{-1} m^{-1} in April 2009 to 1.21 moles d^{-1} m^{-1} in November 2008. Concurrently, ammonium consistently decreased with distance downgradient during each snapshot at rates ranging from -0.48 moles d^{-1} m^{-1} in April 2009 to -0.64 moles d^{-1} m^{-1} in November 2008. DON increased significantly with downstream distance in November 2008 and August 2009 at rates of 0.45 and 0.19 moles d^{-1} m^{-1}, respectively; no DON was detected in the well network in April 2009. Only in April 2009 was a significant decrease in downgradient flux of TN observed, with TN attenuation occuring at a rate of -0.32 moles d^{-1} m^{-1}. In November 2008, TN flux increased with distance downgradient at a rate of 1.16 moles d^{-1} m^{-1}, and no significant trend in TN flux versus distance was observed in August 2009.

Enterococci were detected in Transect A in April 2009 and in all transects in August 2009, allowing for the calculation of fluxes at these locations and times only. In April 2009, flux at Transect A was 1.9 +/- 0.5 log cfu day^{-1}. In August 2009, fluxes at Transects A, B, and C were 4.0 +/- 0.7, 5.0 +/- 0.4, and 6.0 +/- 0.4 log cfu day^{-1},

respectively. The maximum enterococci flux in the sampler network occurred in August 2009 at Transect C. During the Aug 2009 snapshot, a significant increase in flux with distance was observed ($p<10^{-5}$).

5.4.7 FIBV ATTENUATION COLUMN EXPERIMENTS.

F+ coliphage was removed by sediments at a rate above our quantification limits for the method, which we estimate at 1.74 and 2.81 hr^{-1} for the saline and fresh columns, respectively (Figs. S13 and S14). For somatic coliphage, first-order removal was 0.40 hr^{-1} in fresh groundwater as compared to 1.6 hr^{-1} in saline groundwater. For enterococci, first order removal in fresh and saline groundwater was 0.47 hr^{-1} and 0.46 hr^{-1}, respectively. The density of target organisms in the feedstock did not change significantly ($p>0.05$) with time over the course of any experiment.

5.4.8 DENITRIFICATION POTENTIAL ASSAYS.

The denitrification potential rates found at the eight sample locations (DNP1-DNP8) and the autoclave control (DNP9) are shown in Table S5 along with groundwater characteristics from each sample location. DNP rates ranged from 10.8 nmol N hr^{-1} g^{-1} to below the quantification limit of $5.85x10^{-3}$ nmol N hr^{-1} g^{-1}. Along the plume, log-transformed denitrification potential rate decreased significantly with distance oceanward (p=0.014) from DNP1 (10.8 nmol N hr^{-1} g^{-1}) to DNP7 (<$5.85x10^{-3}$ nmol N hr^{-1} g^{-1}) and was significantly negatively correlated to groundwater Eh (p=0.001) and temperature (p=0.020).

5.5 DISCUSSION

Resistivity profiling indicated a resistive freshwater lens thinning toward the ocean sits atop a more conductive saltwater wedge thinning toward the land, as predicted by theory (Dupuit 1863). Limited increases in resistivity from November 2008 to April 2009 were observed at the base of the resistive layer inland of the berm, in the unsaturated zone, and near the beach face seaward of the berm. Considering the observed seasonal changes in hydraulic gradient (Fig. S15), the results indicate a thickening of the freshwater lens, increased moisture content in the vadose zone, a higher water table, and

increased fresh water at the beach face in winter following the rainy winter season. Although field observations and numerical simulations at some coastal locations indicate a fresh groundwater 'tube' discharging below a tidally-driven saline groundwater circulation cell in the beach face (Robinson 1998; Vandenbohede and Lebbe, 2006), no such tube was observed in our field site. This is perhaps due to the shallow beach slope (0.03; de Sieyes et al. 2008), high wave action, and strong mixed semi-diurnal tides.

Significant correlations between measured groundwater characteristics are consistent with the conceptual model of expected plume chemistry. For example, pH and log(DIC) are negatively correlated while pH and log(DOC) are positively correlated, indicative of the production of acid and inorganic carbon during the mineralization of organic carbon in the plume. DIC is positively correlated to ammonium and negatively correlated to nitrate, evidence for the coexistence of mineralized carbon and reduced nitrogen, and consistent with the suggestion that inorganic carbon can be used to indicate 'old' treated septage in the plume (Wilhelm et al. 1994). Carbon species were not significantly different in the plume from in upgradient 'background' wells, suggesting that carbon is an imperfect tracer of septic effluent in groundwater, and that an injected tracer may be necessary for more refined plume tracking in future experiments at the site.

Despite fluxes of 6.2 +/- 0.3 log pfu day^{-1} F+ coliphage, 6.4 +/- 0.5 log pfu day^{-1} somatic coliphage, 9.0 +/- 0.7 log cfu day^{-1} *E. coli* from the septic tank into the leach field, no coliphages and very few *E. coli* were detected in the well network. These results suggest effective removal of these organisms in the vadose zone after they are discharged to the leach field. The saturated column experiments indicate that coliphage would be very effectively removed within the well network even if there were able to pass through the vadose zone. Enterococci were observed throughout the leach field in the August 2009 snapshot, and at Transect A in April 2009. Thus, in April it appears that some enterococci pass through the vadose zone, enter the well network, but are removed before reaching Transect B. This is consistent with the results of the laboratory saturated column experiment showing removal of enterococci in saturated sands. Interestingly, in August 2009, there was a net increase in enterococci flux through the well network suggesting either exogenous inputs of enterococci to the well network or enterococci are growing along the flowpath. Assuming the downgradient increase is due to growth of enterococci,

the data are consistent with a first-order growth rate of approximately 0.28 day^{-1}. This rate of growth is in good agreement with enterococci growth rates observed in intermittently wetted beach sands (0.20 to 0.63 day^{-1}) by Yamahara et al. (2009). If the increase in flux is due to competing growth and removal along the flowpath, the actual rate of growth occurring *in-situ* would be greater than 0.28 day^{-1}.

In August 2009, $1.1x10^6$ cfu day^{-1} enterococci were discharged to the subterranean estuary in concentrations as high as 46 cfu $(100\ ml)^{-1}$, just below half the California single sample standard for recreational contact, 104 cfu $(100ml)^{-1}$. Considering the substantial dilution that occurs in the subterranean estuary and surf zone at Stinson Beach, it is unlikely that a single point source of this concentration would trigger a water quality advisory. However, recent research has documented growth of enterococci on algal wrack (Whitman et al. 2003) as well as in intermittently wetted beach sands with relatively low organic carbon (Yamahara et al. 2009), and it is plausible that the septic system described herein may seed enterococci to the beach environment where they can persist and/or grow and trigger water quality advisories. Additionally, input of enterococci from human sources may be accompanied by input of co-occurring bacterial or viral pathogens which represent health risks.

Significantly increasing fluxes of nitrate with distance downgradient occurred concurrently with decreasing fluxes of ammonium during all three snapshots. This may be evidence of nitirification and is consistent with the fluxes of nitrite, an intermediate in nitrification, which also increased significantly with distance during each snapshot. In November 2008, the increasing flux of nitrate with distance (1.21 moles day^{-1} m^{-1}; Table 5.3) is greater in magnitude than the loss of ammonium flux with distance (-0.64 moles day^{-1} m^{-1}; Table 5.3), suggesting that the increasing nitrate along the flowpath is due not only to nitrification of ammonium. It is possible that additional nitrogen is appearing along the flowpath due to the mineralization of particulate organics to DIN as nitrate. It is also possible that exogeneous inputs of TN are being added to the plume along the flowpath, although the source of such inputs are not immediately obvious. In April 2009, the decrease in ammonium flux along the flowpath (-0.48 moles day^{-1} m^{-1}) was faster than the concurrent increase in nitrate flux (0.15 moles day^{-1} m^{-1}). Considering the particularly low Eh values measured in April 2009 and the net loss of -0.32 moles TN

day^{-1} m^{-1} along the flowpath, this may indicate nitrate attenuation by denitrification at that time.

The Theissen Polygon transect method assumes constant, steady input at the contaminant source, but it is possible that short periods of high contaminant flux to the septic system from high-use weekends at the park contributed to the variability in flux between transects. Such short-term input variability would not have been captured by our bimonthly septic tank sampling, but may explain why in August 2009 nitrate flux was most variable between transects, DIN and TN fluxes did not vary significantly with distance downgradient, and TN concentrations in the plume were the highest of the experiment at 5.8 mM. It is also possible that our monitoring did not capture the entirety of the plume at all transects, another potential source of error posed by the Theissen Polygon approach.

The nitrogen fluxes reported here should be considered 'potential' SGD-associated flux only, since additional attenuation may occur in the subterranean estuary (Kroeger and Charette 2008). However, it is of interest to compare the fluxes calculated in this study with those from during previous SGD studies at the site. In de Sieyes et al. (2008), we used a coastal water mass balance of radium, naturally occuring radioisotopes present in groundwater whose occurance in coastal waters can be used to trace SGD and SGD-associated nutrient fluxes. DIN flux per meter of shoreline from total SGD (fresh + saline groundwater) in the residential Calles area of Stinson Beach in March 2007 was estimated at 1.7 moles DIN day^{-1} m^{-1}. By comparison, the highest mean monthly transect flux measured during our study was 63 moles DIN day^{-1} at Transect B in August 2009. Normalized to the width of the 30m-wide monitoring network, this flux is equivalent to approximately 2.1 moles DIN day^{-1} m^{-1}, and the majority of this flux was DIN. This is in good agreement with the previous estimate. However it should be noted that the 1.7 moles DIN day^{-1} m^{-1} reported in de Sieyes et al. (2008) is the flux from both fresh and saline discharge, while the 2.1 moles DIN day^{-1} m^{-1} reported here is due only to a portion of the fresh groundwater alone. This highlights the importance of individual, highly concentrated point sources like septic systems as controls on total SGD-associated groundwater pollution.

Only in April 2009 was a decrease in TN flux with distance along the flowpath ever observed (Fig. 5.4), indicative of plume attenuation by denitrification. This suggests that during much of the year, TN from the septic system is not being attenuated substantially prior to discharge to the subterranean estuary. This begs the question, if *in situ* conditions for denitrification were optimized, could treatment of the nitrogen plume discharging through the beach be improved, thereby reducing nutrient loads entering the subterranean estuary and, ultimately, the marine environment? This question can be initially approached modeling the beach in the area of the network as a simple box where nitrogen is attenuated at rates measured in the DNP experiments. The dimensions of the well network sediment box are length 30 m, width 15 m, and depth 4.5 m for a total box volume of 2025 m^3. Assuming a bulk density of 2 kg L^{-1}, a value typical of medium-grained beach sands (Fetter 2001), yields a total sediment mass of $4.1x10^6$ kg. The median DNP rate measured in samples collected inside the well network oceanward of the leach field (DNP2 through DNP4) was 0.018 nmol hr^{-1} g^{-1}, or $4.32x10^{-7}$ mol day^{-1} kg^{-1}. The product of this median DNP rate and the total sediment mass in the box yields a rate of 1.8 mol day^{-1}, the total daily potential denitrification rate for the box. Assuming an input of approximately 17 mol day^{-1}, it will take approximately 9.7 days to attenuate the full daily influx of nitrogen to the box. Considering the residence time in the box is on the order of 24 days, the total dentrification potential of the box assuming optimal controlled, well-mixed conditions is approximately 16.3 moles day^{-1}, or 96% of the TN fluxing in the plume. This simple calculation likely overstates the ability of unammended beach sediments to attenuate nitrogen associated with the plume *in-situ* even under the most controlled conditions, but suggests a potential future role for advanced treatment options including *in-situ* reactive barriers for the reduction of TN in this and other similar settings.

Figure 5.1. Plan view of Stinson Beach south lot field site including bathrooms, wet well, leach fields #1 and #2, November 2008 head contours, groundwater flow direction, 2" wells, multi-level well transects A, B, and C, and ERT profile locations. The ocean mean water line is shown at the bottom left corner of the figure.

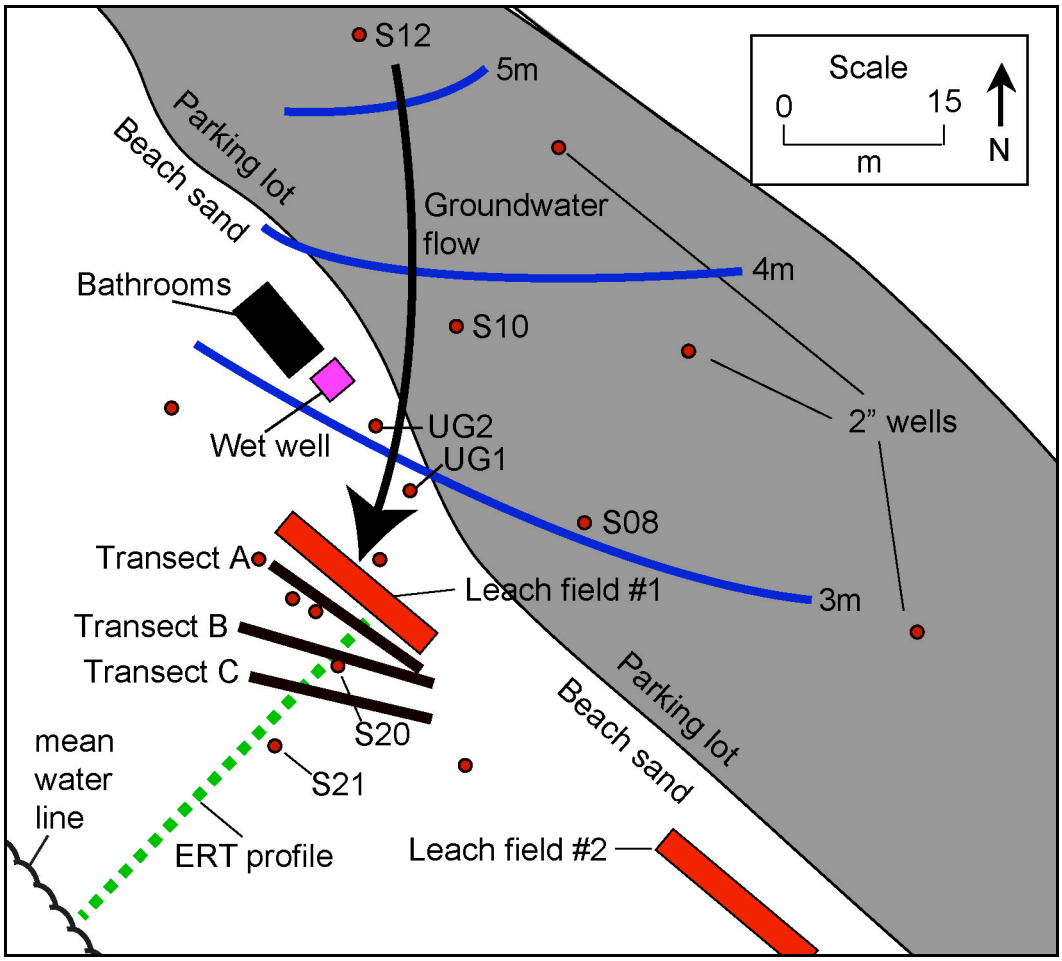

Figure 5.2. Wenner array resistivity profiles from low-low tide on 5 April 2009. The repeat survey from 22 November 2008 and a plot of the absolute change in resistivity between the two surveys are shown in the SI.

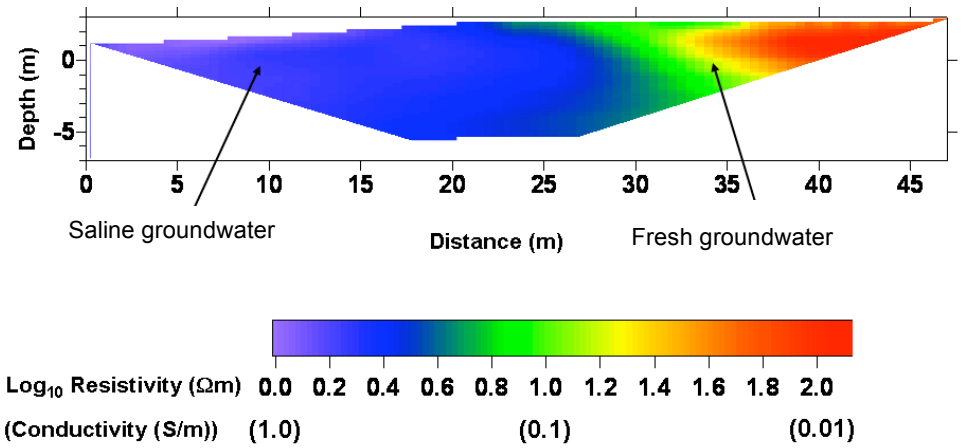

Figure 5.3. Concentration data for TC (a), DIC (b), DOC (c), nitrate (d), ammonium (e), and TN (f) in Transect B during the November 2008 snapshot. Y-axis is depth in meters and the X axis is distance along the transect in meters. Each projection looks upgradient into the plume, which is flowing out of the page. Concentration data are contoured using cubic interpolation and sample locations are designated by open circles. In each subplot, the color limits are based on the maximum and minimum concentrations in the dataset.

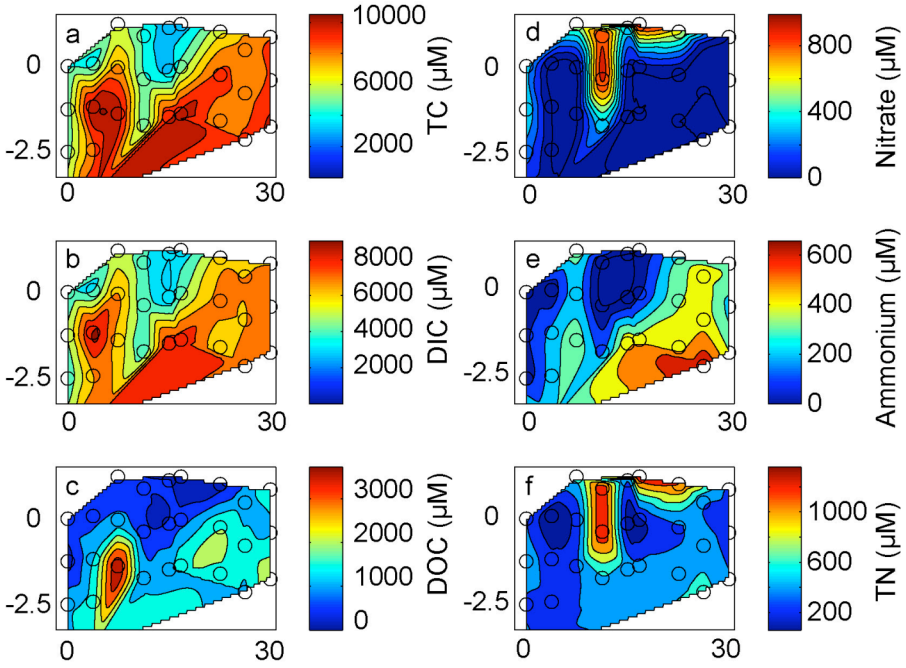

Figure 5.4. Fluxes of nitrate (A), ammonium (B), nitrite (C), DIN (D), DON (E), TN (F) and enterococci (G) associated with septage discharging to the leach field and groundwater discharging through each transect during snapshots. On each box, the central mark is the median, the edges of the box are the 25th and 75th percentiles, and the whiskers extend to the 1st and 99th percentiles. For some boxes, the spread in the data was small and the percentile lines are very close together. Septage fluxes are separated from saturated groundwater fluxes by a vertical dashed line. Fluxes were not calculated when no samples in a given transect during a snapshot were above the detection limit for a given analyte; a color-coded asterisk (*) has been substituted at these locations and times.

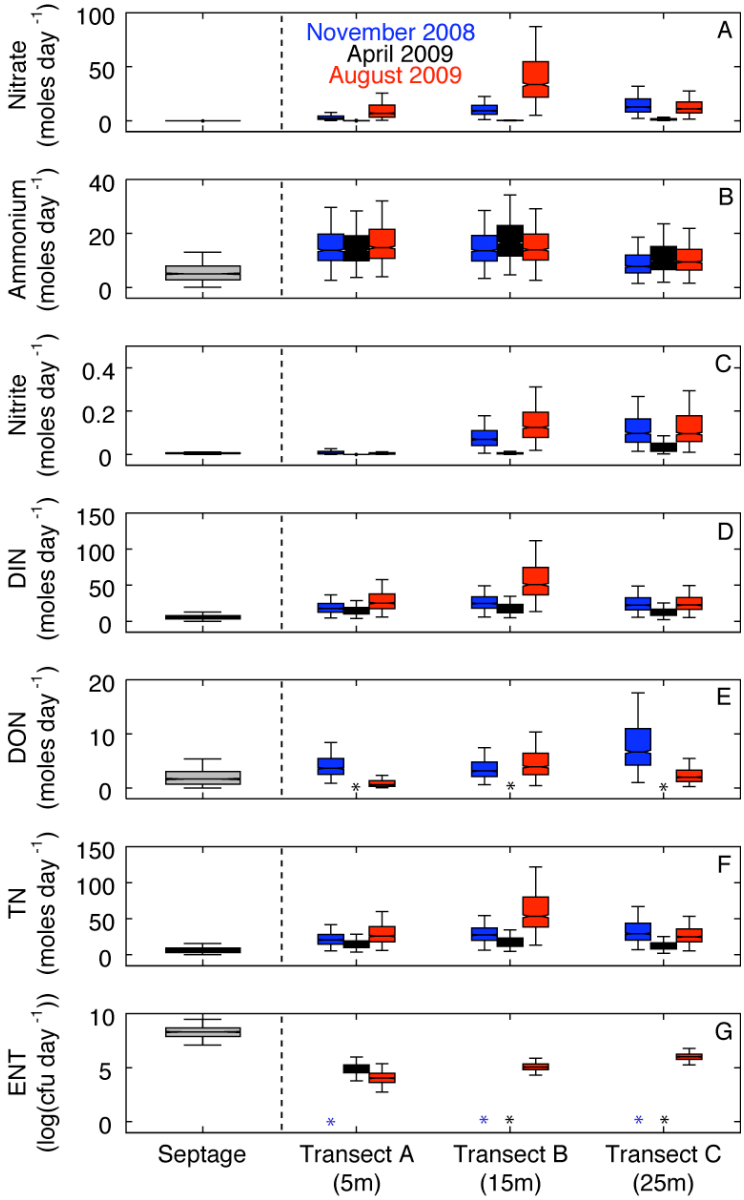

Table 5.1. Mean +/- standard deviation temperature, specific conductivity, dissolved oxygen, pH, salinity and Eh of septic effluent samples.

	Temperature (C)	Specific Conductivity ($\mu S\ cm^{-1}$)	Dissolved Oxygen ($mg\ L^{-1}$)	pH	Salinity (PSS)	Eh (mV)
Mean +/ Standard Deviation	19.4 +/- 1.4	0.7 +/- 0.1	0.9 +/- 1.0	7.1 +/- 0.1	0.34 +/- 0.05	304 +/- 100
n	13	13	13	13	13	13

Table 5.2. Mean +/- standard deviation temperature, specific conductivity, pH, salinity and Eh of groundwater samples collected along the centerline of the plume in wells A05, B05.5, and C06. For each snapshot, n = 12 measurements.

	Snapshot	Temperature (C)	Specific Conductivity ($\mu S\ cm^{-1}$)	Dissolved Oxygen ($mg\ L^{-1}$)	pH	Salinity	Eh (mV)
Mean +/- Standard Deviation	November 2008	18.0 +/- 0.4	1.26 +/- 0.58	0.64 +/- 0.21	6.39 +/- 0.14	0.62 +/- 0.30	414 +/- 156
	April 2009	16.2 +/- 0.6	0.92 +/- 0.23	0.79 +/- 0.41	6.51 +/- 0.07	0.45 +/- 0.12	302 +/- 58
	August 2009	19.2 +/- 1.3	1.06 +/- 0.33	0.32 +/- 0.24	6.50 +/- 0.12	0.52 +/- 0.17	361 +/- 98

Table 5.3. Nitrogen species rates of production or loss with distance presented +/- 95% confidence intervals for nitrate, nitrite, ammonium, DIN, TN, and DON. Pearson's R and the *p* value from each correlation of flux vs. distance is shown in parenthesis. Rates are not shown for DIN and TN in August 2009, whose flux did not change significantly with distance (NS), nor for DON in April 2009 when no samples from the monitoring network had DON concentrations above the detection limit (ND).

	November 2008	April 2009	August 2009
Nitrate (moles day^{-1} m^{-1})	1.21 +/- 0.11 ($R=0.35$, $p<10^{-5}$)	0.15 +/- 0.01 ($R=0.39$, $p<10^{-5}$)	0.29 +/- 0.01 ($R=0.04$, $p=0.024$)
Nitrite (moles day^{-1} m^{-1})	0.01 +/- 0.00 ($R=0.39$, $p<10^{-5}$)	0.00 +/- 0.00 ($R=0.22$, $p<10^{-5}$)	0.02 +/- 0.00 ($R=0.26$, $p<10^{-5}$)
Ammonium (moles day^{-1} m^{-1})	-0.64 +/- 0.10 ($R=-0.19$, $p<10^{-5}$)	-0.48 +/- 0.11 ($R=-0.12$, $p<10^{-5}$)	-0.51 +/- 0.12 ($R=-0.17$, $p<10^{-5}$)
DIN (moles day^{-1} m^{-1})	0.58 +/- 0.15 ($R=0.15$, $p<10^{-5}$)	-0.48 +/- 0.11 ($R=-0.08$, $p<10^{-5}$)	NS
TN (moles day^{-1} m^{-1})	1.16 +/- 0.20 ($R=0.20$, $p<10^{-5}$)	-0.32 +/- 0.11 ($R=-0.08$, $p<10^{-5}$)	NS
DON (moles day^{-1} m^{-1})	0.45 +/- 0.06 ($R=0.21$, $p<10^{-5}$)	ND	0.19 +/- 0.04 ($R=0.16$, $p<10^{-5}$)

5.6 REFERENCES CITED

Bone, S. E., M. A. Charette, C. H. Lamborg, and M. E. Gonneea. 2007. Has submarine groundwater discharge been overlooked as a source of mercury to coastal waters? Environ. Sci. Technol. **41**: 3090-3095.

Borden, R.C., R.A. Daniel, L.E. LeBrun IV, and C.W. Davis, 1997. Intrinsic Biodegradation of MTBE and BTEX in a Gasoline-Contaminated Aquifer. Water Resources Research **33**:1105-1115.

Burnett, W. C., P. K. Aggarwal, A. Aureli, H. Bokuniewicz, J. E. Cable, M. A. Charette, E. Kontar, S. Krupa, K. M. Kulkarni, A. Loveless, W. S. Moore, J. A. Oberdorfer, J. Oliveira, N. Ozyurt, P. Povinec, A. M. G. Privitera, R. Rajar, R. T. Ramessur, J. Scholten, T. Stieglitz, M. Taniguchi, and J. V. Turner. 2006. Quantifying submarine groundwater discharge in the coastal zone via multiple methods. Sci. Total Environ. **367**: 498-543.

Census Bureau, United States Department of Commerce. American Housing Survey for the United States - 1995. Issued September 1997.

Constable, S.C., Parker, R.L., Constable, C.G., 1987. OCCAM's inversion: a practical algorithm for generating smooth models from electromagnetic sounding data. Geophysics **52**: 289–300.

Dale, N. G. 1974. Bacteria in intertidal sediments: factors related to their distribution. Limnology and Oceanography. **19**: 509.

de Sieyes, N. R., K. M. Yamahara, A. Paytan and A. B. Boehm. Submarine groundwater discharge to a high-energy surf zone at Stinson Beach, California, estimated using radium isotopes. Estuaries and Coasts **34**: 256-266.

de Sieyes, N. R., K. M. Yamahara, B. A. Layton, E. H. Joyce, and A. B. Boehm. 2008. Submarine discharge of nutrient-enriched fresh groundwater at Stinson Beach, California is enhanced during neap tides. Limnology and Oceanography **53**: 1434-1445.

D'Elia, C.F., P.A. Steudler, and N. Corwin. 1977. Determination of total nitrogen in aqueous samples using persulfate digestion. Limnology and Oceanography. **22**: 760–764.

Dupuit, J. 1863. Estudes Thèoriques et Pratiques sur le mouvement des Eaux dans les canaux dècouverts et à travers les terrains permèables (Second Edition). Paris: Dunod.

Einarson, M. D., and D. M. Mackay. 2001. Predicting impacts of groundwater contamination. Environmental Science & Technology **35**: 66A-73A.

Ferris, J. G. 1963. Methods of determining permeability, transmissivity and drawdown. U.S. Geol. Survey Water Supply Paper 1536-1.

Fetter, C. W. 2001. Applied Hydrogeology. 4th Edition. Prentice-Hall, Upper Saddle River, NJ. 598 p.

Jin, Y., M. V. Yates, S. S. Thompson, and W. A. Jury. 1997. Sorption of viruses during flow through saturated sand columns. Environmental Science & Technology **31**: 548-555.

Korom, S.F. 1992. Natural denitrification in the saturated zone: a review. Water Resources Research. **28**: 1657-1668.

Kroeger, K. D., P. W. Swarzenski, J. Greenwood, and C. Reich. 2007. Submarine groundwater discharge to Tampa Bay; Nutrient fluxes and biogeochemistry of the coastal aquifer. Mar. Chem. **104**: 85-97.

Laverman, A.M., P. Van Cappellen, D. van Rotterdam-Los, C. Pallud, and J. Abell. 2006. Potential rates and pathways of microbial nitrate reduction in coastal sediments. FEMS Microbiology Ecology **58**: 179–192.

Marin County Open Space District (MCOSD). 1996. The Bolinas Lagoon Management Plan Update.

Millham, N.P. and Howes, B.L. 1995. A comparison of methods to determine K in a shallow coastal aquifer. Ground Water. **33**: 49–57.

Moore, W. S. 1999. The subterranean estuary: a reaction zone of ground water and sea water. Marine Chemistry **65**: 111-125.

Pfenning, K.S., and P.B. McMahon. 1996. Effect of nitrate, organic carbon, and temperature on potential denitrification rates in nitrate-rich riverbed sediments. Journal of Hydrology, **187**: 283-295.

Rivett, M.O., J.W.N. Smith S.R. Buss and P. Morgan. 2007. Nitrate occurrence and attenuation in the major aquifers of England and Wales. Quarterly Journal of Engineering Geology and Hydrogeology. **40**: 335-352.

Robertson, W. D., J. A. Cherry, and E. A. Sudicky. 1991. Groundwater contamination from two small septic systems on sand aquifers. Ground Water **29**: 82-92.

Robinson C., A. Brovelli, D.A. Barry, L. Li2009. Tidal influence on BTEX biodegradation in sandy coastal aquifers. Advances in Water Resources **32**: 16–28

Robinson, M. A., and D. L. Gallagher. 1999. A model of ground water discharge from an unconfined coastal aquifer. Groundwater. **37**: 80.

Stieglitz, T.C. 2005. Submarine groundwater discharge into the near-shore zone of the Great Barrier Reef, Australia. Marine Pollution Bulletin **51**: 51-59.

Stinson Beach County Water District (SBCWD). 1998. Stinson Beach Hydrologic Survey.

Swartz, C. H., S. Reddy, M. J. Benotti, H. Yin, L. B. Barber, B. J. Brownawell, and R. A. Rudel. 2006. Steroid estrogens, nonylphenol ethoxylate metabolites, and other wastewater contaminants in groundwater affected by a residential septic system on Cape Cod, MA. Environ. Sci. Technol. **40**: 4894-4902.

Tiedje, J.M. 1982. Denitrification, pp. 1011-1026. In A.L. Page, R.H. Miller and D.R. Keeney (eds.), Methods of Soil Analysis, Part 2. Agronomy Monograph No. 9., Amer. Soc. Agron., Madison, WI.

U.S. Environmental Protection Agency. 1980. Design manual: Onsite wastewater treatment and disposal systems. Washington, D.C.: Office of Water Program Operations and Office of Research and Development Publication Number 625/1–80–012.

U.S. Environmental Protection Agency. 1998. National Water Quality Inventory: 1996 Report to Congress, EPA 841-R-97-008.

United States Census Bureau. http://factfinder.census.gov. Data retrieved 8 November 2010.

USEPA. 2001. Method 1602: Male-specific (F+) and somatic coliphage in water by single agar layer (SAL). EPA 821-R-01–029. Office of Water, U.S. Environmental Protection Agency, Washington, DC.

USEPA. 2002a. Method 1603: Escherichia coli in water by membrane filtration using modified membrane-thermotolerant Escherichia coli agar (modified mTEC). EPA 821-R-02–023. Office of Water, U.S. Environmental Protection Agency, Washington, DC.

USEPA. 2002b. Method 1600: Enterococci in water by membrane filtration using membrane-Enterococcus-indoxyl-beta-D-glucoside agar (mEI). EPA 821-R-02–022. Office of Water, U.S. Environmental Protection Agency, Washington, DC.

Van Genuchten, M.T. and W.J. Alves. 1982. Analytical Solutions of the One-Dimensional Convective-Dispersive Solute Transport Equation. United States Department of Agriculture, Agricultural Research Service, Technical Bulletin 1661.

Vandenbohede A., and L. Lebbe. 2006. Occurrence of salt water above fresh water in dynamic equilibrium in coastal groundwater flow systems. Hydrogeology Journal. **14**: 462–472

Whitman, R.L., D.A. Shively, H. Pawlik, M. Nevers and M.N. Byappanahalli, Occurrence of Escherichia coli and enterococci in Cladophora (Chlorophyta) in near water and beach sand of lake sand of Lake Michigan. Applied Environmental Microbiology. **69**: 4714–4719.

Wilhelm, S.R., S.L. Schiff, and J.A. Cherry. 1994. Biogeochemical evolution of domestic waste water in septic systems, 1: Conceptual Model. Ground Water **32**: 905-916.

Wilhelm, S.R., S.L. Schiff, and W.D. Robertson. 1996. Biogeochemical Evolution of Domestic Waste Water in Septic Systems: 2. Application of Conceptual Model in Sandy Aquifers. Ground Water. **34**: 853-864.

Yamahara, K. M., S. P. Walters, and A. B. Boehm. 2009. Growth of enterococci in unaltered, unseeded beach sands subjected to tidal wetting. Applied and Environmental Microbiology **75**: 1517-1524.

CHAPTER 6: CONCLUSIONS AND FUTURE WORK

Is SGD occurring at Stinson Beach, and if so, what is the magnitude? What are the important forces driving SGD at the site, and on what timescales do they act?

Submarine groundwater discharge is occurring at Stinson Beach, California, and is modulated by a range of forcing mechanisms including semi-diurnal tides, neap-spring tides, waves, and seasonally-variable precipitation and evapotranspiration. Research presented in Chapter 2 examined the influence of fortnightly spring-neap tidal variability on submarine discharge of fresh and saline groundwater. A groundwater-derived freshening and nutrification of the surf zone during neap tides was observed, and analytical models and a fresh water budget in the surf zone were used to estimate the saline and fresh discharge of submarine groundwater. Fresh SGD estimates were between 1.2 and 4.7 L min-1 m-1 shoreline during neap tides compared to 0.1 and 0.5 L min-1 m-1 during spring tides. Saline SGD calculated as the sum of wave- and tide-driven SGD estimates were 15.9 and 22.0 L min-1 m-1 during neap and spring tides, respectively. The observed fortnightly pulsing of fresh SGD was consistent with seaward hydraulic gradients across the fresh part of the beach aquifer, which varied due to aquifer overheight near the beach face caused by fortnightly-variable infiltration of seawater during high tides. This work confirmed the importance of neap-spring tides as a key control on the magnitude of both fresh and saline SGD at the site. Additional research should be conducted to test whether this neap-spring control on fresh and saline SGD is a widespread phenomenon or is restricted to Stinson Beach and similar locales.

Chapter 3 presents results from field experiments conducted in July 2008 and March 2007 to examine tidal, wave-driven and seasonal variability of submarine groundwater discharge (SGD) at the site using natural radium tracers. SGD was estimated using a mass balance approach. Median SGD estimates based on 223Ra and 224Ra activities were 6 and 8 L min-1 m-1 in July 2006 and 38 and 43 L min-1 m-1 in March 2007, respectively. SGD estimates for July 2007 based on radium were a factor of two to three lower than rates estimated analytically in Chapter 2, but such discrepancies in SGD

estimates obtained by independent methods are not unusual (Burnett et al. 2006). Future experimentation should aim to refine experimental methods to reduce these discrepancies.

During both experiments described in Chapter 3, short-lived radium isotope activities in the surf zone were significantly higher at low tide relative to high tide, indicating the importance of tidal pumping of saline groundwater into and out of coastal aquifers along this coastline. Tidal range correlated significantly with 223Ra and 224Ra activity in the surf zone, suggesting that the magnitude of discharge is controlled to some degree by neap-spring tidal range variability, with maximal discharge occurring during spring tide. These results corroborate the results presented in Chapter 2, which described increased SGD at spring tide. During the March 2007 experiment, surf zone activities of the short-lived isotope 224Ra were significantly positively correlated with breaker height, which explained 38% of the radium variability. This relationship is consistent with increased wave-driven SGD during large winter swell events, as predicted by theory (Longuet-Higgins 1984). To the best of our knowledge, this study was the first to observe a significant relationship between breaker height and groundwater tracer concentrations in open waters receiving SGD, and highlight the importance of wave-driven SGD along high-energy coastlines such as California. Future works should be aimed at resolving the role of waves in both driving SGD and mixing SGD-enriched nearshore waters with offshore waters.

Chapter 4 investigated the role of Mediterranean precipitation-evapotranspiration cycles on the relative magnitude and timing of fresh SGD using a SEAWAT-2000 variable density groundwater model. Monthly average recharge calculated using data collected near the Stinson Beach field site was approximately sinusoidal, with high positive recharge rates dominated by precipitation during the rainy winter season and high negative recharge rates dominated by potential evapotranspiration during the hot, dry summer months. Fresh SGD from two simulated aquifers peaked in January, coincident with maximum precipitation and recharge, and declined until reaching a minimum in September, two months after the minimum recharge period in July. Minimum simulated discharge rates for two simulated scenarios were 17% and 18% lower in September than the maximum discharges simulated in winter, respectively,

highlighting the importance of the Meditternaten climate in driving variation in fresh SGD on the seasonal timescale.

Is SGD an environmentally relevant source of nutrients and/or microbiological pollution to the coastal environment?

Chapters 2 and 3 each addressed the magnitude and environmental relevance of SGD-associated fluxes of nutrients and/or microbial pollution to the coastal ocean at Stinson Beach. In Chapter 2, fresh-, saline-, and total (fresh + saline) groundwater discharge-associated nutrient fluxes were calculated for neap and spring tide conditions. Despite a smaller total discharge of groundwater during neap tide compared to spring tides, a larger fresh discharge component during neap tides raised surf zone silicate, DIN, and SRP by 14%, 35%, and 27%, respectively, relative to spring tides. Following this groundwater-derived freshening and nutrification of the surf zone during neap tides, a 4-day increase in chlorophyll a concentrations was observed. The link between the increase in chlorophyll a concentrations and the neap tide nutrification of the surf zone was investigated in the laboratory using mesocosms phytoplankton growth experiments. Significant increases in chlorophyll in mesocosms containing only a few percent site groundwater highlighted the importance of site groundwater as an ocean fertilizer, confirming the environmental relevance of ocean nutrient enrichment by SGD.

During the experiments described in Chapter 2, high concentrations of enterococci were detected in groundwater at the site. Detection of the human-specific enterococcal surface protein (esp) gene confirmed that some of the enterococci were likely of human origin. However, no increase in enterococci in the surf zone was documented during the period of highest fresh SGD, suggesting that fecal indicator bacteria were not discharging with contaminated groundwater in detectable concentrations during the study.

In Chapter 3, estimates of SGD-associated nutrient flux were compared with that of surface waters discharging to the ocean within 6 km of the study site. Mean +/- standard deviation creek-associated nutrient flux during the March 2007 study was estimated at 10 ± 3 mmol min^{-1} phosphate, 4 ± 1 mol min^{-1} silicate, and 200 ± 50 mmol

min^{-1} dissolved inorganic nitrogen. SGD-associated nutrient flux at the study site in March 2007 was 99 μmol phosphate min^{-1} m^{-1}, 4940 μmol silicate min^{-1} m^{-1}, and 1160 μmol DIN min^{-1} m^{-1}. Thus, SGD from only 200 m of Stinson Beach was responsible for a nutrient flux approximately equal to the total creek-associated flux of phosphate and dissolved inorganic nitrogen discharged within 6 km of the study site in March 2007, highlighting the importance of site groundwater as a major and environmentally relevant nutrient source to the coastal ocean.

Chapter 5 estimates fluxes of nutrients and fecal indicator bacteria from a single septic system plume flowing through the beach to the subterranean estuary. Discharge of substantial total nitrogen associated with the septic effluent plume was documented throughout the year. Only in late summer did we document a flux of fecal indicator bacteria (enterococci) from fresh groundwater to the subterranean estuary. Because the fate of enterococci in the field was variable over time, we conclude that septic systems at the site may at certain times be a source of fecal indicator bacteria to the subterranean estuary and the surf zone. This result should be corroborated using a similar experimental design but where tracers are injected with septage in order to more closely monitor transport of fecal indicator bacteria in coastal septic effluent plumes.

What role do on-site wastewater treatment systems play in contaminating groundwater at the site? Is attenuation in the saturated zone adequate for in-situ treatment septage-derived contamination before discharge to the ocean?

Having documented high concentrations of nutrients and fecal indicator bacteria in Stinson Beach groundwater in Chapters 2 and 3, Chapter 5 documents the characterization of a single plume of septic effluent at the site in order to better understand contaminant fate and transport in the coastal groundwater setting. Specifically, a plume of septic effluent was observed flowing through the beach into the subterranean estuary. Median estimates of total nitrogen fluxing toward the ocean downgradient from the leach field were substantial, ranging from 1.6 to 70.6 moles day-1, depending on season and downgradient location. These fluxes compared well with previous estimates of SGD-associated DIN flux, as reported in Chapter 2. Despite high

concentrations in septage pumped to the leach field, no E. coli or coliphage was detected in the plume, suggesting complete attenuation within the vadose zone and/or the first few meters of transport. These observations were consistent with results from laboratory experiments suggesting fast fecal indicator bacteria and virus attenuation in saturated column experiments. Although attenuation of enterococci was similarly fast in the same laboratory experiments, enterococci were detected throughout the well network during one sampling event during which no attenuation was observed. These results suggested either exogenous inputs of enterococci to the plume within the well network, or growth along the flowpath. Collectively, results from Chapter 5 support the assertions from earlier chapters that septic systems at the site are persistent sources of nitrogen to the subterranean estuary, but also suggest that they may at times also be a source of enterococci.

APPENDIX A: SUPPLEMENTAL INFORMATION TO CHAPTER 5

A.1 SITE HYDROGEOLOGY.

Stinson Beach Park has long been noted by park staff as an area of high water table and substantial fresh SGD. Historical records show a shallow wetland, Willow Camp Lake, also known as Poison Pond, fed by groundwater and a seasonal creek, Easkoot Creek, in the current location of the South Parking Lot at Stinson Beach Park. In the early 1900's, the creek was diverted through the downtown area to Bolinas Lagoon, a large tidal lagoon located just northwest of the town (MCOSD 1996). Poison Pond was subsequently filled in to make an overflow parking lot for the Park. A high water table persists in the northwest corner of the parking lot, closest to the current path of Easkoot creek, the likely vestige of the groundwater-fed wetland that used to exist there.

A.2 WELL INSTALLATION.

The well network at Stinson Beach consisted of three types of monitoring wells and piezometers, each with distinct construction, installation, and purpose (Fig. S1). In November 2003 and April 2004, prior to our experiments, a sparse array of two-inch polyvinyl chloride (PVC) wells was installed by the National Park Service to monitor groundwater head in the South parking lot at Stinson Beach Park. The wells were installed by digging a trench and backfilling with native material around slotted pipe. In Spring 2007, a second set of 2" PVC monitoring wells with 2 m screens were installed by hand auger. A 3-inch hole approximately 1.5 m below the water table was made, the slotted pipe was installed, and native media was allowed to collapse around the slotted pipe. After compiling long-term synoptic and continuous groundwater head data from wells at the site and projecting a flow path downgradient from the leach field, a third array of multi-level nested monitoring wells was installed for measuring mass flux. These multi-level wells consisted of a single rigid 1-inch PVC slotted pipe with a 1.5 m long screen at the base, around which three ¼-inch low-density polyethylene sampling tubes were clustered. The base of each LDPE sampling tube was outfitted 1.5 m of slotted

tubing covered in a 0.01-inch LDPE mesh sleeve. The three sampling tubes were then staggered vertically along the central PVC stalk so as to sample from 1.5-m long depth-discrete intervals. Each multi-level well was then installed using a GeoProbe vibratory sampling rig to approximately 4.5 m below the water table. Multi-level wells were installed along three transects approximately orthogonal to groundwater flow and centered on the projected centerline of the plume. Each well was finished below ground surface, surveyed by standard methods using a scope and stick, and buried to reduce contact with beachgoers.

A.3 HYDRAULIC GRADIENT CALCULATIONS.

Head measurements collected in the vicinity of the septic leach field were binned by month and averaged. Mean heads for each record were then plotted on a base map of the well network. Flow lines passing through each well were traced on the map, and distance from water line along a flow line for each well was measured. All monthly data from each well was plotted against measured distance from water line. Using a y=0 intercept for sea level at the water line, linear regression was used to calculate hydraulic gradient with estimates of error (Fig. S2).

A.4 HYDRAULIC CONDUCTIVITY.

Hydraulic conductivities were estimated using the tidal efficiency method (Ferris 1951), which is based on the concept of tidal wave propagation and dampening with distance in a coastal aquifer with a tidal boundary (Ferris 1963). The relationship between the amplitude of water level fluctuations in the ocean and in a well penetrating the coastal aquifer, and the distance from the well to the tidal boundary, is related to the hydraulic conductivity of the aquifer between the well and the boundary. We measured tidal efficiency at multiple wells during two periods of the study with little or no precipitation. The periods analyzed were 20 April 2008 to 18 June 2008 for wells S10, S12 and S15 and from 12 November 2008 to 10 January 2009 for wells S20 and S21. No open-ocean tide gauge exists at the site; we assumed that tides were well represented by the tide gauge at Point Reyes, CA (http://tidesandcurrents.noaa.gov, Sta. ID 9415020, 37°59’48”N, 122°58’30”W), an assumption made for previous experiments at Stinson

Beach (de Sieyes et al. 2008, de Sieyes et al. 2011). The tidal efficiency method requires estimates of aquifer thickness and storage. For the purposes of this analysis, we assume a uniform beach aquifer thickness of 32 m (SBCWD 1998) and a specific yield of 0.25, a value typical of well-sorted, fine-grained sands (Fetter 2001). For these calculations, head records were de-trended and high pass filtered using a cutoff of 2.5 days to remove longer-term head variations not associated with semidiurnal tides. Tidal efficiency was then calculated at distances from the approximate mean water line as estimated from survey data using the tidal record from the Pt. Reyes buoy as a tidal boundary. In order to reduce sloping boundary affects, which are known to negatively affect tidal efficiency results near the boundary, a second set of tidal efficiency analyses was carried out as follows. Inland distances were measured from well S21, the most seaward monitoring well, and tidal efficiency was calculated at each of the other wells using the S21 head record as a tidal boundary. Results from the two methods agreed reasonably well, and were combined for use in future calculations. Results are reported in Table S1.

A.5 ANALYTICAL METHODS.

Concentrations of nitrate, nitrite, ammonium and orthophosphate were measured by standard colorimetric methods using an automated WestCo SmartChem 200 spectrophotometer (Brookfield, CT). Detection limits are 0.2 μM nitrate, 0.1 μM nitrite, and 0.1 μM ammonium. Dissolved inorganic nitrogen (DIN) is reported as the sum of nitrate, nitrite, and ammonium. Total dissolved nitrogen (TN) was determined by digesting total nitrogen to nitrate using persulfate digestion following D'Elia et al. (1977) and analyzing for nitrate. Dissolved organic nitrogen (DON) was calculated by subtracting DIN from TN. In some samples in which DIN approached TN, sampling or measurement error resulted in negative DON values. Negative DON values were replaced with zeroes for the purposes of our analysis.

Total and inorganic carbon concentrations (TC and DIC, respectively) were analyzed by standard methods using a Shimadzu TOC-5000A autoanalyzer (Kyoto, Japan). Detection limits are 200 μM for both TC and DIC. Dissolved organic carbon (DOC) was calculated as the difference between TC and DIC. Negative DOC values were replaced with zeros for the purposes of our analysis.

Unfiltered water samples for analysis of fecal indicator bacteria and bacteriophage (FIBV) were collected into 10% HCl acid-washed polypropylene bottles and stored on ice until analysis within 6 h of collection. For groundwater samples, duplicate 50-mL unfiltered aliquots were vacuum-filtered onto 47-mm-diameter 0.45-μm cellulose filters (Millipore Inc., Billerica, MA). For septic tank samples, serially diluted duplicates of 1mL, 0.1 mL, and 0.01 mL were filtered using phosphate buffered saline solution as diluent. Colonies of *E. coli* were enumerated after incubation on modified mTEC media (BD Difco, Franklin Lakes, NJ) for 24 hours at 44.5°C according to standard methods (USEPA 2002a); due to constraints in the field laboratory, the 2 h resuscitation incubation step at 35°C was omitted. The second duplicate filter was analyzed for enterococci by enumeration on mEI media (BD Difco) after incubation at 41 ± 0.5°C for 24 hours according to standard methods (USEPA 2001). Unfiltered samples were also collected for two viral indicators of fecal pollution in groundwater, male specific (F+) and somatic coliphage. For a given sample, two unfiltered 40-mL samples were collected into clean polypropylene vials, stored on ice, and analyzed by the single agar layer method following EPA method 1601 (USEPA 2002b) within 24 hours of collection.

A.6 CONTAMINANT FLUX CALCULATIONS.

Fluxes associated with groundwater flowing through control planes made up of multilevel well transects installed orthogonal to flow downgradient from the septic system were calculated via the Theissen polygon transect approach using the following equation:

$$w_{cp} = i_{cp} \sum_{n=1}^{n_{well}} \left(\sum_{m=1}^{n_{ver}} \left(A_{n,m} \bullet K_{n,m} \bullet C_{n,m} \right) \right) \qquad \text{(S1)}$$

where w is total flux (moles time^{-1} or microorganisms time^{-1}), K is hydraulic conductivity (length time^{-1}), A is the area of sampled interval (length^2) for each zone of aquifer monitored by a given monitoring well for which a contaminant concentration C (mass volume^{-1}) is representative, i is hydraulic gradient (-), subscript cp denotes the entire control plane, and subscripts n and m delineate the horizontal and vertical position of a

each well in that control plane, respectively. A description and examples of this method can be found in Einarson and Mackay (2001).

In cases where downstream contaminant flux declines significantly with distance due to destructive attenuative mechanisms, bulk attenuation rates can be calculated from field data (Borden et al. 1997). A number of assumptions are required for such a calculation, and removal processes must be modeled conceptually for nitrogen, fecal indicator bacteria, and bacteriophage fate downgradient from the leach field. Considering the 20-year lifespan of the septic system and the high hydraulic gradients in the area, we assume that plume chemistry had reached steady state with respect to advection and dispersion along the 15 m flowpath between the leach field and the downgradient edge of our monitoring network. We also assume that septage inputs have been approximately constant with respect to volumetric discharge and N, FIB, and phage concentration throughout the lifespan of the septic system, as per discussions with park maintenance staff, and that steady state has been reached with respect to sorption/desorption of each contaminant. Considering our monitoring is mainly above the zone of seasonal erosion and redeposition, we also assume that microbial populations responsible for N cycling are relatively stable in the area of our network. In such a setting, expected losses of TN along the flowpath will be due to denitrification and annamox. Annamox is poorly understood in natural coastal aquifer sediments, and we assume as others have that denitrification is likely the major factor influencing nitrogen bulk attenuation along the flowpath (Rivett et al. 2007). For FIBV, we assume that any attenuation in the field is due to destructive attenuation mechanisms including die-off, attachment, straining and blocking and ultimately die-off. For FIB, the bulk attenuation observed may also reflect the potential shift to the viable but non-culturable (VBNC) state.

A.8 COLUMN EXPERIMENTS.

On 2 December 2009 (C1) and 8 December 2009 (C2), samples were collected into autoclaved glass jars from the depth of the water table using an ethanol-sterilized auger. Using a dedicated sampling tube and a peristaltic pump, 2 L of unfiltered groundwater was then sampled from each bore into a 10% HCl-washed glass bottle. As described in the main text, a sonde and flow-through cell was used to measure additional

water quality characteristics from each bore (Table S2). The soils and groundwater were stored on ice during transport to the laboratory. Once at the lab, the sand and groundwater were stored at 15 °C until use. All experiments were run within 24 hours of sample collection.

Glass columns used in the saturated experiments were 22 cm long by 2.54 cm diameter. Columns were fitted with a Teflon end pieces. The Teflon end pieces were covered with a disk of 200 μm stainless steel mesh to prevent sand grains from entering the inlet or outlet of the column end pieces. Columns were fitted with Teflon tubing and fittings. A Variable Flow Mini-Pump (Fisher Scientific, City, State) with silicon tubing and polypropylene fittings was used to pump solution through each column. All experiments were performed at 15 °C.

Prior to packing, the collected soils were homogenized by hand folding for 10 minutes with a sterile stainless steel spoon. The columns were wet-packed according to (Jin et al. 1997). Groundwater extracted from the sample site was used for the wet-packing. The columns were leached with 4 pore volumes over 30 min of groundwater prior to the start of the experiment to equilibrate conditions. Fractions were tested from each pore volume of the initial flush for enterococci, somatic and male specific (F+) coliphage.

A solution containing groundwater, 10% sewage (v/v), and potassium bromide tracer was prepared at the start of the experiment. This solution is henceforth referred to as the 'working solution'. The sewage used was raw sewage collected from the Palo Alto Water Quality Control Plant within 24 hours of the column experiment. Prior to mixing, the raw sewage was passed through a 200 μm screen to remove large particulates. The bromide tracer concentrations in the fresh and saline columns were 350 ppm and 1000 ppm respectively. These concentrations were chosen to keep the addition of potassium bromide to a minimum, while still allowing detection on the bromide electrode. The saline column required a higher concentration of bromide due to the higher bromide background concentrations in the saline groundwater. Influent concentrations are reported in Table S3.

After the initial flushing of groundwater, the influent solution was switched to the working solution. The working solution was gently mixed using a stir bar and magnetic

stirrer for the duration of the experiment. Five ml fractions were collected from the effluent every 20 minutes for the course 18 hours, which equated to approximately 7 pore volumes of working solution being pumped through the column. The superficial flow rates through the fresh and saline columns were 2.9 +/- 0.30 cm/hr and 3.1 +/- 0.54 cm/hr, respectively. The working solution was sampled every 6 hours and analyzed for concentrations of enterococci, somatic and male specific (F+) phage to account for potential inactivation.

During the experiments, the effluent fractions were tested for enterococci according to EPA Method 1600 (USEPA 2002b; detection limit = 100 cfu $(100\ ml)^{-1}$) and for somatic and male specific (F+) coliphage using the double agar layer (DAL) method of EPA Method 1602 (USEPA 2001; detection limit = 100 pfu $(100\ ml)^{-1}$). Bacterial and viral samples were processed within six and 24 hours of sample generation, respectively. Three dilutions (equivalent to 1 ml, 100 μl and 10 μl of column effluent fraction) were tested for enterococci and somatic phage, and two dilutions (equivalent to 1 ml and 100 μl of column effluent fraction) were tested for male specific (F+) phage. Plates with between 10 and 100 plaque forming units (PFU) are presented and used in calculations.

Bromide concentrations were measured using a Thermo Scientific Orion EA940 outfitted with a Thermo Scientific Orion 9635BNWP ionPlus Bromide Ion-Selective Electrode (Manufacturer, location), pursuant to manufacturer instructions. The probe was rinsed in DI water and dried between measurements.

The convection-dispersion equation (CDE; Eq. S1) was fit to column effluent data to estimate colloid transport and removal parameters in each saturated column experiment (van Genuchten and Alves, 1982).

$$R\frac{\partial C}{\partial t} = D\frac{\partial^2 C}{\partial z^2} - V\frac{\partial C}{dz} - \mu RC \qquad \text{(S2)}$$

The equation assumes uniform water content and steady state flow conditions and includes terms for linear equilibrium sorption and first order removal such as filtration, inactivation, and irreversible sorption. In Eq. S1, C is the viral or bacterial concentration in the liquid phase (cfu ml^{-1} or pfu ml^{-1}), D is the hydrodynamic dispersion coefficient

(cm^2 min^{-1}), V is the water velocity (cm min^{-1}) and μ is the first order virus or bacteria removal rate coefficient (min^{-1}). R is the retardation factor, as defined in Eq. S2:

$$R = 1 + \frac{\rho_b K_d}{\theta} \quad \text{(S3)}$$

where ϱ_b is the bulk density of the sand (g/cm^3, dry weight), K_d is the equilibrium distribution coefficient between the liquid and sorbed phases (cm^3 g^{-1}), and Θ is the volumetric water content (cm^3 cm^{-3}). Parameters were calculated using STANMOD Version 2.2 from UC Riverside & US Salinity Laboratories. Tracer data was input into the CXTFIT2 package to estimate D and V for each column. For the bromide tracer it was assumed that there was no removal (μ=0) and no retardation (R=1). Next the calculated D and V for bromide were used as inputs along with the virus and bacteria concentrations to the CXTFIT2 package; this approach assumes that D and V are equal for both bromide and the colloid being modeling. The CXTFIT2 package was then used to calculate μ and R values for the virus and bacteria in each column. Results are reported in Table S4. For the somatic phage, data beyond the first 3 pore volumes was poorly described by the model, so only the data from the first 3 pore volumes were used for the calculation of μ and R calculations.

A.9 DENITRIFICATION POTENTIAL ASSAYS.

Samples analyzed for denitrification potential analysis were collected on 24 August 2009 (DNP1-8, Fig. S1). At each sampling location, a 70% ethanol-cleaned, dry hand auger was used to sample approximately 1 kg of sediment from the water table into an autoclaved glass jar. The sample was then bubbled with 99.999% nitrogen gas (Alliance Gas) to remove oxygen introduced by the soil extraction process. The samples were capped and stored on ice for transport back to the laboratory. In the laboratory, the samples were stored at 15 Cº until analysis (within 24 h of collection). Prior to testing, the samples were allowed to warm to 21.5 +/-0.5 ºC and then were homogenized by folding using a 70% ethanol cleaned, dry steel spatula.

The acetylene block slurry method was used to estimate denitrification potential of the sediment samples, following Tiedje (1982). Prior to testing, a solution of sterilized DI water was prepared with 2 mM sodium nitrate and with 2 mM sodium acetate as a labile organic carbon source (Pfenning and McMahon 1996; Laverman et al. 2006). Hereafter, this is referred to as 'working solution'. The solution was vigorously bubbled with 99.998% nitrogen (Praxair, Medipure) for one hour prior to testing in order to purge dissolved oxygen.

The eight samples were run in triplicate. In addition, a control consisting of autoclaved sands from site DNP2 was included. For each sample, three sterile 250 ml serum bottles were weighed and then packed with approximately 130 grams of sediment. Once packed, the bottles were weighed again. 65 ml of the previously described working solution were added to each bottle. A needle connected to the 99.998% nitrogen was inserted into each bottle and the solution was bubbled for 30 minutes prior to the start of the test. Each bottle was then sealed with a septa and crimp top, maintaining a nitrogen headspace.

At the start of the experiment, acetylene gas was generated by exposing calcium carbide to water (Pfenning and McMahon 1996). Each sealed serum bottle was injected to 10% acetylene by volume. Bottles were shaken vigorously, vented, and resealed, marking the start of the assay. The serum bottles were placed on an orbital shaker table set at 200 RPM, following Laverman (2006). Samples of the head space were collected from each serum bottle at 15, 30, 45 and 60 min elapsed time, after shaking vigorously. Prior to sampling, a syringe with stopcock and needle was flushed three times with gas from the headspace, after which 4 ml of headspace gas was sampled and sealed in the syringe for analysis on the gas chromatograph. All experiments were performed at 21.5 +/-0.5 ºC. Gas samples from the headspace were tested for nitrous oxide concentrations on a Shimadzu GC-14A gas chromatograph equipped with and ECD (^{63}Ni) detector (Tiedje 1982). After each test, the bottles were opened, dried at 105 ºC, and re-weighed to determine the weight of dry sand in each bottle.

Nitrous oxide peak heights from the gas chromatograph were converted to nitrous oxide concentrations based on a linear calibration curve established with standard gas injections. The concentration of nitrous oxide in the headspace was converted to the

number of total moles of nitrous oxide for each time point, in each of the triplicate samples. This conversion was done by assuming ideal gas behavior in the headspace, and assuming equilibrium behavior for Henry's Law for the number of moles dissolved in solution. A linear regression was used with all data points from the triplicate samples to determine the rate of nitrous oxide production (nmol N hr^{-1}). The rate at which nitrous oxide is produced is assumed to be equal to the rate of denitrification. The rates were finally normalized by the dry weight of sand (nmol N hr^{-1} (g dry sediment)$^{-1}$. Data from three sample bottles confirmed for NO_2 contamination or leaky septa seals were omitted from analysis. DNP rates are reported in Table S5.

The minimum DNP quantifiable rate limit (nmol N hr^{-1}) was estimated by assuming a headspace nitrous oxide concentration equal to the detection limit (0.110 ppm nitrous oxide) at the end of a 1-hour experiment. The estimate assumes the average mass of dry sand used during all assays. This DNP limit was found to be 5.85×10^{-3} nmol N hr^{-1} g^{-1}.

Figure S1. Plan view of Stinson Beach south lot field site including bathrooms and wet well, leach fields #1 and #2, 2" wells S12, S10, and S08, multi-level well transects A, B, and C, sample locations for the fresh and saline FIBV attenuation column studies, and denitrification potential sample locations DNP1-DNP8.

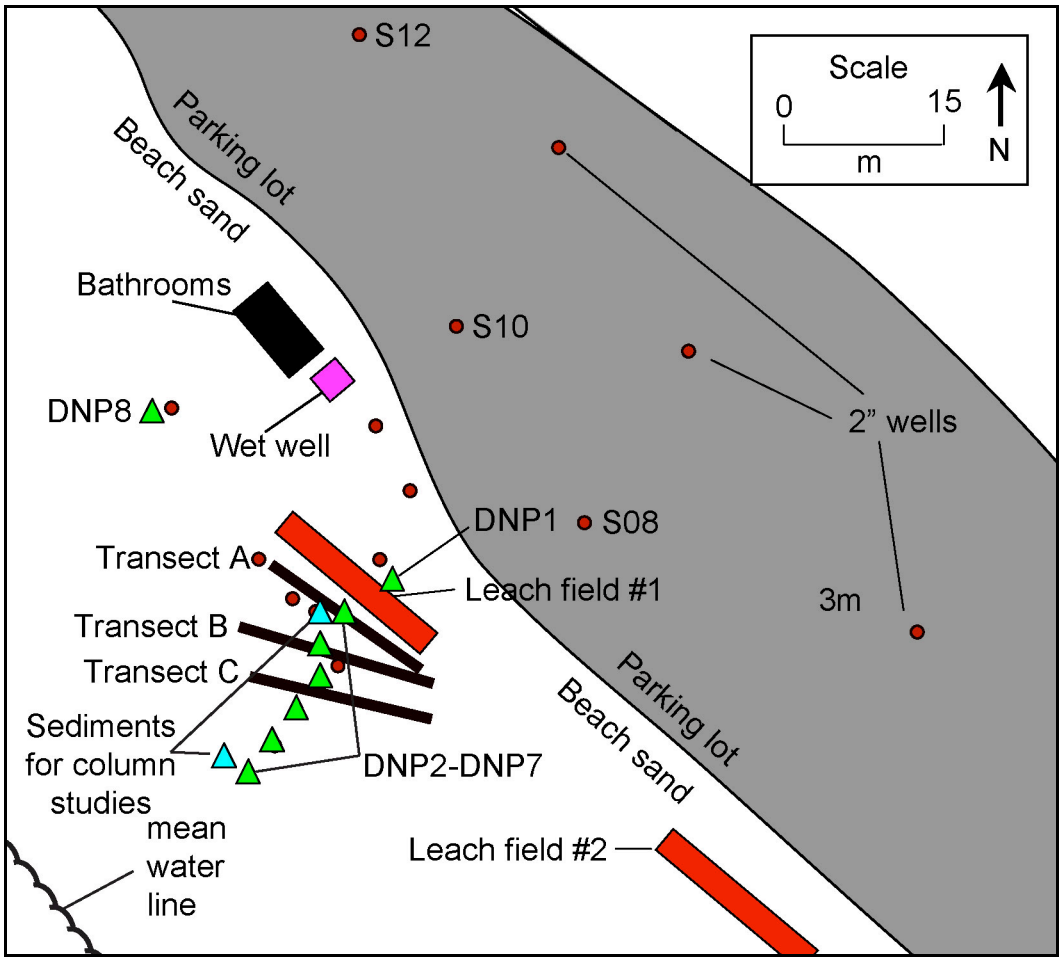

Figure S2. Monthly mean +/- standard deviation hydraulic gradients. Positive gradients indicate downward slope in the direction the ocean. Hydraulic head data are missing for August 2008 due to equipment failures in the field. Standard deviations are shown for all months but are sometimes too small to be seen in the figure.

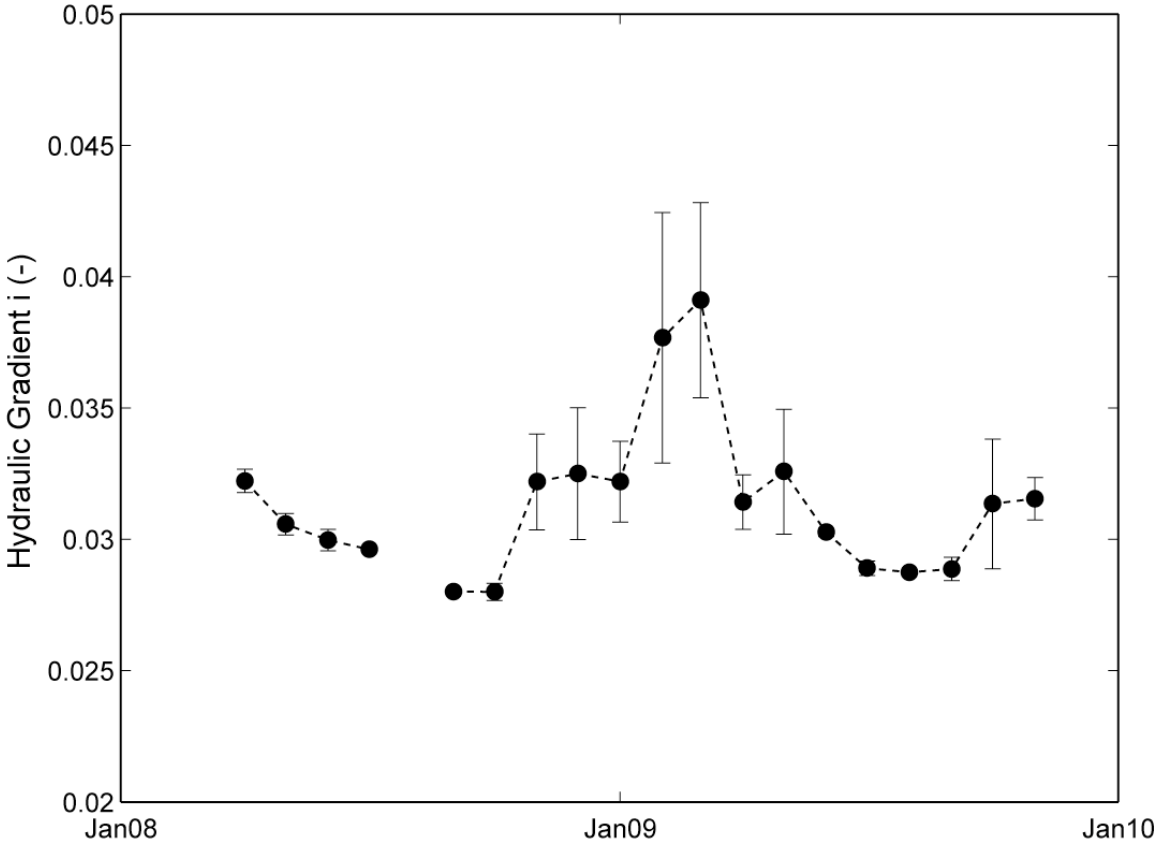

Figure S3. Wenner array resistivity profiles from low-low tide on 22 November 2008 and a plot of the absolute change in resistivity between the Wenner array profiles collected on 5 April 2009 and 22 November 2008.

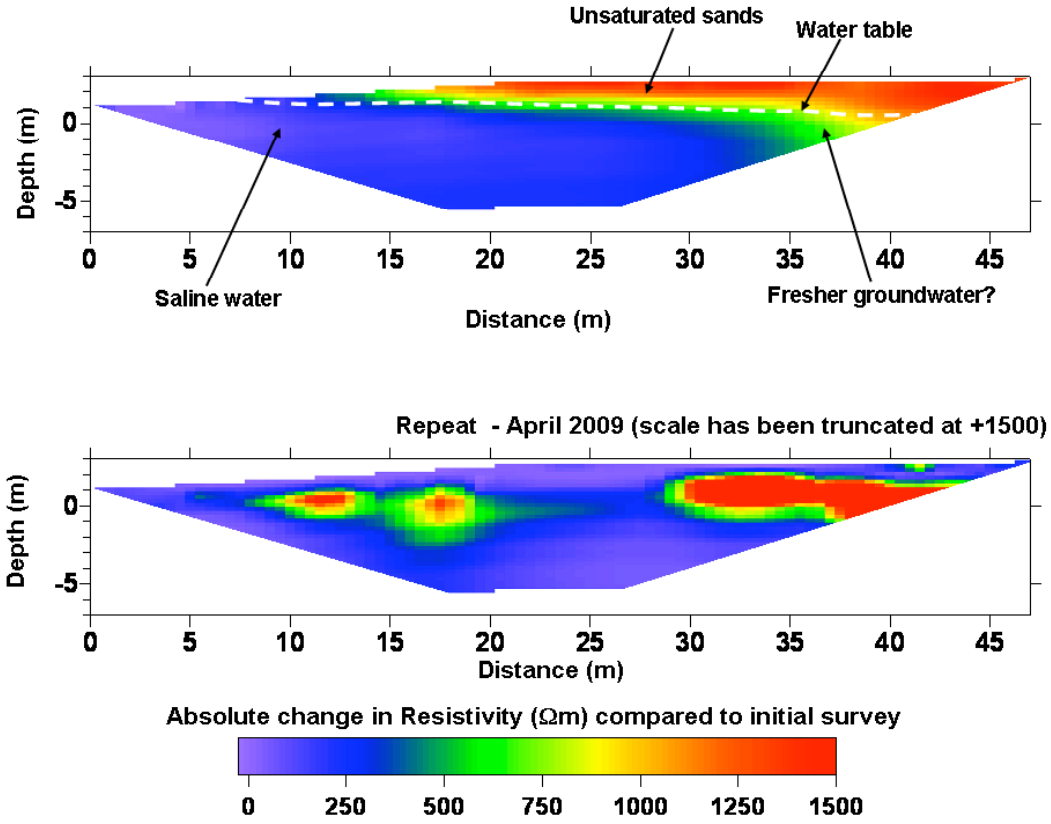

Figure S4. Cross-sectional contour plots of TC (a), DIC (b), DOC (c), pH (d; no data collected), nitrate (e), nitrite (f), ammonium (g), DIN (h), DON (i), and TN (j) concentrations in Transect A in November 2008. Open circles in the plot delineate locations where samples were collected. The color bar limits for each plot are based on the limits of concentrations along the cross section.

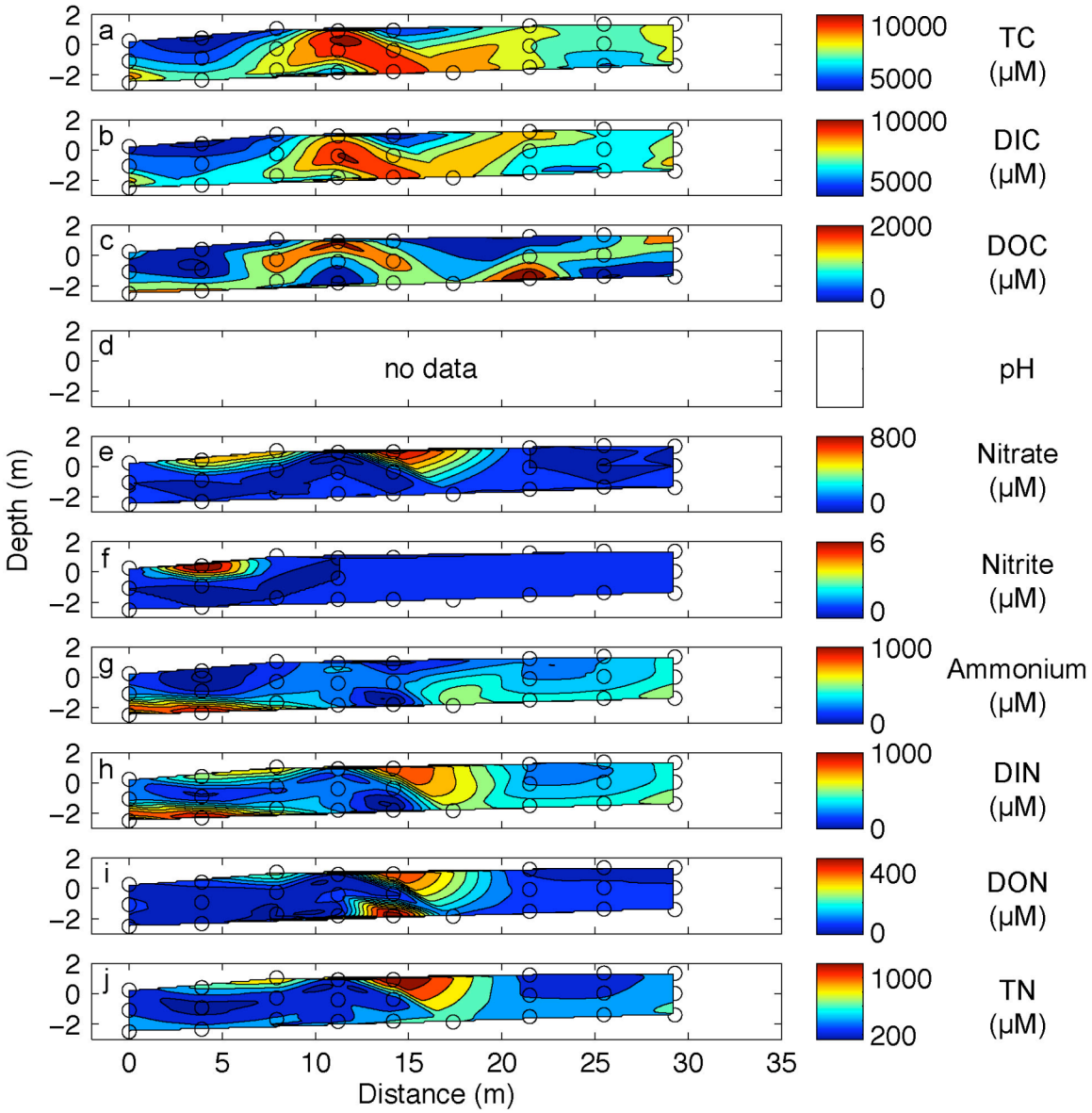

Figure S5. Cross-sectional contour plots of TC (a), DIC (b), DOC (c), pH (d; no data collected), nitrate (e), nitrite (f), ammonium (g), DIN (h), DON (i), and TN (j) concentrations in Transect B in November 2008. Open circles in the plot delineate locations where samples were collected. The color bar limits for each plot are based on the limits of concentrations along the cross section.

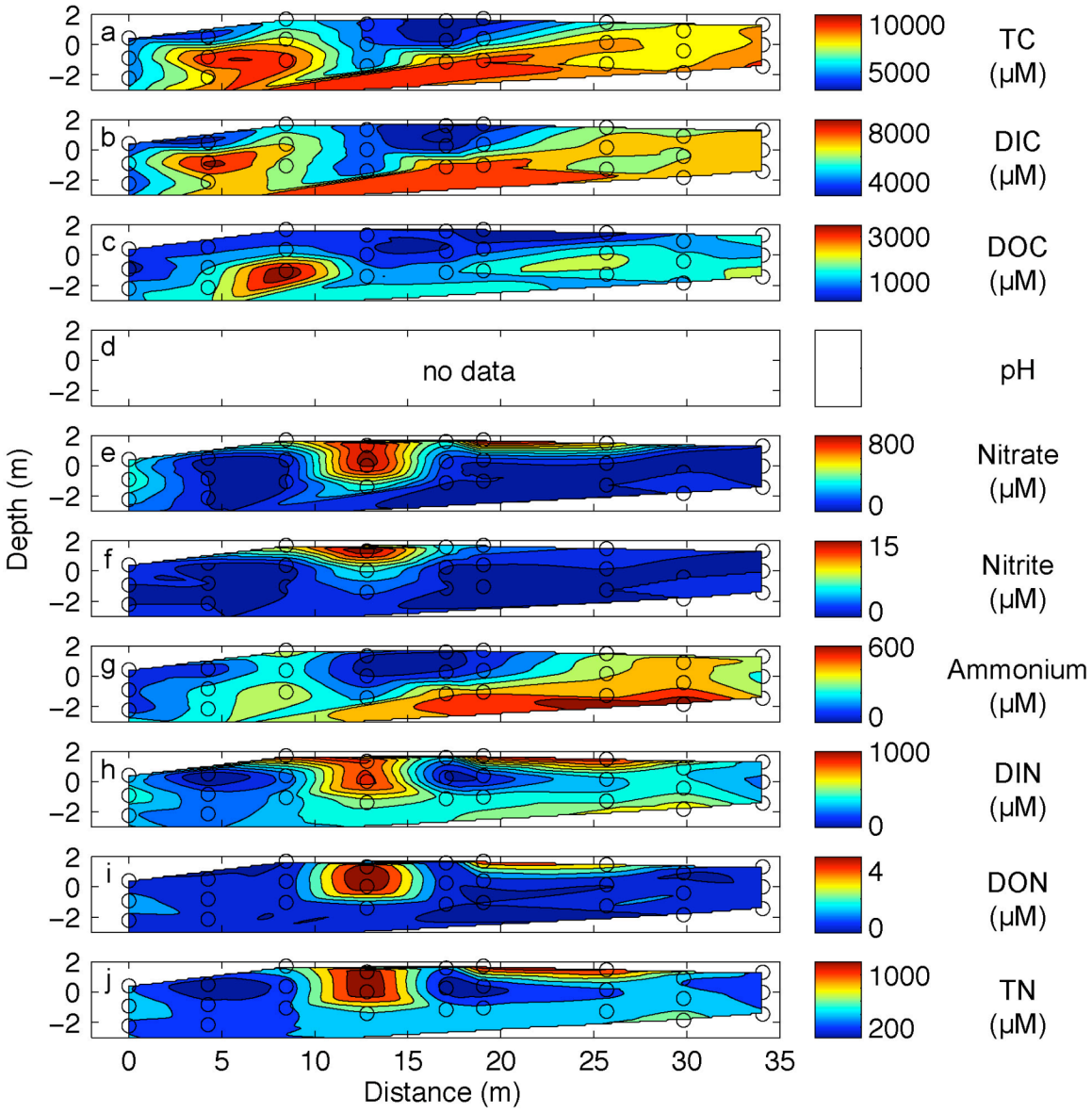

Figure S6. Cross-sectional contour plots of TC (a), DIC (b), DOC (c), pH (d; no data collected), nitrate (e), nitrite (f), ammonium (g), DIN (h), DON (i), and TN (j) concentrations in Transect C in November 2008. Open circles in the plot delineate locations where samples were collected. The color bar limits for each plot are based on the limits of concentrations along the cross section.

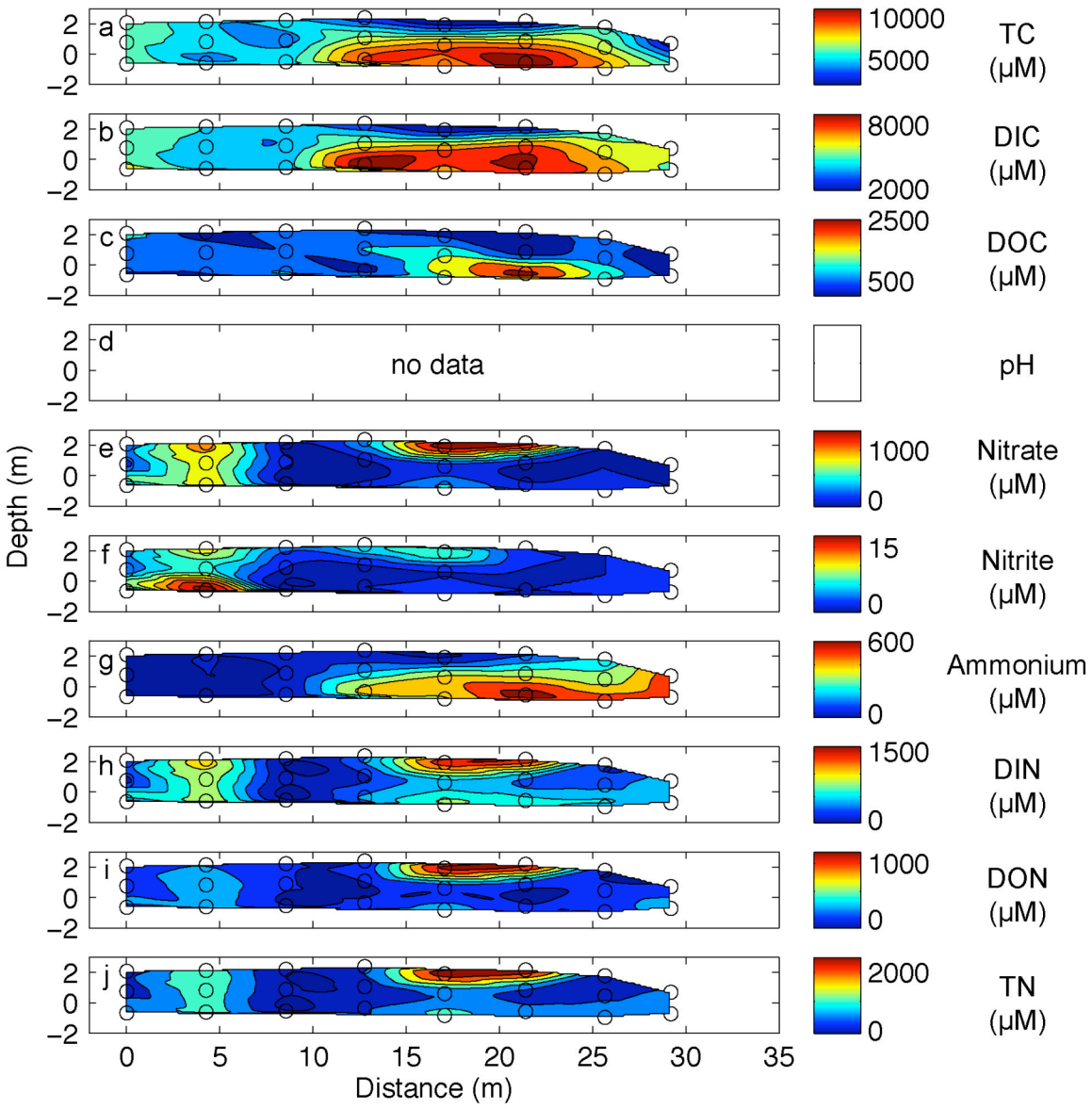

Figure S7. Cross-sectional contour plots of TC (a), DIC (b), DOC (c), pH (d), nitrate (e), nitrite (f; all data below detection limit (<DL)), ammonium (g), DIN (h), DON (i; all data below detection limit (<DL)), and TN (j) concentrations in Transect A in April 2009. Open circles in the plot delineate locations where samples were collected. The color bar limits for each plot are based on the limits of concentrations along the cross section.

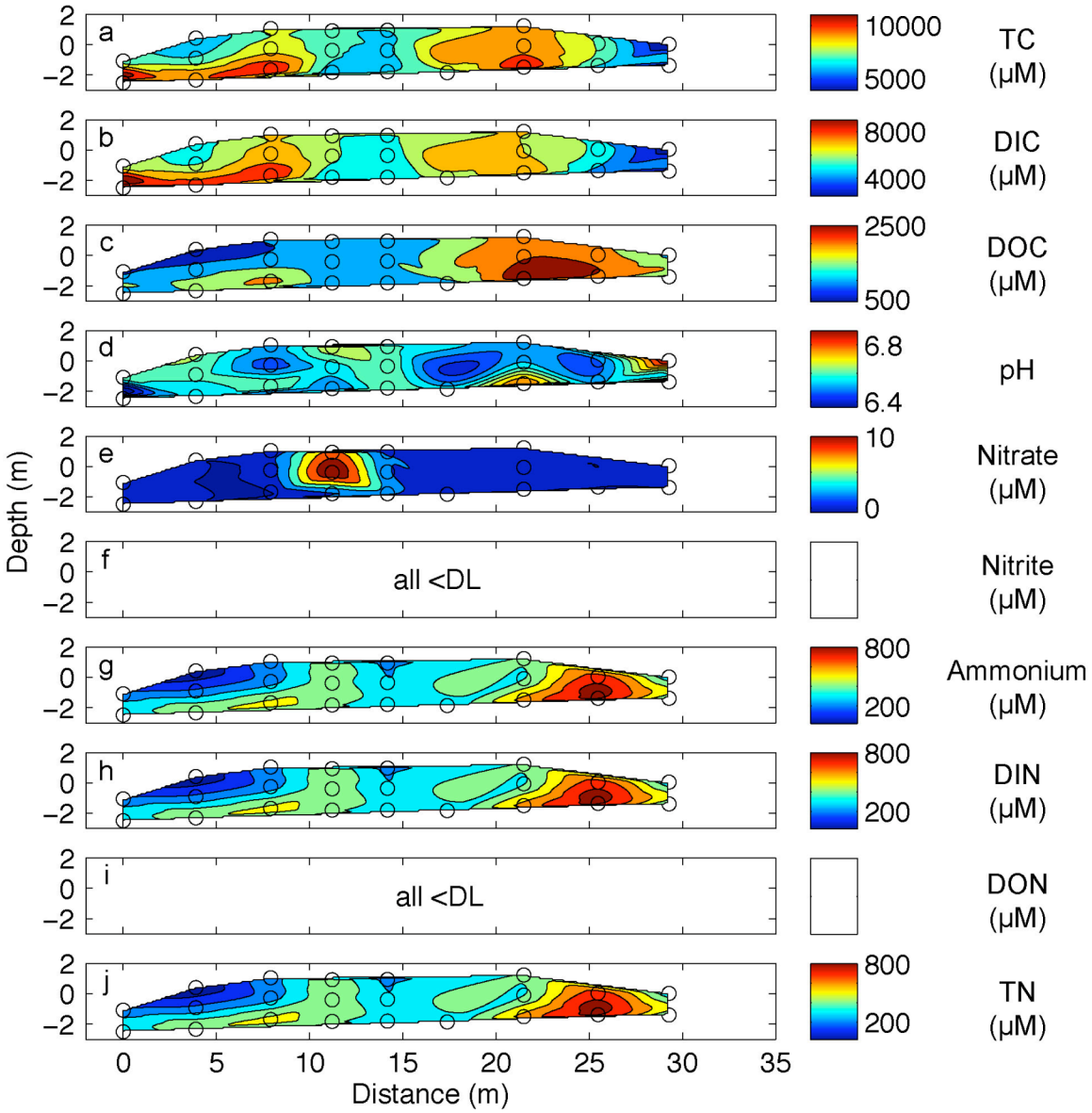

Figure S8. Cross-sectional contour plots of TC (a), DIC (b), DOC (c), pH (d), nitrate (e), nitrite (f), ammonium (g), DIN (h), DON (i; all data below detection limit (<DL)), and TN (j) concentrations in Transect B in April 2009. Open circles in the plot delineate locations where samples were collected. The color bar limits for each plot are based on the limits of concentrations along the cross section.

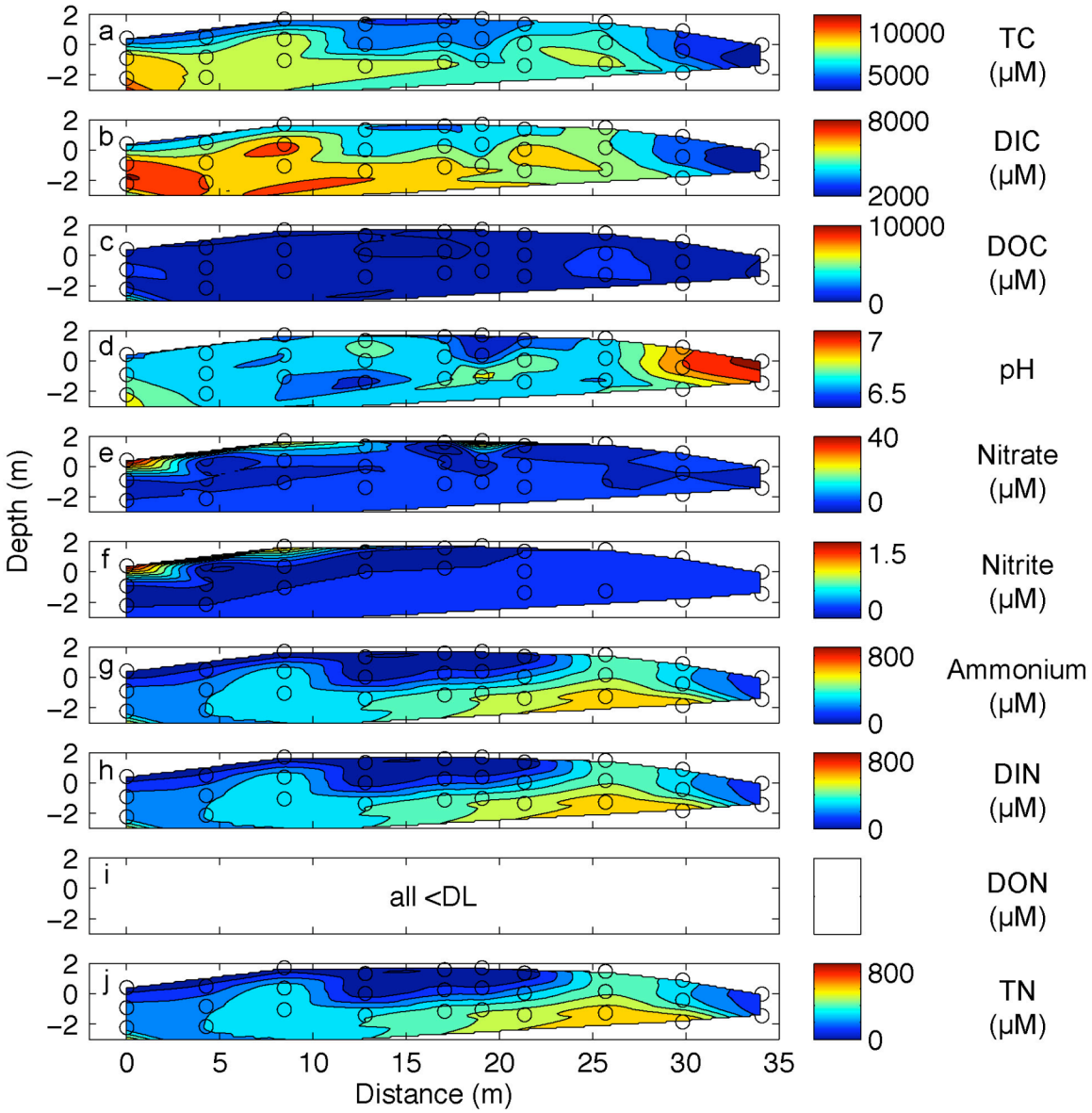

Figure S9. Cross-sectional contour plots of TC (a), DIC (b), DOC (c), pH (d), nitrate (e), nitrite (f), ammonium (g), DIN (h), DON (i; all data below detection limit (<DL)), and TN (j) concentrations in Transect C in April 2009. Open circles in the plot delineate locations where samples were collected. The color bar limits for each plot are based on the limits of concentrations along the cross section.

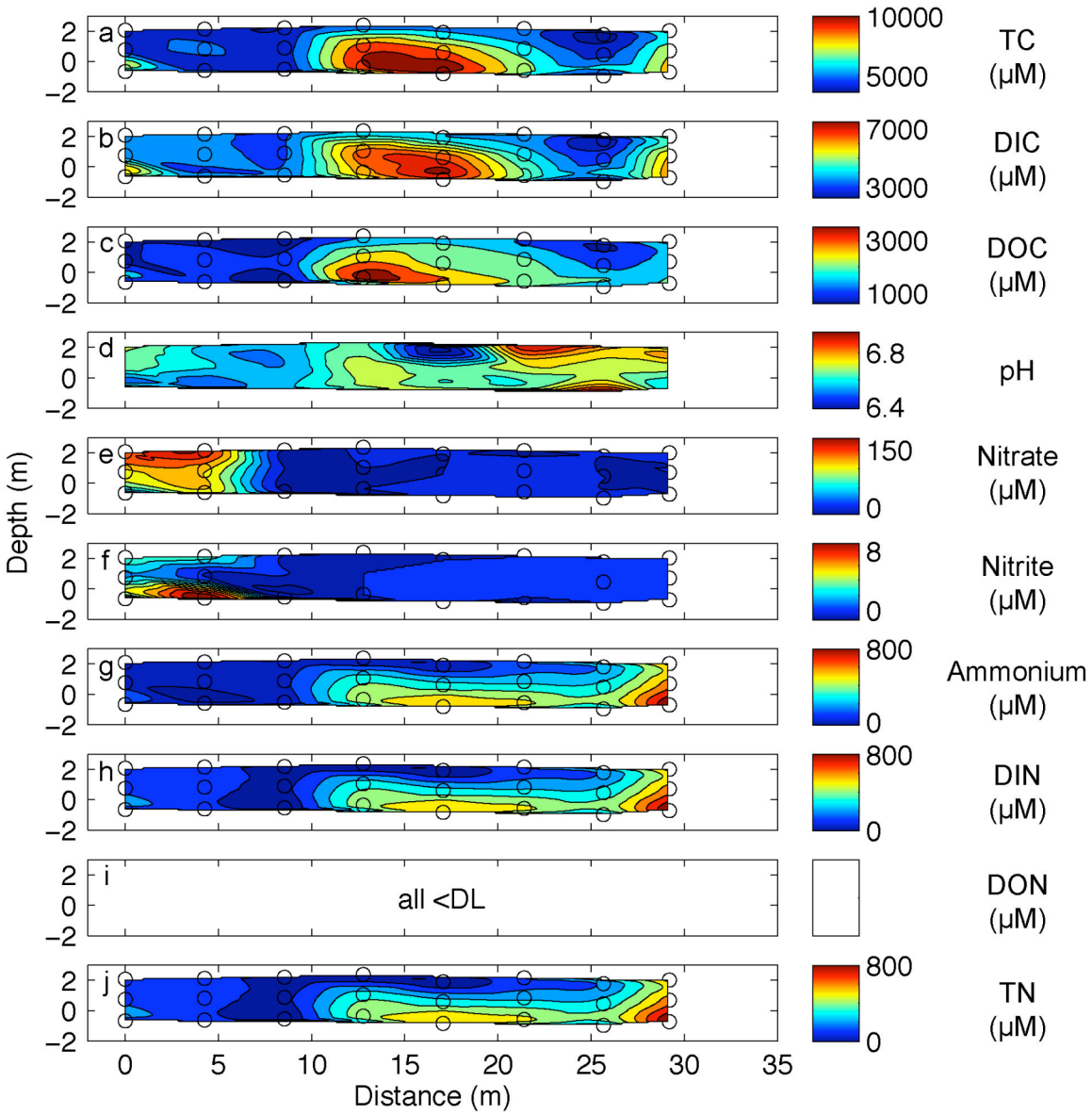

Figure S10. Cross-sectional contour plots of TC (a), DIC (b), DOC (c), pH (d), nitrate (e), nitrite (f), ammonium (g), DIN (h), DON (i), and TN (j) concentrations in Transect A in August 2009. Open circles in the plot delineate locations where samples were collected. The color bar limits for each plot are based on the limits of concentrations along the cross section.

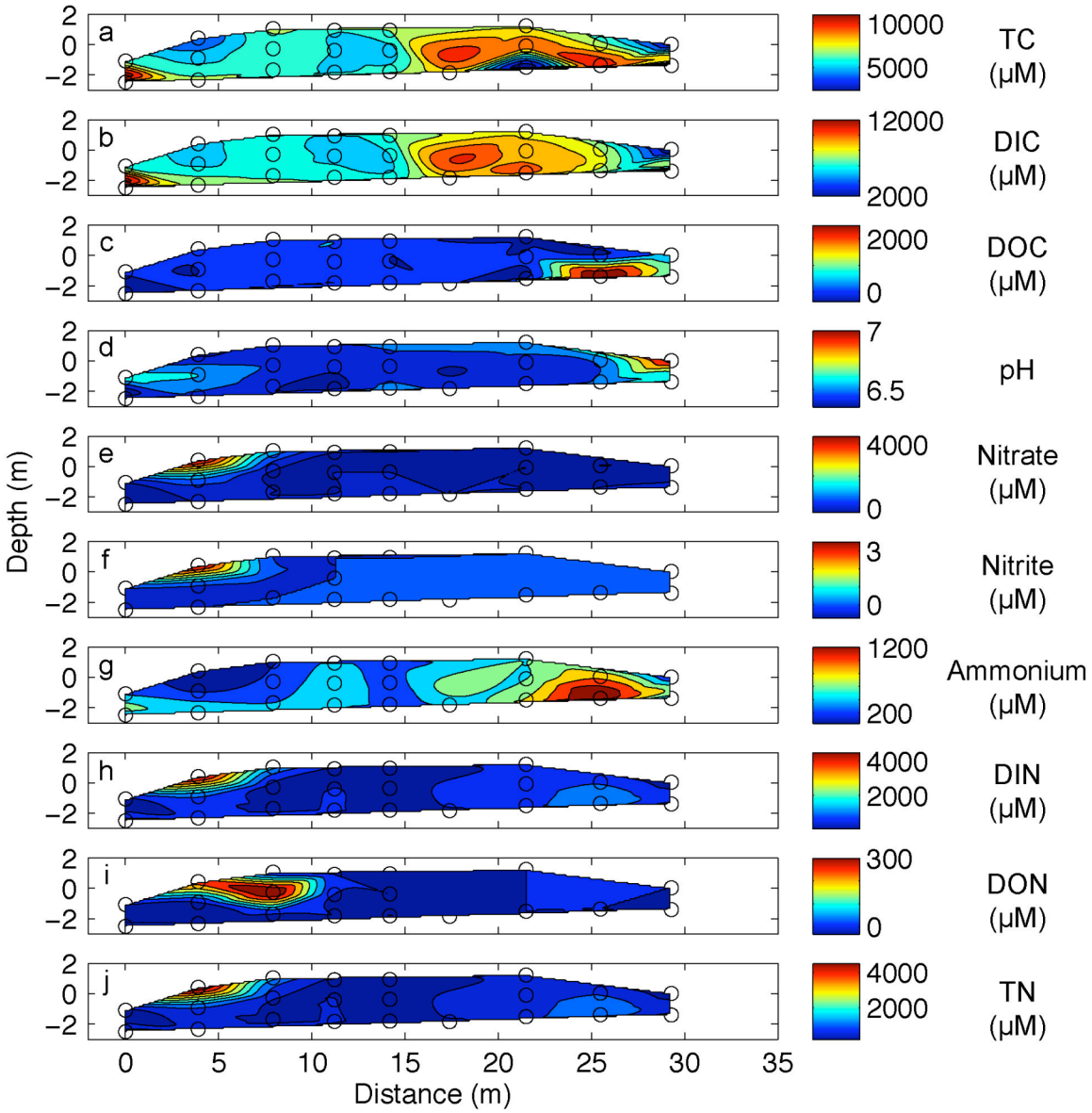

Figure S11. Cross-sectional contour plots of TC (a), DIC (b), DOC (c), pH (d), nitrate (e), nitrite (f), ammonium (g), DIN (h), DON (i), and TN (j) concentrations in Transect B in August 2009. Open circles in the plot delineate locations where samples were collected. The color bar limits for each plot are based on the limits of concentrations along the cross section.

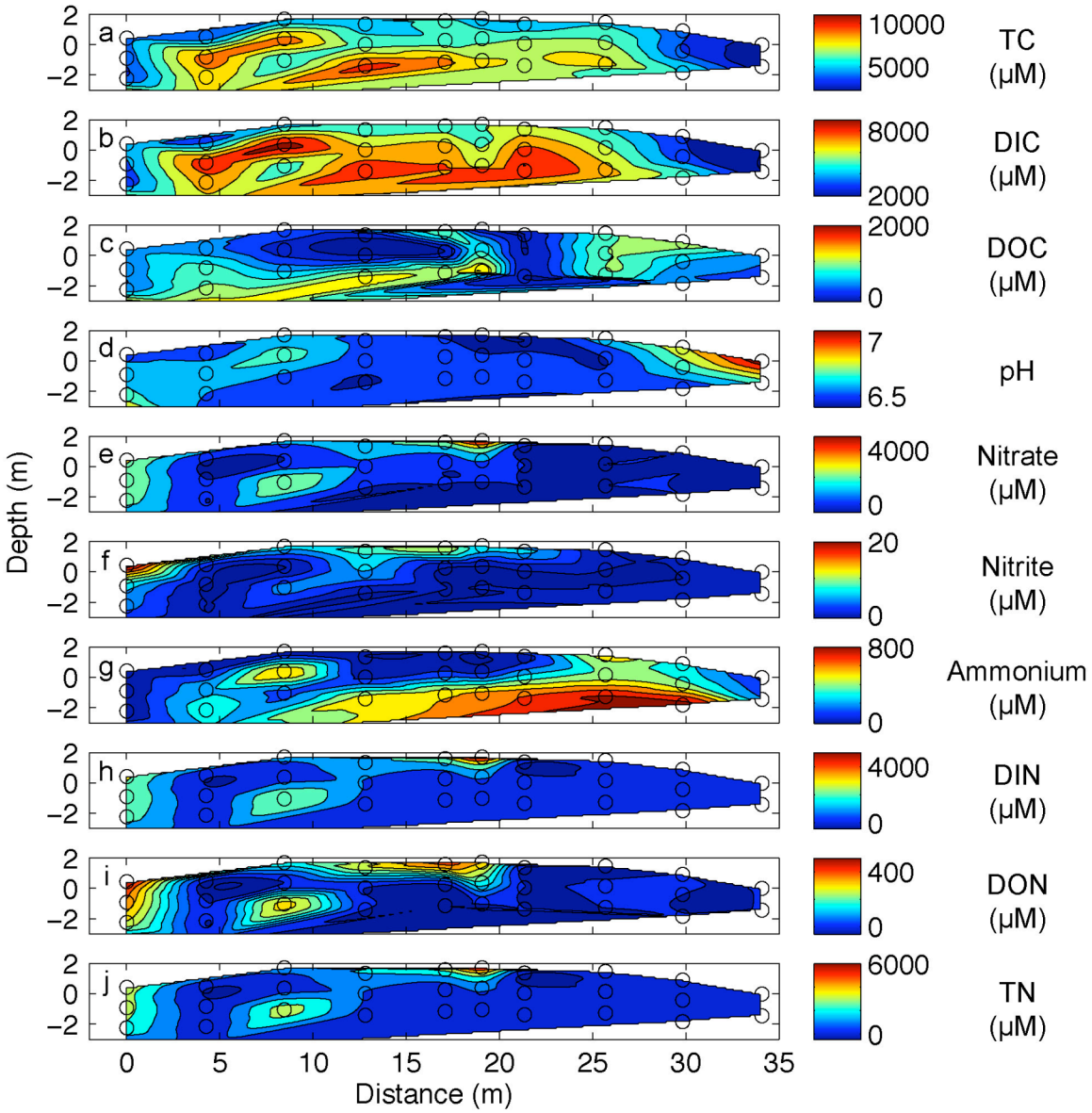

Figure S12. Cross-sectional contour plots of TC (a), DIC (b), DOC (c), pH (d), nitrate (e), nitrite (f), ammonium (g), DIN (h), DON (i), and TN (j) concentrations in Transect C in August 2009. Open circles in the plot delineate locations where samples were collected. The color bar limits for each plot are based on the limits of concentrations along the cross section.

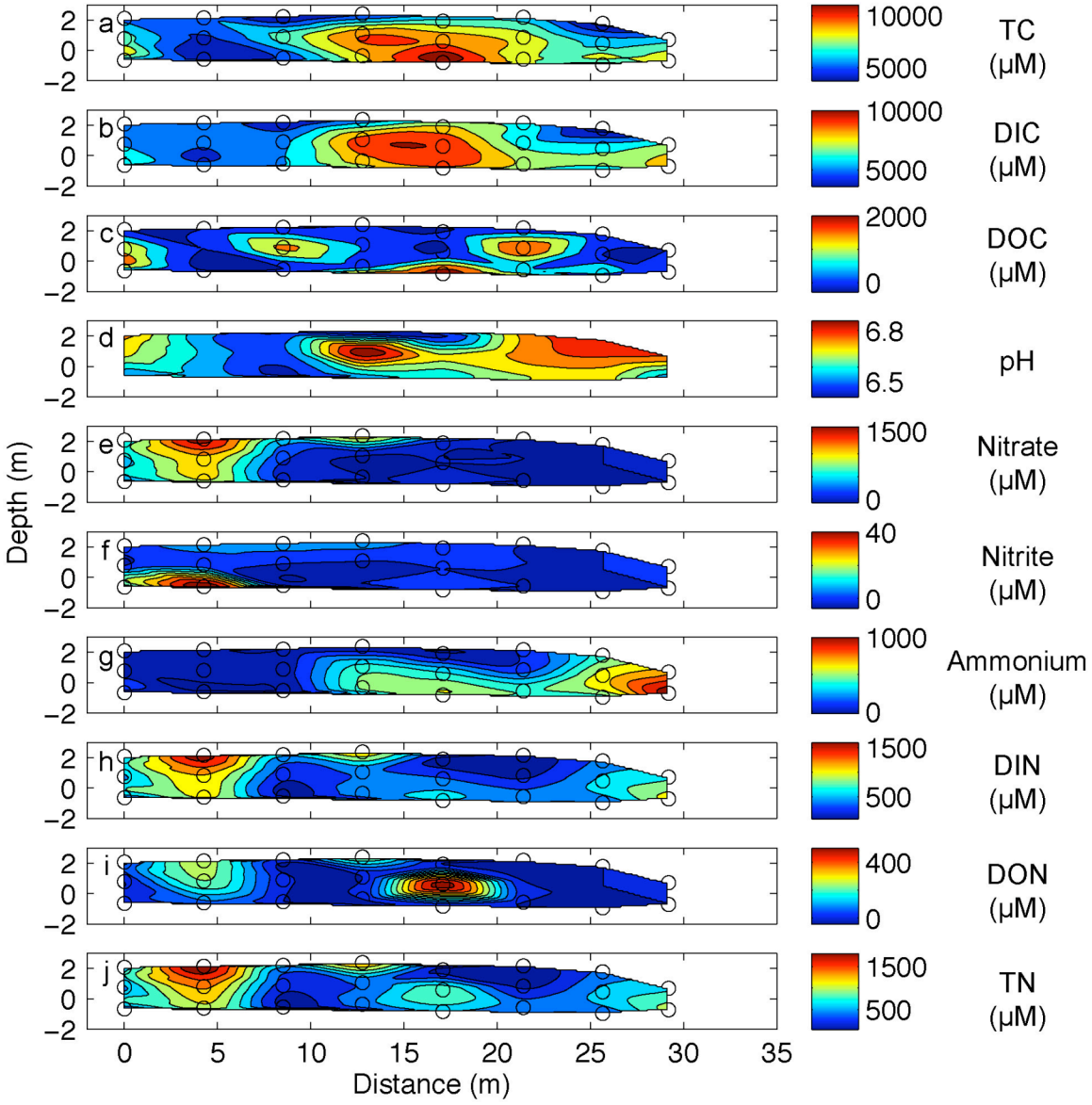

Figure S13. Concentrations of bromide tracer, enterococci, somatic coliphage and F+ coliphage in the fresh column, all normalized to influent concentrations.

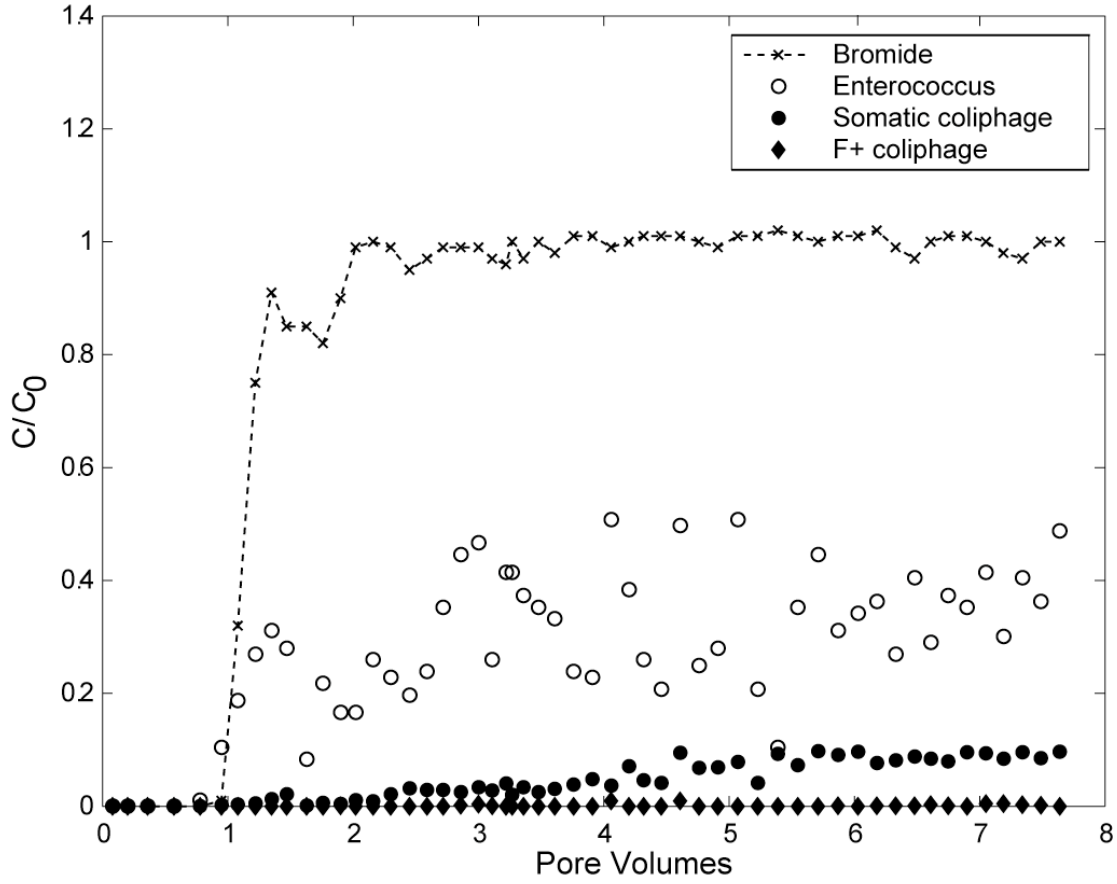

Figure S14. Concentrations of bromide tracer, enterococci, somatic coliphage and F+ coliphage in the saline column, all normalized to influent concentrations.

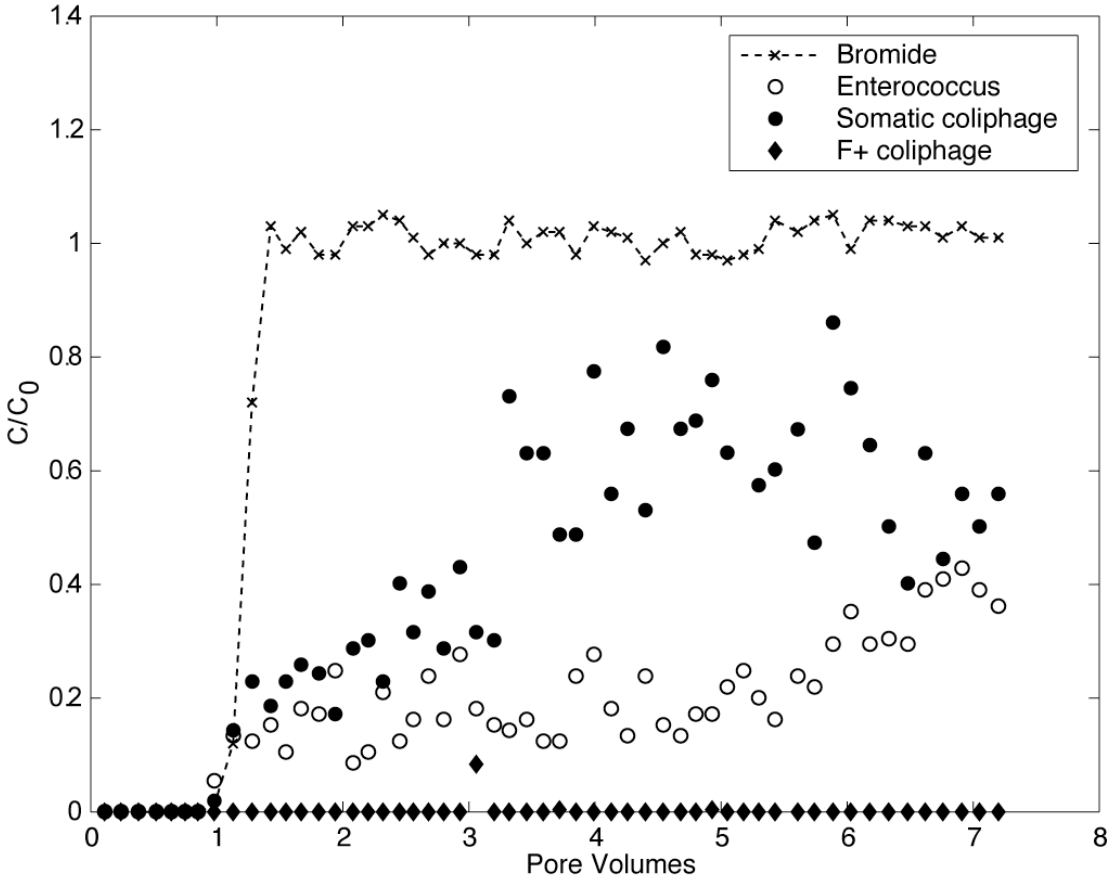

Table S1. Hydraulic conductivities based on tidal efficiency.

Well ID	K (m day^{-1}) based on Pt. Reyes record	K (m day^{-1}) based on S21 record
S21	20.3	n/a
S20	7.4	2.2
S15	5.4	1.9
S10	15.8	13.7
S12	31.3	35.9

Table S2. Groundwater characteristics for the fresh and saline sediment and water samples used in the column experiments, as measured in the field upon collection.

Sample Site	Temperature (ºC)	Conductivity (mS/cm)	DO (mg/L)	pH (-)	Salinity (-)	Eh (mV)
Fresh Groundwater (Column A)	15.1	0.725	1.42	6.63	0.35	577
Saline Groundwater (Column B)	12.1	35.5	7.42	7.88	21.9	545

Table S3. Mean +/- standard deviation concentrations of bromide, log(enterococci), log(somatic coliphage) and log(F+ coliphage) in the feed stock for the fresh and saline FIBV attenuation column experiments.

	Fresh Column	Saline Column
Bromide (mg L^{-1})	35 +/- 1	121 +/- 1
Enterococcus (log (cfu (100 mL)$^{-1}$))	5.03 +/- 0.11	4.97 +/- 0.15
Somatic coliphage (log (pfu (100 mL)$^{-1}$))	4.84 +/- 0.06	4.98 +/- 0.14
F+ coliphage (log (pfu (100 mL)$^{-1}$))	4.37 +/- 0.17	5.04 +/- 0.04

Table S4. Results and confidence intervals from saturated fresh and saline FIBV attenuation column experiments. In the table, V is the water velocity (cm min^{-1}), D is the hydrodynamic dispersion coefficient (cm^2 min^{-1}), and μ is the first order virus or bacteria removal rate coefficient (min^{-1}), and R is the retardation factor (-), as defined in Eq. S2.

		Fresh Column		Saline Column	
Parameter	Unit	Value	95% Confidence Interval	Value	95% Confidence Interval
V	cm hr^{-1}	6.83	6.79-6.89	8.88	8.70-9.06
D	cm^2 hr^{-1}	0.255	0.175-0.335	1.72	0.900-2.55
Enterococci, μ	hr^{-1}	0.476	0.439-0.511	0.462	0.426-0.499
Enterococci, R	[]	0.924	0.822-1.03	0.917	0.766-1.07
Somatic, μ	hr^{-1}	0.406	0.367-0.444	1.65	1.52-1.79
Somatic, R	[]	0.935	0.877-0.991	1.23	.936-1.53
Male Specific (F+), μ	hr^{-1}	1.8	1.36-2.31	2.82	2.57-3.01
Male Specific (F+), R	[]	2.39	0.54-4.24	2.77	1.44-4.10

Table S5. Denitrification potential assay results, including groundwater characteristics at each sediment sample site and denitrification potential rates. Salinity is reported using the unitless practical salinity scale. Denitrification potential rates are shown with standard errors from triplicate analysis. Rates below the quantification limit are designated "BQL".

Sample	Description	Temperature (°C)	Conductivity (mS/cm)	Dissolved Oxygen (mg/L)	pH	Salinity (-)	Eh (mV)	Denitrification Potential Rate +/- Standard Error [nmol N hr^{-1} g^{-1}]
DNP1	Up gradient of leach field	17.6	0.83	.52	6.59	0.40	286	10.8 +/- 1.09
DNP2	Down gradient of leach field	18.6	0.97	.38	6.36	0.48	489	.023 +/- .0033
DNP3	Down gradient of leach field	19.3	0.95	.49	6.40	0.46	517	.012 +/- .0036
DNP4	Down gradient of leach field	19.8	1.2	2.35	6.40	0.61	584	.018 +/- .0063
DNP5	Down gradient of leach field	20.4	0.87	2.11	6.40	0.43	605	.0073 +/- .0082
DNP6	Down gradient of leach field	20.8	1.72	1.53	7.14	0.87	551	BQL
DNP7	Down gradient of leach field	19.5	11	4.18	7.98	6.4	549	BQL
DNP8	North of impacted aquifer	18.8	0.79	0.51	7.09	0.38	339	.075 +/- .042
DNP9	Autoclaved control	n/a	n/a	n/a	n/a	n/a	n/a	BQL

A.10 REFERENCES CITED

Bear J.A., H.D. Cheng, S. Sorek, D. Ouuzar, I. Herrera, editors. 1999. Seawater intrusion in coastal aquifers — concepts, methods and practices. Dordrecht, the Netherlands: Kluwer Academic Publishers. 625 pp.

Borden, R.C., R.A. Daniel, L.E. LeBrun IV, and C.W. Davis, 1997. Intrinsic Biodegradation of MTBE and BTEX in a Gasoline-Contaminated Aquifer. Water Resources Research **33**: 1105-1115.

de Sieyes, N. R., K. M. Yamahara, A. Paytan and A. B. Boehm. 2001. Submarine groundwater discharge to a high-energy surf zone at Stinson Beach, California, estimated using radium isotopes. Estuaries and Coasts. DOI: 10.1007/s12237-010-9305-2

de Sieyes, N. R., K. M. Yamahara, B. A. Layton, E. H. Joyce, and A. B. Boehm. 2008. Submarine discharge of nutrient-enriched fresh groundwater at Stinson Beach, California is enhanced during neap tides. Limnology and Oceanography **53**: 1434-1445.

D'Elia, C.F., P.A. Steudler, and N. Corwin. 1977. Determination of total nitrogen in aqueous samples using persulfate digestion. Limnology and Oceanography. **22**: 760–764.

Einarson, M. D., and D. M. Mackay. 2001. Predicting impacts of groundwater contamination. Environmental Science & Technology **35**: 66A-73A.

Ferris, J. G. 1963. Methods of determining permeability, transmissivity and drawdown. U.S. Geol. Survey Water Supply Paper 1536-1.

Fetter, C. W. 2001. Applied Hydrogeology. 4th Edition. Prentice-Hall, Upper Saddle River, NJ. 598 p.

Jin, Y., M. V. Yates, S. S. Thompson, and W. A. Jury. 1997. Sorption of viruses during flow through saturated sand columns. Environmental Science & Technology **31**: 548-555.

Korom, S.F. 1992. Natural denitrification in the saturated zone: a review. Water Resources Research. **28**:1657-1668.

Laverman, A. M., P. Van Cappellen, D. Van Rotterdam-Los, C. Pallud, and J. Abell. 2006. Potential rates and pathways of microbial nitrate reduction in coastal sediments. Fems Microbiology Ecology **58**: 179-192.

Marin County Open Space District (MCOSD). 1996. The Bolinas Lagoon Management Plan Update.

Moore, W. S. 1999. The subterranean estuary: a reaction zone of ground water and sea water. Marine Chemistry **65**: 111-125.

Pfenning, K.S., and P.B. McMahon. 1996. Effect of nitrate, organic carbon, and temperature on potential denitrification rates in nitrate-rich riverbed sediments. Journal of Hydrology, **187**: 283-295.

Stinson Beach County Water District. 1998. Stinson Beach Hydrologic Survey. Stinson Beach: Stinson Beach County Water District.

Tiedje, J.M. 1982. Denitrification, pp. 1011-1026. In A.L. Page, R.H. Miller and D.R. Keeney (eds.), Methods of Soil Analysis, Part 2. Agronomy Monograph No. 9., Amer. Soc. Agron., Madison, WI.

USEPA. 2001. Method 1602: Male-specific (F+) and somatic coliphage in water by single agar layer (SAL). EPA 821-R-01–029. Office of Water, U.S. Environmental Protection Agency, Washington, DC.

USEPA. 2002a. Method 1603: Escherichia coli in water by membrane filtration using modified membrane-thermotolerant Escherichia coli agar (modified mTEC). EPA 821-R-02–023. Office of Water, U.S. Environmental Protection Agency, Washington, DC.

USEPA. 2002b. Method 1600: Enterococci in water by membrane filtration using membrane-enterococcus indoxyl-beta-D-glucoside agar (mEI). EPA 821-R-02–022. Office of Water, U.S. Environmental Protection Agency, Washington, DC.

Van Genuchten, M.T. and W.J. Alves. 1982. Analytical Solutions of the One-Dimensional Convective-Dispersive Solute Transport Equation. United States Department of Agriculture, Agricultural Research Service, Technical Bulletin 1661.